IN SILICO-GUIDED DESIGN, SYNTHESIS AND ANTIMICROBIAL ACTIVITY OF PIPERAZINE-LINKED 8-HYDROXYQUINOLINE-ISATIN HYBRIDS

A MINI THESIS SUBMITTED IN PARTIAL FULFILMENT OF THE

REQUIREMENTS FOR THE DEGREE OF MASTER OF SCIENCE

(CHEMISTRY)

OF

THE UNIVERSITY OF NAMIBIA

BY

Elvira Van Wyk

9271428

April 2025

Main Supervisor: Dr R. Hans (Department of Physics, Chemistry & Material Science, University of Namibia)

Co-Supervisor: Prof V. Uahengo (Department of Physics, Chemistry & Material Science, University of Namibia)

ABSTRACT

Drug-resistant pathogenic bacteria and fungi render existing antimicrobials ineffective, fuel the global antimicrobial resistance (AMR) crisis, and ultimately serve as impetus for the discovery of new antimicrobial agents. Hybrid drugs formed by covalently binding two pharmacophores, have shown promise in combating resistance. Monomers selected for this study include 8-hydroxyquinoline and isatin. There exist reports on the versatility of the 8-hydroxyquinoline ring and the antimicrobial, anticancer, and antifungal activity ascribed to its derivatives, while the isatin scaffold known for rendering high hit rates, in targeted drug discovery. The aim of the study was to synthesize piperazine-linked 8-hydroxyquinoline-isatin hybrids, with and without the thiosemicarbazide unit, and to evaluate their antimicrobial activities. *In silico* studies of the hybrids were done using open-source absorption, distribution, metabolism, excretion, and toxicity (ADMET) prediction platforms, SwissADME and pkCSM, to guide the selection of constructs with favourable pharmacokinetics and druglike properties. According to the docking studies, compounds **14a-c** and **15a-c** showed significant binding energy with *Escherichia coli*'s outer membrane protein A (OmpA) and DNA gyrase as the key target enzymes. Both **14c** and **15c** showed binding energies of -9.8 kcal/mol with OmpA. In the case of DNA gyrase, a binding energy of -8.9 kcal/mol was recorded for **14c**, whereas **15c** showed satisfactory interaction with a binding energy of -8.5 kcal/mol. Synthesis of the target hybrids began with the reaction of 5-chloromethyl-8-hydroxyquinoline **10** with piperazine to yield 5-(piperazin-1-ylmethyl)quinolin-8-ol **11**. The Mannich reaction of unsubstituted/5-substituted isatin with **11**, yielded Mannich bases **14a-c** with yields ranging between 56 - 60%. Proposed structures of the novel hybrids, **14a-c** were confirmed by means of infrared, ^{1}H- and ^{13}C-NMR spectroscopy. Antimicrobial activity testing of hybrids **14a-c** and advanced intermediates, against *Klebsiella pneumonia* ATCC10556, *Escherichia coli* ATCC700928, *Candida albicans* ATCC13933 and *Staphylococcus aureus* ATC12600 was done using the agar disk diffusion method. Hybrids **14a-b** as well as intermediate **10** displayed activity against all four strains. Equipotent activity with MIC values of 1.25 mg/mL against all bacterial strains was recorded for hybrid **14b** and intermediate **10**. This study revealed the antimicrobial activity of novel piperazine-linked 8-hydroxyquinoline-isatin hybrids and that they warrant further studies.

Key words: 8-hydroxyquinoline, isatin, hybrids, in silico ADMET, antimicrobial

CONFERENCE PARTICIPATION

1. Virtual Conference on Chemistry and its Applications: Transforming Chemistry and Interdisciplinary Research (VCCA), 12th to 16th August 2024. Oral presentation**.**

   Title: Synthesis and Antimicrobial Activity of Piperazine-Linked 8-Hydroxyquinoline-Isatin Hybrids.

2. National Students' Research Symposium (NCRST), 21-22 August 2024. Poster presentation.

   Title: Synthesis and Antimicrobial Activity of Piperazine-Linked 8-hydroxyquinoline-Isatin Hybrids.

TABLE OF CONTENTS

LIST OF FIGURES

LIST OF SCHEMES

LIST OF TABLES

ABBREVIATIONS

8HQ:	8-Hydroxyquinoline
ADMET:	absorption, distribution, metabolism, excretion, and toxicity
AMR:	Antimicrobial resistance
Caco-2:	human colorectal adenocarcinoma cell line
CADD:	Computer-Aided Drug Design
CD_3OD:	methanol-d_4
$CDCl_3$:	chloroform-d
$(CD_3)_2SO$:	dimethyl sulfoxide-d_6
DMSO:	dimethyl sulfoxide
ESKAPE:	*Enterococcus faecium*, *Staphylococcus aureus*, *Klebsiella pneumoniae*, *Acinetobacter baumannii*, *Pseudomonas aeruginosa*, and Enterobacter spp.
GOLD:	Genetic Optimization for Ligand Docking
HRMS:	High-resolution mass spectrometry
HOB:	human oral bioavailability
IR:	infrared
LBDD:	ligand-based drug design
LogP:	the logarithm of the *n*-octanol/water partition coefficient
MIC:	Minimum inhibitory concentrations

MR: molecular refractivity

MRSA: Methicillin-resistant *Staphylococcus aureus*

MW: molecular weight

NMR: Nuclear magnetic resonance

NP: natural products

OmpA: outer membrane protein A

PDB: Protein Data Bank

PSA: polar surface area

QSAR: quantitative structure–activity relationship

Ro5: Lipinski's rule of five

SBDD: Structure-based drug design

SMILES: simplified molecular input line entry system

sSA: sub-Saharan Africa

SAR structure-activity relationship

TLC: thin layer chromatography

TPSA: topological polar surface area

TSC: Thiosemicarbazide

WHO: World Health Organization

ZOI: zone of inhibition

ACKNOWLEDGEMENTS

First and foremost, I have to thank my Lord and Savior Jesus Christ who has been with me and guiding me through the whole blood sweat and tears.

I would express my sincere gratitude to my supervisor Dr Renate Hans for all her patience, guidance, and unwavering support throughout this study. I have learned more from her than just academics and for that I am forever grateful. Dr Mukakalisa for her help in the biological testing and Mr. Petrus Shanika for his help with the computational studies.

I would like to thank my family, especially my daughter Tiffany for their encouragement and support.

DECLARATION

I, Elvira. B. Van Wyk hereby declare that this study is a true reflection of my own research and that this work or part thereof has not been submitted for a degree from any other institution of higher education.

Elvira. B. Van Wyk	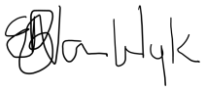	26 November 2024
Name	**Signature**	**Date**

1. INTRODUCTION

1.1 Background

Antimicrobial resistance (AMR) remains a pervasive global threat that calls for the application of innovative and pioneering strategies to discovery novel drugs with new mechanisms of action. According to predictions, deaths due to AMR could increase to 10 million per year by 2050 in the absence of effective and timely interventions [1]. Sub-Saharan Africa (sSA) bears the highest clinical burden of AMR [2,3], with the latter typified by lengthy periods of hospitalization and increased mortalities. Furthermore it exerts a heavy strain on the already compromised healthcare facilities in low-resource settings [4]. AMR represents a formidable global challenge and is exacerbated by a poorly stocked antimicrobial drug development pipeline, and an increasing number of critical priority microbial pathogens.

The monumental contribution of natural products to the arsenal of antimicrobial agents, albeit primarily sourced from microbial taxa, is worthy of note [5]. Privileged natural product (NP) scaffolds such as isatin and 8-hydroxyquinoline, serve as validated “blueprints” in the design of compound libraries, and are synthetically versatile with their derivatives displaying a spectrum of biological activities, including antimicrobial activities [6,7]. Both scaffolds have been documented as pre-validated for drug development because of their suitable molecular geometry for target binding and the ability to be modified to boost activity or selectivity. More importantly, the antimicrobial potential of isatin and 8-hydroxyquinoline is well-documented, and both scaffolds have been extensively studied for their ability to inhibit the growth of various microorganisms [8,9]. Thiosemicarbazide (TSC) derivatives are typically synthesized via the condensation of thiosemicarbazide with aldehydes or ketones. They have

gained significant interest due to their ability to form complexes with various metals. TSC derivatives have been studied for their antimicrobial properties, and several studies reported promising results [10]

A rewarding drug design approach which contributes toward the enhancement of the structural diversity and pharmacokinetic profile of natural products, entails hybridization [11]. Hybrid drugs are formed by the linkage of two or more pharmacophores to yield a molecule with a dual mode of action. According to reports, molecular hybrids offer improved binding interaction at the target site, a reduced side effect profile, simplified drug-drug interactions and, more importantly, a reduced susceptibility for the development of drug resistance [12].

The high attrition rate of potential drug molecules can, in part, be ascribed to poor pharmacokinetic properties [13]. Advances in computational chemistry and the evolution of *in silico* drug discovery tools, for example, online absorption, distribution, metabolism, excretion, and toxicity (ADMET) prediction software, de-risk drug discovery during the initial stages by prioritizing "druglike" Lipinski's rule of 5 (Ro5) compliant compounds for synthesis [14].

1.2 Statement of the problem

Listed among the critical intervention strategies is the development of effective antimicrobial drugs with new modes of action, and a reduced propensity for the development of resistance. The isatin and 8-hydroxyquinoline scaffolds are pre-validated templates for designing compound libraries, by virtue of their privileged status. A literature review revealed that hybrid compounds containing these core structures, i.e. isatin and 8-hydroxyquinoline, linked with a piperazine unit and

enriched with a TSC group, have not been synthesized before nor explored for their potential as antimicrobial agents.

1.3 Objectives of study

(i) To design, synthesize and characterize piperazine-linked 8-hydroxyquinoline-isatin hybrids with and without a TSC group.

(ii) To evaluate the antimicrobial activity of hybrids and advanced intermediates.

1.4 Significance of the study

This research aims to demonstrate and endorse the application of *in silico*-guided drug design and the molecular hybridization of privileged natural product scaffolds, isatin and 8-hydroxyquinoline, for the discovery of potential novel antimicrobial compounds. It is envisaged that the isatin-8-hydroxyquinoline hybrids from this study can be further explored as potential antimicrobial lead compounds and as ligands in bioactive metal complex formation. Overall, the study aims to contribute to the synthesis of new antimicrobial lead compounds.

1.5 Limitation of the study

The synthesis of six hybrids, of which three serve as advanced intermediates were identified for this study due to the unavailability of reagents and the costly nature of Nuclear magnetic resonance (NMR) spectroscopy analysis. The full characterization of compounds which require, in addition to NMR data, high resolution mass spectroscopy and elemental analysis, could not be done because of the lack of local infrastructure.

2. LITERATURE REVIEW

2.1 Antimicrobial Resistance (AMR)

AMR renders antimicrobial medications ineffective and complicates the treatment of microbial infections by increasing the risk of the spread of infections, and by causing serious illness, disability, and death [15]. There exists a paucity of data on the true extent and prevalence of antimicrobial resistance in sub-Saharan Africa (sSA), which is partly due to a lack of laboratory infrastructure, diagnostics and poor AMR surveillance [2, 16]. In 2019, almost 5 million people died due to drug-resistant microbial infections and the highest number of deaths, 1.07 million were recorded for sSA. Furthermore, the consequences of unchecked AMR extend to longer and more severe illnesses, with infections that were once manageable becoming untreatable. Surgical procedures including organ transplants and cancer treatments which rely heavily on effective antimicrobial agents to avert post-operative infections, are at risk [4]. Less than 25% of the drugs currently in development are new or function in a novel manner, and none of them appear to be effective against the most virulent and resistant bacteria such as ***E****nterococcus faecium*, ***S****taphylococcus aureus,* ***K****lebsiella. pneumoniae,* ***A****cinetobacter baumannii,* ***P****seudomonas aeruginosa,* and ***E****nterobacter* spp., also known as (ESKAPE pathogens, or the World Health Organization's (WHO) critical threat pathogens [17].

2.2 Natural product (NP) scaffolds and natural product hybrids as antimicrobial agents

Compared to synthetic compounds, NPs are structurally diverse, have higher molecular weights, more sp^3 hybridized carbon and oxygen atoms, and fewer nitrogen

and halogen atoms. They also have an increased number of hydrogen bond acceptors and donors, lower calculated octanol–water partition coefficients (cLogP), and enhanced molecular rigidity compared to synthetic compounds [18]. NPs fulfill specific biological functions, including the regulation of an organism's defense mechanisms and its competitive interactions with other organisms, making them particularly relevant for tackling infectious diseases and cancer [19]. However, using plant chemicals, also known as phytochemicals as a source of antimicrobial agents or as templates in drug design continues to be a viable approach for the discovery of new drugs. [17].

Natural product scaffolds selected for this study include the 8-hydroxyquinoline and isatin moieties, which are categorized as privileged structures. The term "privileged structure" was introduced by Evans and coworkers [20] and describes structural motifs that bind to various biological targets indiscriminately. These flexible binding characteristics allow them to change functional groups thus providing efficient and specific ligands for a variety of distinct biological targets [21]. These scaffolds often serve as a valuable starting point for the design of natural-product-based compound libraries in drug discovery and have been extensively studied in various disease models. [7].

2.2.1 Isatin and its derivatives as antimicrobial agents

Isatin **1, (Figure 1)** is a 2-oxoindole derivative that is found in plants of the genus *Isatis* and is a metabolite of adrenaline in humans [22]. The isatin scaffold is synthetically versatile and its chemical reactive functional groups allow a range of transformations like oxidation, aldol condensation, Friedel-Crafts reactions, and ring

expansion. Other reactions include addition and condensation reactions at positions 2 and 3 **(Figure 1)**, as well as *N*-alkylation, *N*-acylation, Mannich, and Michael reactions [22]. Schiff and Mannich base derivatives of isatin exhibit a broad spectrum of biological and pharmacological properties, including antitumor [23], antimicrobial [24], anti-inflammatory [25], analgesic [26], antimycobacterial [24], anticonvulsant [27], antiviral [28], anthelmintic, anti-HIV [29], antioxidant, and CNS depressant activities [30].

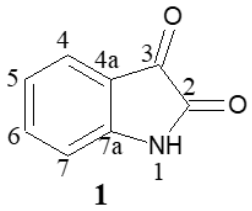

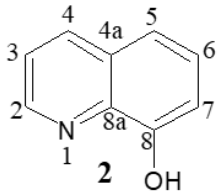

isatin 8-hydroxyquinoline

Figure 1. Chemical structures of privileged natural product scaffolds selected for this study, isatin **1** and 8-hydroxyquinoline **2**.

According to reports, antibacterial active isatin derivatives exert their mechanism of action by inhibiting fatty acid production or by binding to various targets, for example, DNA, efflux pumps, protein tyrosine phosphatases [31], Filamenting temperature-sensitive mutant Z(FtsZ), and virulence factors [31]. In a reported study, Schiff bases of isatin, were prepared by a condensation reaction of TSC and substituted *N*-aryl isatins **(Figure. 2)** [32]. These isatin derivatives were screened for in vitro antimicrobial activities by using microbroth dilution assay against eight bacterial strains: *S. aureus*, *S. epidermidis*, *Escherichia coli*, *Salmonella species*, *Bacillus cereus*, *Enterobacter faecalis*, *P. aeruginosa*, Methicillin-resistant *Staphylococcus aureus* (MRSA), and two fungal strains: *Candida albicans*, and *Aspergillus niger*.

Minimum inhibitory concentrations (MICs) recorded ranged between 30 and 80 μg/mL, with compound 3 **(Figure 2)** displaying the best antifungal activity with MIC values of 30 μg/mL against *C. albicans* and 40 μg/mL against *Aspergillus niger* [32].

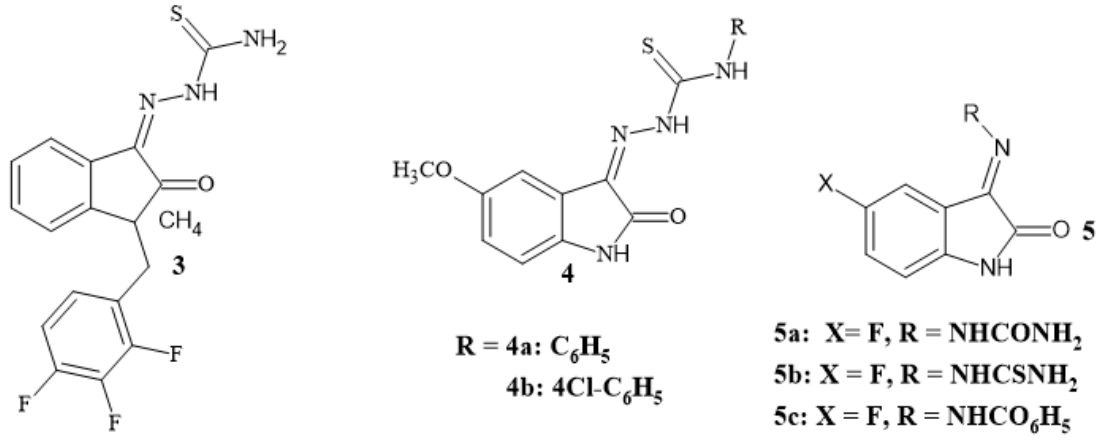

Figure 2. Chemical structures of antimicrobial isatin Schiff bases.

Novel isatin-thiosemicarbazones **4a**, **b (Figure 2)** was synthesized and evaluated for antimicrobial activity against two Gram-positive bacteria, *S. aureus* (ATCC 29213) and *B. cereus* (ATCC 11778), two Gram-negative bacteria *E. coli* (ATCC 25922), *P. aeruginosa* (ATCC 27853), and two yeasts C. *albicans* (ATCC 10231) and *C. tropicalis* (DSM 11953), using the broth microdilution method. **4 a** and **b (Figure 2)** were the most active and equipotent with a MIC value of 0.039 mg/mL against *S. aureus* [33]. In another study, a series of novel isatin Schiff bases were synthesized by combining amine and hydrazide derivatives with 5-substituted isatin derivatives. These novel derivatives were tested for antimicrobial activity against *P. aeruginosa (*ATCC 27853*), E. coli* (ATCC 25922), *E. faecalis (ATCC 29212), S. aureus* (ATCC 25923) and *Methicillin resistant Staphylococcus aureus* (MRSA, ATCC 43300), using a microtiter plate method. The derivatives displayed antimicrobial properties, with

compounds **5a-c (Figure 2)**, being equipotent against *P. aeruginosa* with an MIC value of 6.25 μg/mL [34].

2.2.2 8-Hydroxyquinoline and its derivatives as antimicrobial agents

Skraup et al (1953), successfully synthesized 8-hydroxyquinoline (8HQ) **2 (Figure 1)**, which comprises a phenol ring fused to a pyridine ring. The 8HQ scaffold exhibits versatile binding properties, chelating abilities towards various transition metal ions, displaying multitarget-molecule properties and acquiring privileged structure status in heterocyclic chemistry [35]. The presence of the phenol group makes 8HQ derivatives prone to several chemical reactions and/or structural modifications. This includes electrophilic aromatic substitution, diazonium coupling, and molecular rearrangements [36]. The hydroxyl group, being an electron donating group directs ortho- and/or para-functionalization of the aromatic ring. Easy modification of the 5- and 7-positions **(Figure 1)** can therefore be affected through electrophilic aromatic substitutions such as sulfonation, nitration, and nitrosation. Typically, the 5-position is the primary site of attack, but polysubstitution may also occur. Collectively, these reactions demonstrate the potential for further derivatization of the 8HQ scaffold [37]. In essence, the combined features of the hydroxyl group, chelation capabilities, and hydrophobic regions collectively support the antimicrobial potential of 8-HQ derivatives [38].

In 2016, Faydy et al. synthesized a series of novel 8-HQ derivatives **7 (Figure 3)** [39]. The synthesis involved a nucleophilic substitution reaction between piperazine derivatives and 5-chloromethyl-8-quinolinol hydrochloride, **6** (**Figure 3**) and the resulting compounds were screened for activity against both gram-positive and gram-negative bacterial strains. Compound **6** exhibited the best activity against the bacterial

strains with inhibition zones of 25, 24, 29 mm against S. *aureus, E. coli* and *Xanthosomas fragariae*, respectively at a concentration of 500 µg/mL [39]. In a separate study, the synthesis of 8-hydroxyquinoline derivatives **8 (Figure 3)** was undertaken and evaluated against Gram-positive and Gram-negative bacterial strains. The hybrid **8a** showed promising activity with a MIC value of 2 µg/mL against *S. aureus*. MIC values of 2, 4 and 2 µg/mL were recorded for compound **8b** against *E. coli, A. baumanii* and *S. aures* respectively, whilst compound **8c** showed activity with a MIC value of 2 µg/mL against *E. coli* and *A. baumanii* each [40].

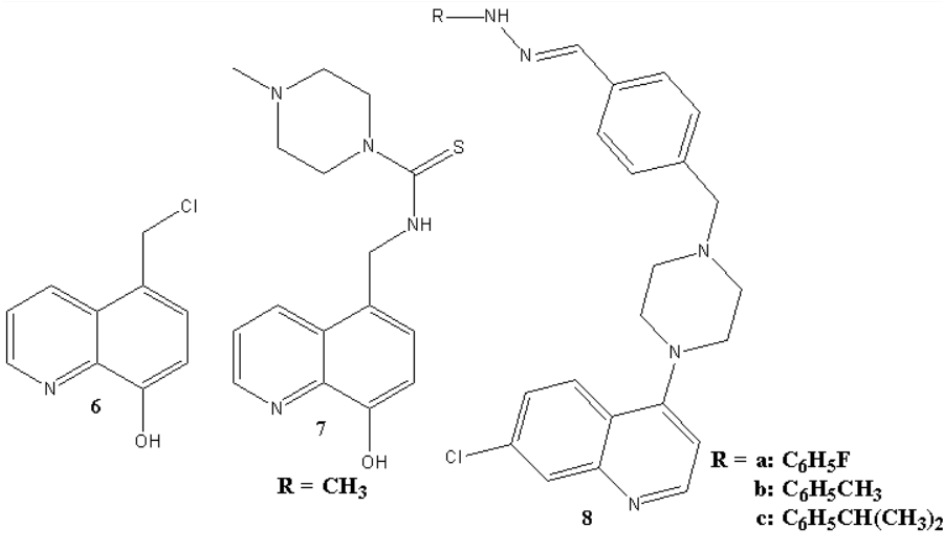

Figure. 3 Chemical structures of derivatives of 8-hydroxyquinoline

In addition to the 8HQ scaffold the above antimicrobials contain the piperazine ring system used in the design of the envisaged hybrids for this study.

2.2.3 Natural Product Hybrids

Hybridization entails the linking of two pharmacophores, each with its own distinct mechanism of action, to yield a construct that displays a dual mode of action and improved pharmacokinetics [11]. This drug design approach is rewarding in that the

combined pharmacophores reportedly have a reduced resistance, show enhanced activity, and improved binding affinity by modulating multiple targets [31, 12]. Hybrid drugs can be classified as linked, fused or merged. Merged hybrids are created when two structural motifs or pharmacophores overlap, while fused hybrids result from the joining of two pharmacophores without a linker. Linked hybrids are bound together by hydrolysable or non-hydrolyzable linkers [41.42]. The choice, position and stability of the linker is crucial in ensuring the desired therapeutic effect [12]. One limitation of hybrid compounds is their high molecular mass and bulky size that hinders passage through nonselective porin channels and delay cell entry through passive diffusion [43].

In 2011, Prakash et al. synthesized ciprofloxacin-isatin hybrids **(Figure 4)** as potential antimicrobials [44]. Most hybrids displayed strong antibacterial and antifungal activity compared to the reference drug ciprofloxacin. Compound **9a** showed equipotent activity against *S. aureus* and *P. aeruginosa* with an MIC value of 7.8 µg/mL, while the MIC for ciprofloxacin was 15.62 µg/mL and 7.81 µg/mL, respectively. Furthermore, compared to ciprofloxacin, compound **9b** showed equipotent activity with a MIC value of 7.81 µg/mL against *M. luteus.* Compound **9c** showed equipotent activity as ciprofloxacin against *S. epidermidis* and *M. luteus* with a MIC value of 7.81 µg/mL for each, and finally compound **9d** showed the same activity as ciprofloxacin against *K. pneumoniae* with an MIC value of 3.9 µg/mL. [44].

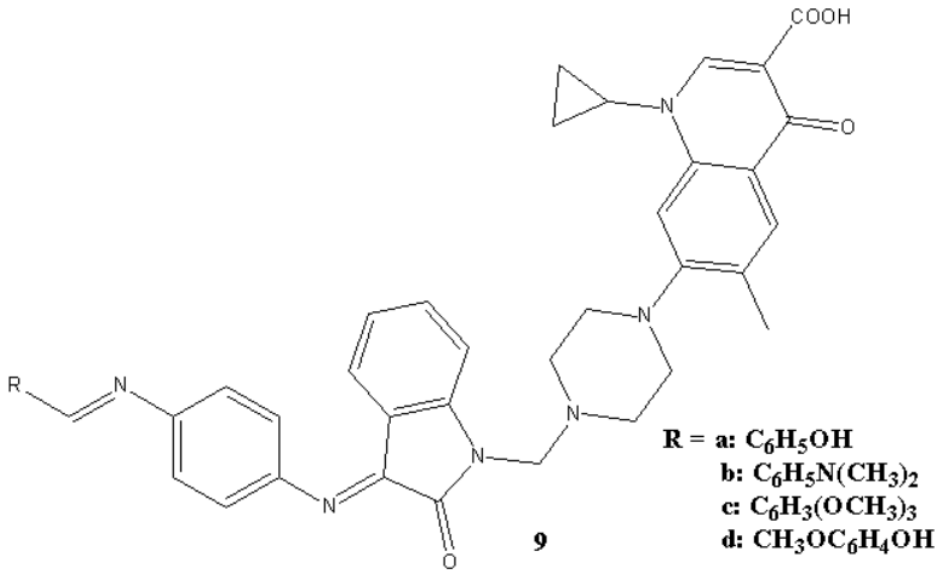

Figure. 4 Chemical structures of ciprofloxacin-isatin hybrids

Furthermore, dual-acting, hybrid candidates that have passed phase two clinical trials are rifampicin-fluoroquinolone hybrid (TNP-2092) and rifamycin-nitroimidazolehybrid (TNP-2198) [45]. The rifamycin class are potent DNA-dependent RNA polymerase (RNAP) inhibitors but are prone to resistance due to point mutations. Quinolones, broad-spectrum antibiotics targeting topoisomerase IV and DNA gyrase, also encounter resistance via chromosomal mutations and resistance plasmids. It is proposed that the rifamycin-quinolone hybrids can overcome resistance [46]. One hybrid, TNP-2092, showed success in phase II trials for acute bacterial skin infections and was designated for treating prosthetic joint infections. Additionally, it demonstrated strong efficacy in murine *C. difficile* models and against urease-producing bacteria, including *Helicobacter pylori* (*H. pyori*) [47].

Rifamycins were also combined with nitroimidazoles. TNP-2198, a rifamycin-nitroimidazole hybrid, outperformed metronidazole by showing a fourfold potency

against rifamycin-resistant *H. pylori* and up to 500-fold potency against rifamycin- and ciprofloxacin-resistant *C. difficile*; thus, displaying strong bactericidal synergy [45].

2.3 Computer-Aided Drug Design: *In silico* ADMET profiling and molecular docking studies

Computer-Aided Drug Design (CADD) is a key component of contemporary drug discovery. It combines computational procedures with biological knowledge to discover and enhance potential drug candidates. [48]. For the past 30 years, the increase in computational aided methods and available data on small molecule libraries made CADD an indispensable part of drug discovery [49]. CADD can be subdivided into two categories: Structure-based drug design (SBDD) and ligand-based drug design (LBDD). SBDD utilizes the three-dimensional structures of the biological target (usually proteins) to comprehend how potential drugs could fit and interact with it. Conversely, LBDD does not rely on understanding the target structure; instead, it concentrates on existing drug molecules and their pharmacological characteristics to develop novel drug candidates [48].

The evolution of computational approaches in optimizing pharmacokinetic and toxicity properties has facilitated the effective progression of discovery leads into drug candidates, and there exist numerous examples of evidence to this [50]. Molecular docking studies were employed to predict the binding of oseltamivir, used for treating influenza, to the influenza neuraminidase enzyme [51]. Similarly, for rivaroxaban, an oral anticoagulant used to prevent blood clots; *in silico* ADME predictions were used to assess its absorption, metabolism, and excretion, aiding in dose selection and safety considerations [52].

A few examples of *in silico* methods include Quantitative Structure–Activity Relationship (QSAR), molecular modeling and molecular docking. QSAR studies explores the relationship between the structure of molecules and their biological activities. It can be used to envisage the pharmacological activity of compounds according to their structural characteristics [48]. Molecular modeling is a fast-expanding field with applications across numerous research areas including physics, chemistry, and biology. It serves as the common link that connects key areas in pharmaceutical and biomedical research, medicinal chemistry, and (enantio)separation science. [53]. It uses three-dimensional structures of molecules to gain an understanding of the molecules structural and functional characteristics, and to provide a better understanding of how potential drugs might react within a biological system [48]. A few examples of these tools include Avogadro, a free and open-source molecular editor and visualizer [54], MolView, an open-source structural formula editor and a 3D model viewer [55] and Biovia Discovery Studio Visualizer, a graphics visualization tool for viewing, sharing, and analyzing protein and modeling data [56]. Molecular Docking entails predicting the orientation and position of one molecule (ligand) relative to a receptor molecule (usually a protein) forming a stable complex. The way the molecules bind together is used to predict their binding affinity, which is influenced by intermolecular interactions such as hydrogen bonding, electrostatic interactions, hydrophobic interactions and Van der Waals forces [57]. Examples of docking tools include AutoDock Vina [58], AutoDock-GPU [59] Genetic Optimization for Ligand Docking (GOLD) [60], Glide [61] and others. However, these *in silico* models have limitations as they focus on a predetermined database of structures, which when used, can result in new chemical structures that are outliers of the experimental data used to construct the initial models, being prematurely excluded

[62]. Because of this aforementioned limitation, interpretation of *in silico* data must be validated with in vitro biological data.

This study used molecular docking, more specifically blind docking to identify the binding regions of the protein and predict the binding pose of a molecule.

2.3.1 *In silico* physicochemical and pharmacokinetic profiling

Profiling the absorption, distribution, metabolism (biotransformation), elimination, and toxicity (ADMET) of potential drug compounds during the early stages, plays a key role in evaluating the prospective success of a new compound and can potentially reduce the risk of attrition [63]. Considering the limitations of virtual screening, *in vitro* and *in vivo* biological testing is required as it provides a comprehensive understanding of a drug's behavior, guiding its development and ensuring patient well-being [64]. Examples of free ADMET applications available online include pkCSM (Predicting Small-Molecule Pharmacokinetic and Toxicity Properties) [13], SwissADME [14], ADMETlab [65], ADMET-AI [66], preADMET [67], to mention a few.

The pkCSM method employs graph-based modeling to predict ADME/T properties and mutagenicity in drug development. By representing molecules as g/raphs with atoms as nodes and bonds as edges, it produces descriptors for structural and chemical features. It achieved 83.8% accuracy in predicting mutagenicity compared to Toxtree [68] which has 75.8% accuracy. It also provides predictions for many key indicators such as LD_{50}, Ames test, maximum daily dose and hepatotoxicity. [14]. Moreover, pkCSM claims confidentiality, in that no molecule information will be kept on their system after being uploaded by the user. However, even after covering a larger range

of parameters shows lower accuracy in its predictive ability compared to SwissADME [15].

SwissADME serves as a predictive model for physicochemical properties encompassing molecular weight (MW), molecular refractivity (MR), the count of specific atom types, and polar surface area (PSA). In terms of PSA calculation, SwissADME employs the topological polar surface area (TPSA) based on a fragmental technique, considering sulfur and phosphorus as polar atoms [69]. It is widely used for its simplicity in assessing the drug-likeness profile of compounds. This involves the incorporation of Lipinski's rule, to assess the likelihood of a substance being orally active by determining specific physicochemical parameters conducive to the possibility of becoming an oral drug. [70]. SwissADME, uses different methods to estimate log P. For example, iLOGP is formulated using a physics-based method that utilizes solvation-free energies, MLOGP follows a topological method, and XLOGP3 derives from an atomistic approach, WLOGP is based upon a fragmental system, while the determination of (SILICOS-IT) logP follows a hybrid method that uses both fragment and topological descriptors. The consensus of logP represents the mean of the five lipophilic character predictions, i.e. iLOGP MLOGP, XLOGP3, WLOGP and (SILICOS-IT) logP [62]. Privacy and confidentiality of personal data is ensured when using the webserver. SwissADME however, does not predict all the absorption parameters. For example, it does not provide predictions for Caco-2 (human adenocarcinoma cells) and HOB (human oral bioavailability) related to oral drugs, nor does it estimate any toxicity parameters [62]. Also, of note, is that SwissADME and pkCSM use different methods for counting rotatable bonds. pkCSM engages graph-based signatures in accordance with the original Veber rule, except for amide C-N bonds due to their high rotational energy barrier, whereas SwissADME's makes use of

the JpGraph an object-oriented graph creating library for PHP (hypertext preprocessor) to produce a radar plot bearing six axes for six properties of oral bioavailability which include lipophilicity (XLOGP3), size (MW), polarity (TPSA, topological polar surface area), solubility (log S), saturation (fsp^3) and flexibility (number of rotatable bonds). The six axes are adjusted to present the ideal one as a hexagon [62]. Additionally, the two tools differ in their approaches to predicting hydrogen bond acceptors. pkCSM focuses on central ADMET properties and may consider structural and chemical properties, while SwissADME rely on the presence of functional groups like oxygen or nitrogen atoms. These distinct measures used for identifying hydrogen bond acceptors may contribute to differences in predicted properties [71, 13]. In light of the aforementioned differences, this study used both pkCSM and SwissADME for physicochemical and pharmacokinetic profiling.

2.3.2 Molecular Docking

Molecular docking is a crucial tool in drug discovery, using *in silico* structure-based computational techniques to study ligand-protein interactions, and predicting how drug molecules bind to specific target sites [72]. In this process, a prototype based on the target protein structure is used, obtained from a protein data bank, and potential ligands are tested for binding efficacy within the protein's active site. To predict the preferred orientation of the ligand relative to the receptor, there are two methods used to explore the protein surfaces namely blind docking and site-specific docking. Site-specific docking is used when the binding site of the protein is known, and the docking is focused on a specific binding pocket or region. Blind docking is performed when there is no information about the binding sites in a protein. Even though site-specific

docking has shown great success rates, it is less practical when screening a large number of molecules against a big number of binding sites. However, blind docking results in a loss of accuracy and speed as it enables a simultaneous search of the entire protein surface [73]. The docking process evaluates interactions, measured by docking scores. As mentioned earlier, real-life tests, including MIC, enzyme inhibition, and cytotoxicity assays, offer a more accurate validation of potential compounds before drug development [74]. In this study, blind docking was used, wherein the hybrid was docked across the entire protein. This approach is useful for identifying unknown binding pockets, as the hybrids are novel and specific binding sites are not predetermined. It is particularly useful for discovering new binding sites. In contrast, a site-specific docking approach assumes that the hybrid would bind to a specific site, potentially overlooking areas where it might exhibit a higher binding affinity.

3. RESEARCH METHODS

3.1 Research Design

The design of the envisaged hybrids commenced with the acquisition and analysis of reported structure-activity relationship (SAR) data on antimicrobial activity of isatin and 8-hydroxyquinoline derivatives. Incorporated in the design process were *in silico*, physicochemical, pharmacokinetic profiling and docking studies of the intermediates and hybrids of which the results obtained endorsed the selected hybrids. The hybrids were then synthesized and spectroscopically characterized before being tested for antimicrobial activity against four microbial strains: *S. aureus*. *E. coli*, *K. pneumonia*, and *C. albicans*.

3.2 General Experimental

All reagents and solvents used were of analytical grade and used without further purification. The progress of the reactions was monitored with thin layer chromatography (TLC), using silica gel-coated aluminium-backed plates (Merck). TLC solvent systems used include: (i) chloroform: methanol: ammonia in the ratio 9:1:0.25, (ii) ethyl acetate: methanol: water (10:1:0.5) and (iii) ethyl acetate: hexane (4:6). Visualization of the developed TLC plates was done with the naked eye, UV light and by using vanillin-sulfuric acid as spray reagent. Melting points were recorded using a Stuart melting point apparatus SMP 30 and were uncorrected. The infrared (IR) spectra of compounds were recorded in the range of 4000 – 400 cm^{-1} on a Perkin Elmer Fourier-Transform Infrared Spectrophotometer 65 as thin films. ^{1}H-NMR and ^{13}C-NMR spectra were recorded on a 400 MHz Agilent NMR spectrometer at the Central Analytical Facilities (CAF), at Stellenbosch University, with deuterated

solvents, chloroform-d ($CDCl_3$), methanol-d_4 (CD_3OD) or dimethyl sulfoxide-d_6 ($(CD_3)_2SO$). In accordance with the format of most international journals, the ^{13}C NMR chemical shift values for each compound were listed without being assigned to a specific carbon atom. High-resolution mass spectrometry (HRMS) and elemental analysis data are needed to confirm the purity of the advanced intermediates and hybrids. However, due to limited funds and lack of access to the above facilities, these analyses were not performed.

3.3 Procedures

3.3.1 Virtual screening

3.3.1.1 *In silico* physicochemical and pharmacokinetic screening

Profiling the pharmacokinetic and toxicological properties of compounds during the early discovery stages, using validated computational methods, allows for the prioritization of compounds for synthesis. For this study *in silico/*Tox profiling of the hybrid constructs and advanced intermediates was done using the SwissADME [75] from the Swiss Institute of Bioinformatics and pkCSM [76] from the Biosig Lab University of Melbourne. Computational work commenced with the conversion of structures of the advanced intermediates and hybrids to their canonical simplified molecular input line entry system (SMILES) format, which was then submitted to the SwissADME and pkCSM webserver tools. As mentioned in section 2.3.1, the SwissADME Web tool allows for the computation of important physicochemical, pharmacokinetic, drug-like, and associated parameters [69], whereas the pkCSM webserver tool allows for the pharmacokinetic and toxicity profiling of compounds [49].

3.3.1.2 Docking studies

Docking studies were carried out using AutoDockTools-1.5.7 and PyRx Virtual Screening tool, Discovery Studio Visualizer v21.1.0.20298, as visualizers. 3D structures of synthesized hybrids were prepared using ChemBioDraw Ultra version 14.0.0.117 and their geometry optimized in Avogadro version 1.2.0 by adding polar hydrogens and Gasteiger charges.

One of the enzyme targets selected for this study is the *E. coli* DNA gyrase B, which is absent in the human host and therefore allow the sourcing of selective potential antimicrobial drugs using the structure-based drug design approach [77]. The *E. coli* DNA gyrase B (PDB code: 1KZN) was retrieved from the RCSB Protein Data Bank (PDB) [78]. Another protein selected for this study is the outer membrane protein A (OmpA) of *E. coli*, which contributes towards the virulence of *E. coli* and promotes the development of resistance by *E. coli* to different antibiotics [79, 80]. The 3D structures of OmpA (PDB code: 1BXW) were retrieved from the RCSB Protein Data Bank (PDB) [81]. The co-crystalized ligand for OmpA is (hydroxyethyloxy)tri(ethyloxy)octane(hydroxyethyloxy)tri(ethyloxy)octane [82] and for DNA gyrase, clorobiocin [83]. These co-crystalized ligands reveal the active site of the enzyme targets and can be used in site-specific binding to draw the grid box. The removal and redocking of the co-crystalized ligand will aid in validating the docking results. Further validation of molecular docking results requires molecular simulation dynamics, which was not done for this study.

The protein preparation was carried out using UCSF ChimeraX version 1.6.1 [56] in a two-step process, which involved preparation and removal of water molecules. The low-energy conformers were generated using AutoDock Tools. The receptor grid

generation panel in Glide module was used to define receptor, and the size of the grid box was fixed to maximum. The generated low-energy conformers of all ligands were blindly docked into the receptor grid. The binding free energy, hydrogen bonding and π–π interactions with the surrounding amino acids were studied to elucidate the binding affinities and appropriate alignment of all the ligand into the best binding pocket of OmpA and DNA gyrase B using Discovery Studio Visualizer and UCSF ChemeraX.

3.3.2 Design and synthesis

3.3.2.1 Rationale for the design of the piperazine linked, 8-hydroxyquinoline-isatin hybrids

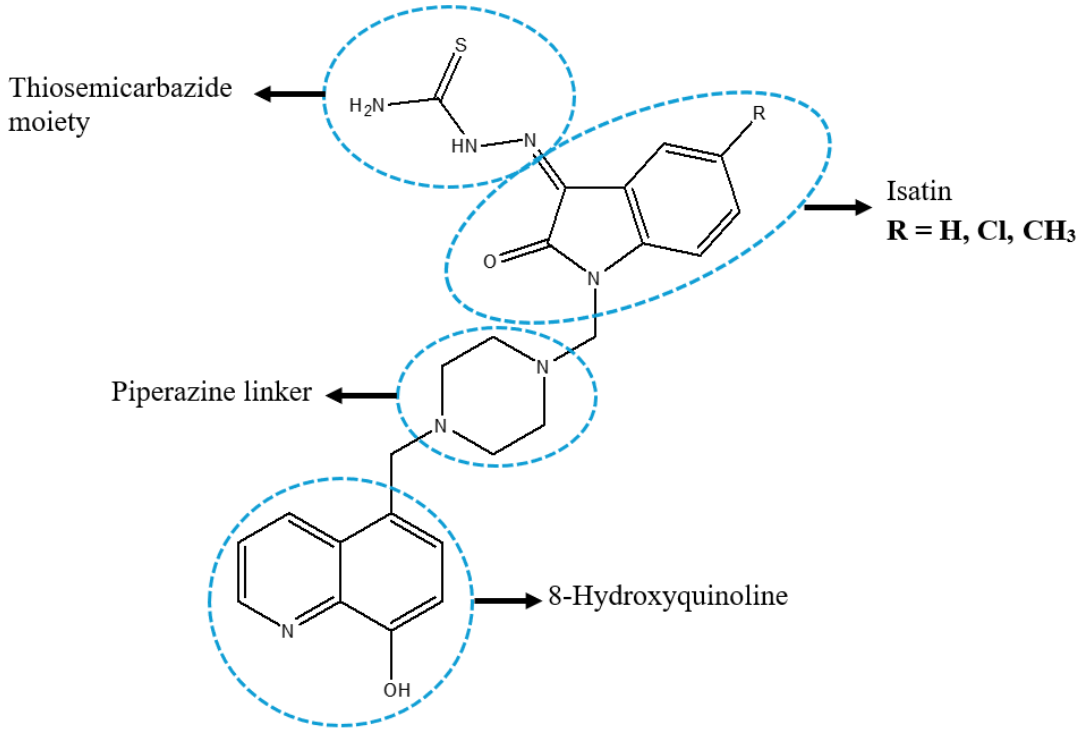

Figure 5 Rationale for the design of target hybrids

The general chemical structure of the hybrids envisaged for this study is shown in **Figure 5**. As mentioned in section 2.2.1, design of the proposed structure was guided

by previously reported SAR studies on antimicrobial derivatives based on the isatin and 8-hydroxyquinoline scaffolds. The key SARs which guided this study are summarized below:

(i) Reference was made to the privileged status of the 8-hydroxyquinoline scaffold (section 2.2.2), which renders it able to bind to various and diverse biological targets with high affinity [35]. The 8-HQ scaffold is hydrophobic, planar and allows for interactions with biological targets through hydrophobic (π-π stacking) interactions [36]. According to reports, the hydroxyl group's close proximity to the heterocyclic nitrogen affords 8-hydroxyquinolines the ability to act as a monoprotic bidentate chelating agents [37]. This chelating ability of 8-HQ derivatives reportedly enhances their antimicrobial efficacy. It was for this reason that the hydroxyl group was retained and not alkylated or acylated [6].

(ii) Also known for its privileged status is the natural product scaffold, isatin (section 2.2.1) onto which other bioactiphores, that is, functional groups or moieties that enhance biological activity, can be added. The promising antimicrobial activity displayed by Schiff base and Mannich bases derivatives of isatin was also discussed in section 2.2.1. It was therefore deemed necessary to append the TSC unit at the C-3 ketonic carbonyl group through Schiff base formation.

(iii) The presence of the piperazine moiety in biologically active compounds has been well-documented [84, 36]. As a linker, it provides flexible molecular conformations and interacts well with biological targets. This moiety can improve the bioavailability of compounds by means of enhanced solubility offered by the nitrogen sites [36]. In addition to improved bioavailability, modification of pharmacokinetics through pK_a and the introduction of hydrogen bond acceptors are among the drug-like

features imparted on compounds which incorporate the piperazine scaffold [85]. The piperazine scaffold is considered privileged due to its effectiveness, selectivity and is widely present in biologically active compounds across therapeutic fields [86]. The piperazine moiety was therefore selected as a linker for the envisaged hybrids.

(iv) According to Chiyanzu et al. (2005), the TSC moiety offers bioactive sites (the imine and thiol carbonyl) for the alkylation of the enzymes [87]. Additionally, TSCs can form coordination bonds with metal ions, which enables the formation of metal complexes with antibacterial properties [86]. Worthy of note is the poor water solubility associated with TSC derivatives [88] which presents a challenge for drug synthesis and development. This study aims to compare the activity of hybrid constructs that contain the TSC group to those without it.

3.3.2.2 Retrosynthesis of thiosemicarbazone, piperazine-linked 8 hydroxyquinoline-isatin hybrids

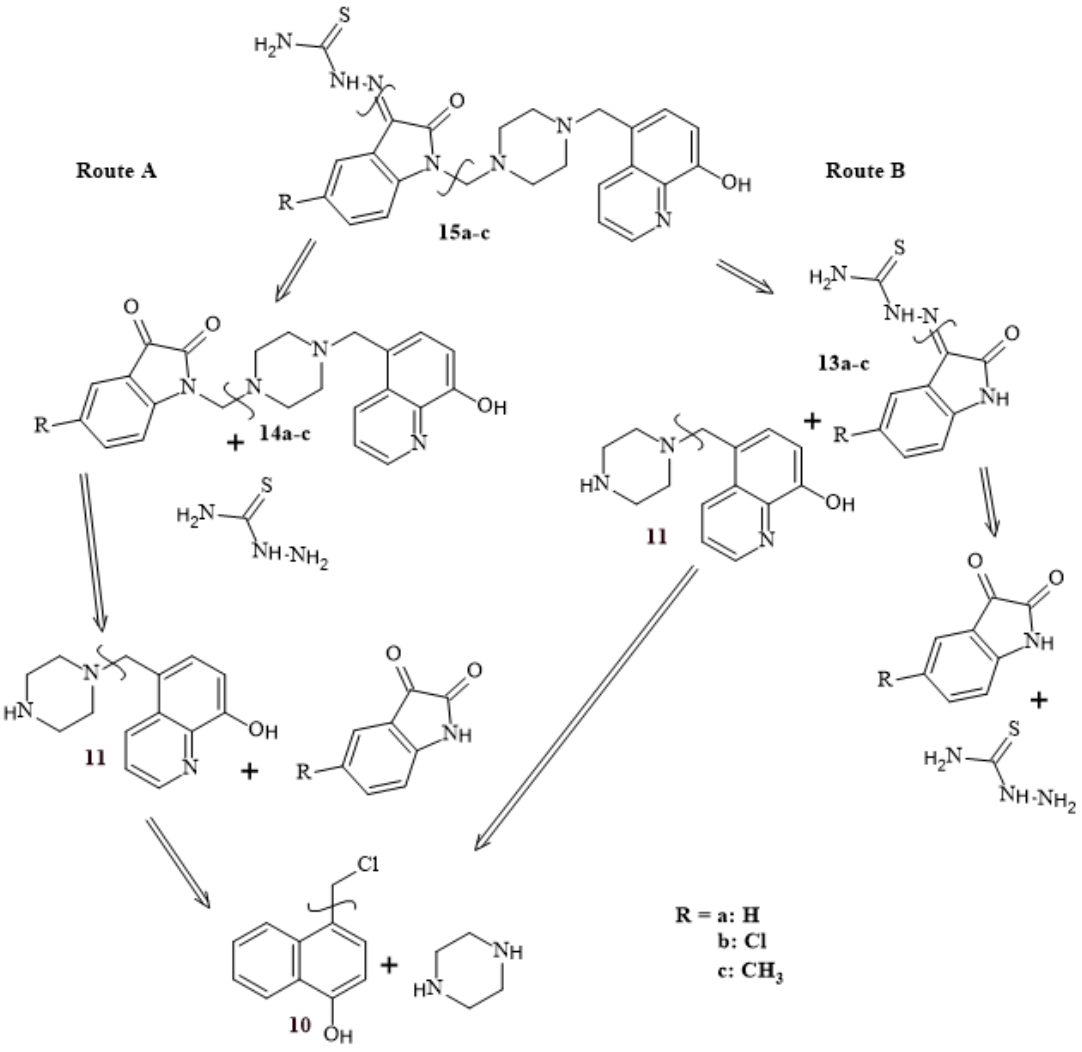

Scheme 1: Retrosynthetic pathways for the 8-hydroxyquinoline- isatin thiosemicarbazone hybrids

Scheme 1 outlines the retrosynthesis of the target molecule through two pathways. According to route A, synthesis of the piperazine-linked, thiosemicarbazone 8-hydroxyquinoline-isatin hybrid **15a-c**, is envisioned from the condensation reaction of TSC with the piperazine-linked hydroxyquinoline-isatin hybrid **14a-c**. The latter can be obtained from the Mannich reaction of commercially available isatin with 5-

(piperazin-1-yl)quinoline-8-ol **11**. Compound **11** can be derived from the reaction of piperazine with 5-chloromethyl-8-hydroxyquinoline hydrochloride **10**, which in turn can be prepared by the chloromethylation of commercially available 8HQ. Route B grants access to the envisaged hybrids **15a-c** through the Mannich reaction of 5-(piperazin-1-yl)quinoline-8-ol **11** with isatin β-thiosemicarbazone derivatives **13(a-c)**. The latter can be obtained using the Schiff base reaction of commercial substituted and unsubstituted isatin with TSC.

In principle, both pathways can yield the envisaged hybrids but for this study, and for reasons described in the discussion section **4.3**, pathway A was used to afford the piperazine-linked hydroxyquinoline-isatin hybrid **14a-c** and pathway B was followed to attempt the synthesis of piperazine-linked, thiosemicarbazide 8-hydroxyquinoline-isatin hybrid **15a-c**.

3.3.2.3 Synthesis of piperazine-linked 8-hydroxyquinoline-isatin 14a-c

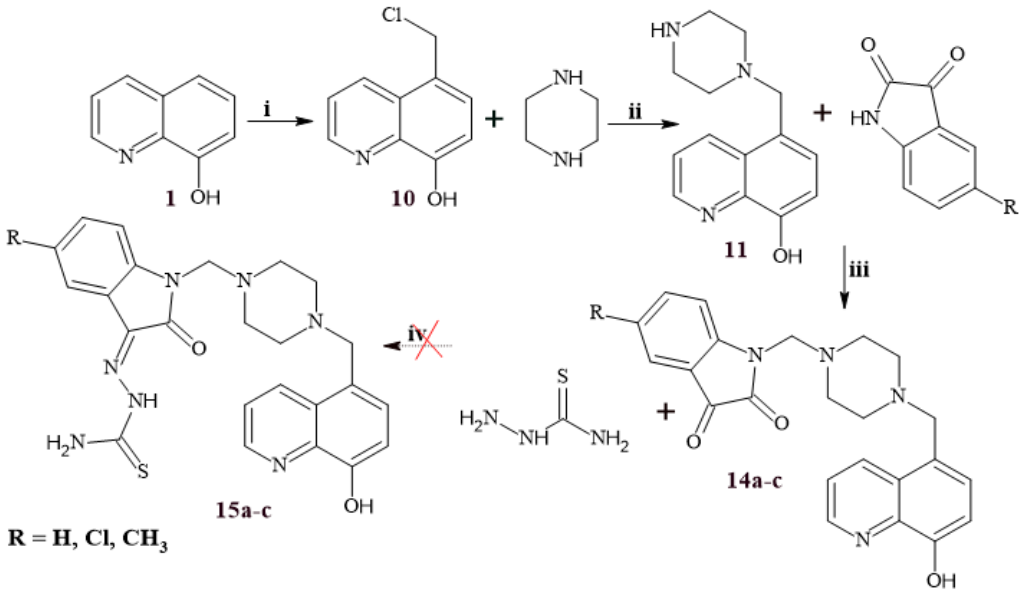

Scheme 2 Synthesis according to route A. *Reagents and conditions*: (i) formalin (37%), concentrated hydrochloric acid (36%), 25ºC, 24 h, (ii) chloroform, 0ºC, then

25ºC for 24 h, (iii) EtOH, formaldehyde, reflux for 1 h then 25ºC for 24 h (iv) EtOH, reflux, 2h

Synthesis of the first intermediate, 5-chloromethyl-8-hydroxyquinoline hydrochloride **10 (Scheme 2)** involved a chloromethylation reaction. Commercially available 8-HQ was reacted with formalin and concentrated HCl using the protocol reported by Faydy, et. al (2015) [48]. *N*-alkylation of piperazine with intermediate **10** to yield 5-(piperazin-1-yl)quinoline-8-ol **11**, **(Scheme 2)** was done based on a method reported by Zhou A, et. al (2015). Anhydrous piperazine (9 g) was dissolved in chloroform (30 mL), and 5-chloromethyl-8-hydroxyquinoline hydrochloride in chloroform (15 mL) was added dropwise at 0°C. The resulting reaction mixture was stirred for 24 hours at room temperature [89]. Because of the poor solubility of 5-chloromethyl-8-hydroxyquinoline hydrochloride **10** in chloroform, the reaction mixture was spiked with a few drops of dimethyl sulfoxide (DMSO). Upon completion, the product mixture was worked up using the procedure reported by Warshawsky et al. The mixture was neutralized by adding 25 mL of saturated $NaHCO_3$ and 25 mL water and stirred for 45 minutes. Chloroform (150 mL) was added, and the mixture was stirred for a further 30 minutes. The two phases that formed were separated and the organic layer was dried over anhydrous Na_2SO_4. [90]. The detailed synthesis procedure for each intermediate is outlined in the experimental section **3.4**

For the final step the *N*-Mannich reaction was used. Intermediate **11** was reacted with commercially available 5-substituted or unsubstituted isatin and formaldehyde using a method reported by Afsah EM et. al (2015) to obtain hybrids **14a-c**.

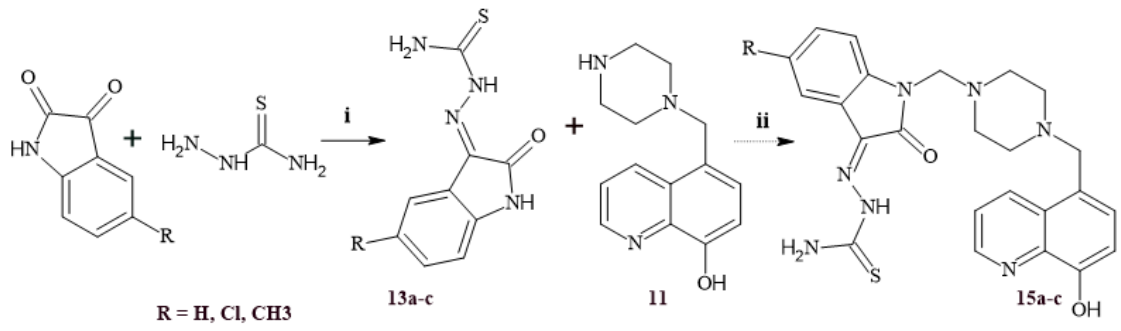

Scheme 3. Synthesis of route B. *Reagents and conditions*: (i) EtOH, reflux, 2h at 100 °C (ii) glacial acetic acid, EtOH, reflux, 2h at 100 °C

3.3.2.4 Synthesis of thiosemicarbazone, piperazine-linked 8-hydroxyquinoline-isatin hybrids 15a-c

As shown in **scheme 2**, equimolar amounts of the piperazine linked 8-hydroxyquinoline-isatin **14a-c** and TSC were refluxed in ethanol. Upon completion, the product mixture was kept at room temperature for 45 min. Filtration of the reaction mixture followed by washing with cold ethanol and recrystallisation from EtOH [91]. The reaction was not successful as revealed by TLC, and an alternative route was followed which involved first reacting the 5-substituted or non-substituted isatin with TSC via the Schiff base condensation reaction to produce intermediates **13a-c (Scheme 3)** The intermediates **13a-c** was then reacted with intermediate **11** via the *N*-Mannich base reaction to attempt the synthesis of hybrids **15a-c (Scheme 3)** [92].

3.3.3 Antimicrobial activity testing

3.3.3.1 Test microorganisms and growth conditions

The microorganisms selected for this study included *Candida albicans* ATCC13933, *Escherichia coli* ATCC700928, *Staphylococcus aureus* ATC12600, *and Klebsiella pneumoniae* ATCC10556. They were rehydrated in nutrient broth for 48 hours. Stock cultures were prepared and kept at -70ºC until needed. The strains were grown in nutrient broth at 37ºC. To standardize the inoculum, the culture was grown overnight on an agar plate. One or two colonies were transferred into a test tube containing 6 mL broth and incubated at 37ºC.

3.3.3.2 Screening for antimicrobial activity and MIC determination of synthesized compounds

Screening of antimicrobial activity was done using the agar well diffusion method as described by Zeidan; Khleifat and Matar (2013) with minor modifications [93]. Overnight, activated microbial strains were inoculated on nutrient agar plates by streaking the swab over the entire agar surface. The plates were allowed to dry and left at room temperature for 1hr. Using a cork borer, 6 mm diameter wells were cut in the agar. Into the wells, 50 µL of 25 mg/mL concentrated sample was introduced. Same was done for negative control (25% v/v DMSO) and positive control, ampicillin. The plates remained at room temperature for 30 min, then incubated at 37°C for 24 hours, after which zones of inhibition (ZOI) were measured. The assay was performed in independent duplicates and the averages of the two experiments were recorded. Only the strains which showed ZOI were selected for MIC. The concentrations for MIC were 10 mg/ml, 5 mg/ml, 2.5 mg/ml and 1.25 mg/ml.

4. RESULTS AND DISCUSSION

4.1.1 *In silico* physicochemical and pharmacokinetic profiling

The benefits and limitations of computer-aided drug design (CADD) methods were discussed in section 2.3. Results obtained using *in silico* ADMET models serve as a guiding tool to de-risk and accelerate the drug discovery process, but require experimental validation with in vitro and in vivo ADMET, biological and toxicity studies [94]. For this study, eleven compounds comprising intermediate **10,** advanced intermediates **11, 13** and hybrids **14-15** were analyzed using the SwissADME and pkCSM web tools. The physicochemical descriptors: molecular weight (MW), hydrogen bond acceptors (HBA), hydrogen bond donors (HBD), number of rotatable bonds (nRotb), molar refractivity (MR) and polar surface (PSA), of the compounds are shown in **Table 1**. For an orally active compound to be drug-like, guiding principles known as Lipinski's Ro5 states that a molecule should have a molecular weight (MW) less than 500 Da, no more than 5 hydrogen bond donors, less than 10 hydrogen bond acceptors, and an n-octanol–water partition coefficient or log P of less than 5. Reportedly, compounds with more than two Ro5 violations are unlikely to be orally active drugs [95]. **Table 1** shows that all the compounds comply with Lipinski's rule of five, except for compound **15b** that has a MW of 510.02 Da. This observation evidences a limitation of hybrid compounds, that is, their high molecular weight that hinders their permeability [12].

Table 1. *In silico* predicted physicochemical parameters calculated using SwissADME and pkCSM

Compound	Molecular Weight/ g.mol^{-1}	Log P	#Rotatable Bonds/ pkCSM	#Rotatable bond /SwissADME	#HBAcceptors/ pkCSM	#HBAcceptors/ SwissADME	#HBDonors	molecular refractivity (MR)/ m^3.mol^{-1}	Topological Polar surface area (TPSA)/ Å^2	Fraction Csp^3	iLOGP	XIOGP3	W LOGP	MLOGP	Silicos-IT Log P	Consensus Log P	Lipinski #violations	PAINS #alerts
10.	193.63	2.679	1	1	2	2	1	53.53	**33.12**	**0.1**	1.98	2.28	2.53	1.78	2.91	2.3	0	0
11.	243.31	1.346	2	2	4	4	2	79.37	**48.39**	0.36	2.32	1.07	0.43	0.87	1.94	1.33	0	0
13a	220.26	0.176	1	2	3	2	3	63.53	111.6	**0**	1.44	1.2	-0.4	-0.06	1.5	0.74	0	**1**
13.b	254.70	0.829	1	2	3	2	3	68.54	111.6	**0**	1.6	1.71	0.26	0.51	2.15	1.25	0	**1**
13.c	234.28	0.484	1	2	3	2	3	68.49	111.6	**0.1**	1.44	1.45	-0.1	0.24	1.97	1	0	**1**
14.a	402.45	2.245	4	4	6	6	1	124.41	**76.98**	0.26	2.32	2.25	0.95	1.22	2.12	1.79	0	0
14.b	436.90	2.898	4	4	6	6	1	129.42	**76.98**	0.26	2.52	2.88	1.6	1.7	2.84	2.31	0	0
14.c	416.48	2.553	4	4	6	6	1	129.38	**76.98**	0.29	3.09	2.62	1.26	1.43	2.73	2.23	0	0
15a	475.58	1.600	5	6	7	6	3	**145.78**	142.41	0.25	3.36	2.62	0.31	1.01	2.27	1.91	0	**1**
15.b	**510.02**	2.253	5	6	7	6	3	**150.79**	142.41	0.25	3.75	3.25	0.96	1.49	2.92	2.47	1	**1**
15.c	489.61	1.908	5	6	7	6	3	**150.75**	142.41	0.28	3.76	2.98	0.61	1.22	2.8	2.28	0	**1**

Cut-off values for MR = 40-130 mol^{-1}, Log P ≤ 6, nRotB ≤ 9, HBD < 5, HBA < 10, fraction Csp^3 = at least 0.25 and TPSA = 20 Å^2 and 130 Å^2. [62, 95]

Lipophilicity, expressed as the logarithm of the *n*-octanol/water partition coefficient (log P), describes a compound's affinity for lipids, and may influence its permeability, potency, selectivity, ADME properties, and toxicity [96]. SwissADME uses different computational methods to estimate log P (section **2.3.1**). According to the implicit log P(iLOGP), all the compounds exhibit lipophilicity values within the acceptable range of 1 - 4, which predicts high solubility and potential high oral absorption **(Table 1**). Another parameter for drug likeness is the molecular refractivity (MR) which gives information about the electronic polarizability of individual ions in solution. MR results can be used to explain molecular interactions in solution and the value should ideally range between 40 and 130 m^3mol^{-1} for good absorption and oral bioavailability [97]. As shown in Table 1, the thiosemicarbazone hybrids **15a-c** do not display acceptable MR values (142.41 $m^3.mol^{-1}$), which suggests that they are more polarizable than typical drug-like compounds and will most likely display poor solubility and permeability.

SwissADME calculates the polar surface area (PSA) using the topological polar surface area (TPSA) technique. [62] For optimal drug absorption and distribution, the TPSA of a compound should be between 20 $Å^2$ and 130 $Å^2$ [68]. A value >140 $Å^2$ indicates poor intestinal adsorption and a value < 60 $Å^2$ predicts blood brain barrier (BBB) permeability [98]. For hybrid compounds **14a-c** TPSA values of 76.98 $Å^2$ were calculated (**Table 1**), which indicate good cell permeability whereas hybrids **15a-c** with TPSA of 142.41 $Å^2$ might display poor intestinal absorption. According to the TPSA, intermediates **10**, **11** display potential of causing BBB permeability, that is, they can enter the Central Nervous System, with the potential of causing adverse reactions [99]. Fraction Csp^3 indicates the number of sp^3 hybridized carbons/total

carbon count. A fraction Csp^3 value of at least 0.25 is favoured [62], and from the results obtained, the hybrids **14** and **15 (Table 1)** with values ranging between 0.25-0.29, meet the minimum requirement for carbon saturation, while intermediate **11** shows an increased level of saturation (fraction Csp^3 of 0.35). It is worth adding that 3D descriptor, fraction Csp^3 correlates with the solubility of a compound, the higher the Csp^3 value the more potential interaction with the solvent resulting in better solubility [62]. SwissADME uses two topological methods for the prediction of water solubility. The water solubility of the compounds affects their absorption and enhances their elimination through the urinary track system; it is qualitatively assessed using log S values as given in table 2 [62].

Pan Assay Interference compounds (PAINS) identify chemical substructures that can potentially interfere with biological assays, yielding false positive results or nonspecific effects [100]. As shown in table 1, the TSC unit present in intermediates **13a-c** and hybrids **15a-c** is flagged as a promiscuous substructure or PAINS alert. This is in line with reports that the functional groups of thiosemicarbazones (imines and thiocarbonyl) can react nonspecifically with assay components. They exhibit redox cycling behavior which interferes with assays that rely on redox processes, and can bind to multiple targets, leading to nonspecific effects [100]. Although flagged as promiscuous, thiosemicarbazones display a spectrum of biological activities [38]. Compounds **13a-c** and **15a-c** therefore merit further investigation.

Table 2. *In silico* Pharmacokinetic and toxicity prediction using SwissADME and pkCSM

Compound	**10**	**11**	**13a**	**13b**	**13c**	**14a**	**14b**	**14c**	**15a**	**15b**	**15c**
Absorption											
Water Solubility (log *S*, mol/L)	-2.615	-1.486	-3.104	-3.587	-3.22	-3.492	-3.709	-3.587	-2.867	-3.384	-2.914
Caco-2 permeability (log P_{app}, 10^{-6}cm/s)	1.355	1.226	0.676	0.687	0.689	1.191	1.208	1.218	0.075	1.027	0.727
Intestinal absorption (human) / (% Absorbed)	93.322	92.825	82.424	84.546	80.772	95.758	94.556	96.015	72.831	71.624	73.243
Bioavailability Score/ SwissADME	0.55	0.55	0.55	0.55	0.55	0.55	0.55	0.55	0.55	0.55	0.55
Distribution											
VDss (human) (log L/kg)	0.142	1.645	-0.528	-0.561	-0.496	1.57	1.586	1.642	1.294	1.265	1.302
BBB permeability (log BB)/ pkCSM	0.386	-0.158	-0.717	-0.9	-0.746	-0.928	-1.105	-0.952	-0.942	-1.279	-0.975
BBB permeability/SwissADME	**Yes**	No	No	No	No	No	No	No	No	No	No
Metabolism											
CYP2D6 inhibitor	No	No	No	No	No	**Yes**	**Yes**	**Yes**	**Yes**	**Yes**	**Yes**
CYP3A4 inhibitor	No	No	No	No	No	**Yes**	**Yes**	**Yes**	No	**Yes**	No
Excretion											
Total Clearance (log ml/min/kg)	0.225	0.907	-0.179	-0.309	0.291	1.004	0.969	0.985	0.599	-0.629	0.586
Toxicity											
AMES toxicity	No	No	**Yes**	No	No	No	No	No	No	No	No
Hepatotoxicity	No	No	No	No	No	**Yes**	**Yes**	**Yes**	**Yes**	**Yes**	**Yes**

insoluble < − 10 < poorly < − 6 < moderately < − 4 < soluble < − 2 < very < 0 < highly [62]

The ADMET descriptors of the compounds are shown in **Table 2.** Solubility of the compounds ranges between -1.486 mol/L and -3.492 mol/L meaning they are all soluble with hybrid **14b** being the least soluble and intermediate **11** being the most soluble **(Table 2)**. Experimentally we found that compounds **11** and hybrids **15a-c** showed poor solubility (section 3.3.2.1), which evidences a discrepancy between the *in silico* data and what was found experimentally. The poor water solubility of hybrids **15a-c** can impact their effectiveness as potential lead compounds.

Caco-2 is the colorectal adenocarcinoma cells used as a model of human intestinal permeability. The permeability experimental data for model drugs is expressed using permeability coefficient (P_{app}) values; P_{app} value determines the rate of transport of the substance across the Caco-2 monolayer [101]. A compound is considered to have high Caco-2 permeability if its log P_{app} value is more than 0.90 x 10^{-6} cm/s [62]. Results obtained show that all sulphur containing intermediates, **13a-c** and **15a-c** have poor Caco-2 permeability with a P_{app} value of less than 0.9 x 10^{-6}cm/s **(Table 2)**. Another parameter is bioavailability which is defined as the fraction (%) of the drug that makes it into the systemic circulation [102]. As indicated in table 2, all compounds have 55% bioavailability which shows that they have good absorption.

Correlation with pkCSM and SwissADME results was noted for the blood-brain barrier (BBB) descriptor; it shows the drugs' ability to cross the brains semipermeable membrane that offers protection to the central nervous system against pathogen toxins and xenobiotics. A log BB value higher than 0.3 indicates brain barrier permeability was noted for intermediate **10 (Table 2)** and correlates with the results of the TPSA descriptor**.** Drug metabolism involves the biotransformation of drugs into compounds that can be easily excreted from the body and is catalyzed by specialized enzymes

[103]. The heme-containing hepatic cytochrome P450 (CYP) enzymes are the most important drug metabolizing enzymes in humans, and of the 57 functional CYP isoforms, CYP3A4 and CYP2D6 contribute to more than 50% of the CYP-related drug metabolism [104]. It is reported that inhibition of CYP3A4 and CYP2D6 will result in a reduction of drug metabolism which, in the case of multidrug therapies, can be the cause of pharmacokinetic-related drug-drug interactions [104]. According to the inhibitory prediction all the hybrids **14a-c** and **15a-c** are potential substrates of CYP2D6, and in the case of CYP3A4 inhibitory activity was predicted for hybrids **14a-c** and **15b (Table 2**).

Excretion is the final step and involves the elimination of the drug and/or its metabolites from the body. The total clearance of a given compound is measured in log(mL/min/kg) and is a combination of both hepatic and renal clearance. Clearance is fundamentally linked to bioavailability and plays a crucial role in determining dosing rates necessary to achieve steady-state concentrations. Higher levels of renal excretion result in decreased plasma half-lives. Factors such as increased plasma protein binding and a larger volume of distribution can reduce renal excretion. Some charged molecules may undergo active secretion, whereas neutral and lipophilic compounds might be reabsorbed back into the plasma [105]. According to the results in table 2 hybrids **14 a-c** show the highest levels of total clearance whereas intermediates **13 a, b** and hybrid **15 b** show the lowest levels of total clearance.

Toxicity predictions, for example mutagenicity (Ames toxicity) and hepatotoxicity, were done using pkCSM. According to the toxicity descriptors **13a** has the ability to cause changes to DNA of genetic mutations, these changes could potentially cause

cancer. All the hybrids, **14 a-c** and **15 a-c**, are potentially hepatotoxins, that is, they have the potential to cause liver damage.

4.1.2 Molecular Docking Studies

Molecular docking provided information on the interaction between the compounds synthesized and biological macromolecules OmpA [78] and DNA gyrase [106]. It furthermore predicted how strongly a ligand binds to a target protein and identified potential binding sites on the protein surface. OmpA is an outer membrane protein of the bacterial strain *E. coli*, it is a multi-virulent strain responsible for several life-threatening diseases and can express many virulent factors [107]. DNA gyrase is a key bacterial protein necessary for replication and transcription. It catalyzes the negative supercoiling of circular bacterial DNA. Given its critical role, the inhibition of its function will plausibly lead to bacterial mortality [106]. Blind docking as opposed to site-specific docking was chosen as it explores the whole protein surface in search of a feasible binding pose [108]. Blind docking may not be precise but is unbiased in seeking out other binding sites, including allosteric ones. Site-specific docking reportedly gives more accurate binding poses [109].

Molecular docking studies were conducted successfully on novel hybrids **14a-c** and **15a-c** as well as all intermediates **10, 11 and 13**. The results of the molecular docking of the intermediates and hybrids with OmpA and *E. coli* DNA gyrase are given in **Tables 3** and **4.** Overall the hybrids **14 a-c and 15 a-c** show good binding scores with both OmpA and DNA gyrase. It is suggested that a binding energy of less than -7 kcal/mol is often considered good, and less than -10 kcal/mol is considered very good.

Table 3. Molecular docking scores and binding interactions with OmpA.

Compound	Binding energy / kcal/mol	Binding interactions with amino acids of OmpA
10	-7.6	ALA 74, TRP 102, ASN 146, THR 144, MET 100, ASP 158
11	-8.7	TRP 102, ASP 56, ASN 146, ASP 158, MET 100
13a	-7.8	MET 100, ASP 158, THR 144, ASN 146 TRP 102, ALA 104
13b	-8	ASN 146, THR 144, ASP 158, HIS 19, TRP 102, ALA 104, TYR 72
13c	-8.1	ALA 104, TRP 102, HIS 19, ASP 158, THR 144, ASN 146
14a	**-9.8**	ALA 74, MET 100, LEU 58, GLN 142, HIS 19, ASP 116, ARG 156
14b	-9.6	ALA 150, ASN 146, HIS 19, MET 100, MET 161, ALA 74, LEU 58
14c	-9.7	ASN 146, HIS 19, MET 100, MET 161, ALA 74, LEU 58
15a	-9.5	ASN 146, MET 161, ALA 74, LEU 58, HIS 19, MET 100, GLN 142
15b	-9.7	THR 117, TRP 102, ASP 116, ASN 146, HIS 19, MET 100, MET 161, ALA 74, LEU 58
15c	**-9.8**	GLN 142, MET 100, HIS 19, LEU 58, ALA 74, MET 161, ASN 146, TYR 72, ASP 116
(hydroxyethyloxy)tri(ethyloxy) octane	-5.1	ARG 156, ASP 158, GLY 148, VAL 119, TRP 102, HIS 19, MET 100, ALA 74

The best docking scores with OmpA protein were recorded for hybrids **14a** and **15c** with binding energies of -9.8 kcal/mol each, which is much higher than the binding score of the co-crystalized ligand, (hydroyethyloxy)tri(ethyloxy)octane. Promising binding interactions were also noted for the remaining hybrids **15 a-b** and **14 b-c** with binding scores ranging between -9.5 kcal/mol and -9.7 kcal/mol **(Table 3)**.

(a)

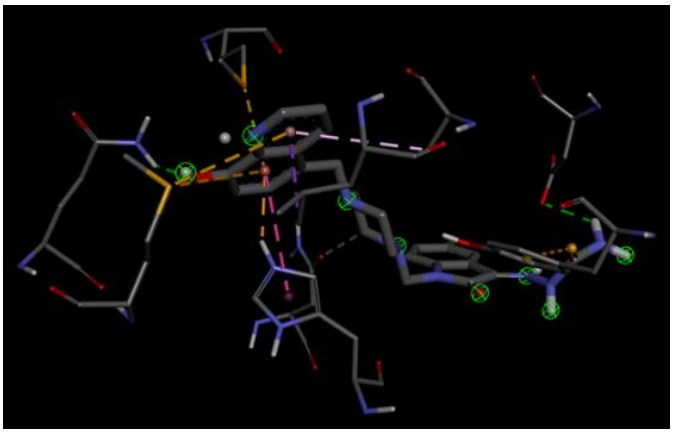

(b)

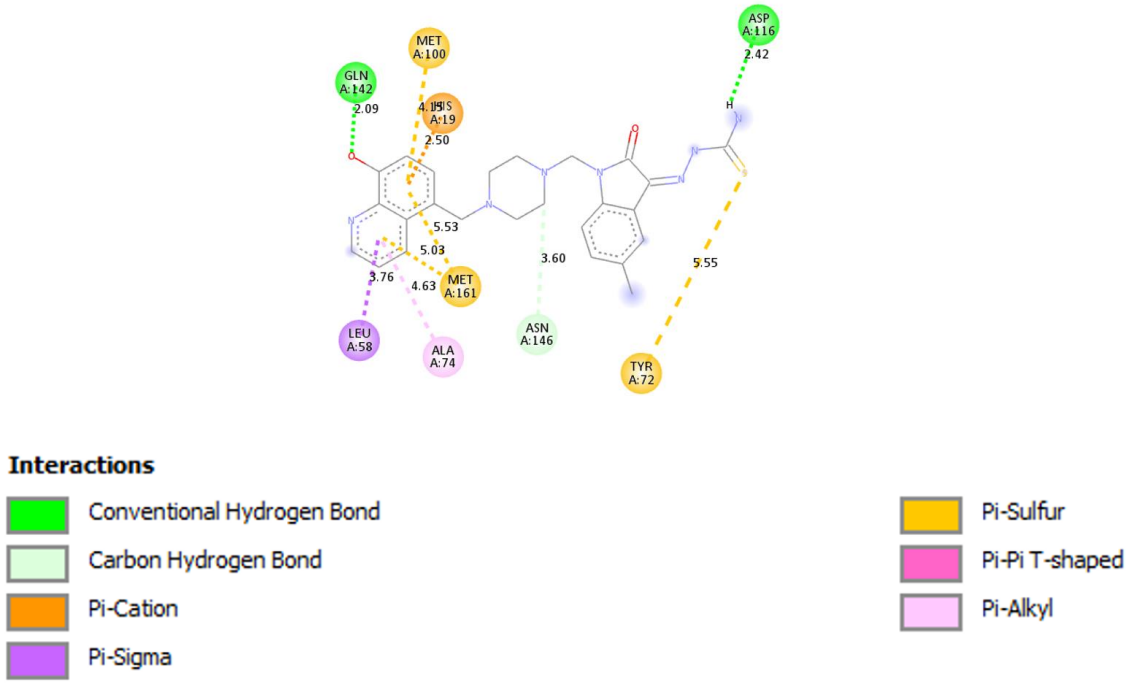

Figure 6. Representations of the molecular model of complex formed between compound **15c** and OmpA. **(a)** 3D representation of the ligand-enzyme binding interactions; **(b)** 2D schematic representation of the hydrogen bonding and hydrophobic interactions.

Figure 6 shows the interactions between hybrid **15c**, and amino acid residues of enzyme OmpA. Hybrid **15c** interactions include strong hydrogen bonds with GLN 142 via the alcohol group on hydroxyquinoline ring and with ASP 116 through the NH

group of the primary amide of thiosemicarbazone. Arene-cation interaction with the benzene ring of hydroxyquinoline and HIS 19 as well as interactions of the same benzene ring with the sulfur atoms of MET 100 and MET 161, were observed. The pi-sulfur interaction with TYR 72 is the only interaction not found in **15 a** and **15 b** which could be the reason for the higher binding score.

(a)

(b)

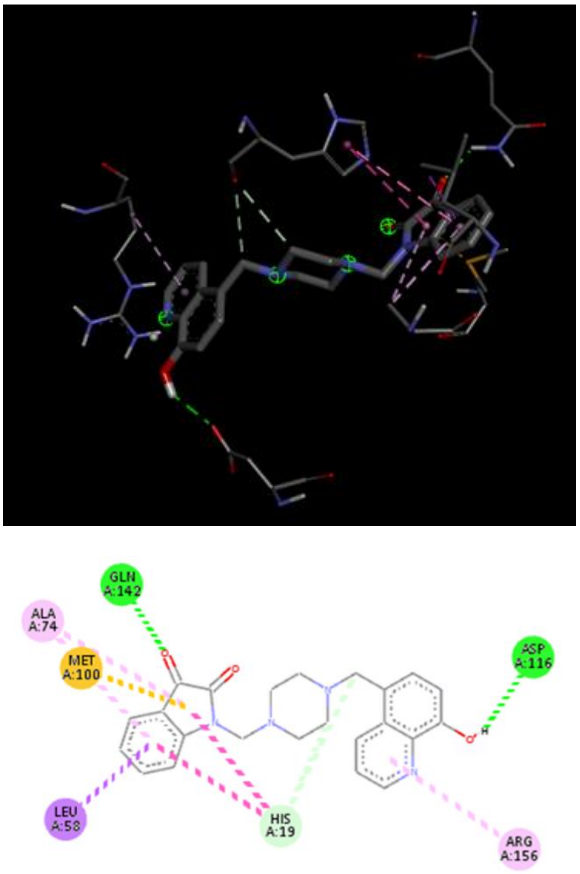

Figure 7. Representations of the molecular model of complex formed between compound **14a** and OmpA. **(a)** 3D representation of the ligand-enzyme binding interactions; **(b)** 2D schematic representation of the hydrogen bonding and hydrophobic interactions.

Compound **14a** shows the same docking score of -9.8 as that of **15 c**. Strong hydrogen bond interactions were observed with GLN 142 and the ketonic group of isatin and with ASP 116 and the alcohol group on hydroxyquinoline,as well as hydrophobic π-σ interactions with LEU 58. The strong hydrogen bond interactions with GLN142 and ASP 116 were not present in **14b** or **14c** which could be the result of the higher binding score for **14a**. Interactions with similar amino acid residues were expected and observed because of the structural similarity between hybrids **14** and **15.**

Table 4. Molecular docking scores and binding interactions with DNA gyrase

Compound	Binding energy / kcal/mol	Binding interactions with amino acids of DNA gyrase
10	-6.6	VAL 120, ILE 90, ALA 47, MET 91, ILE 78, VAL 167, THR 165, ASP 73
11	-6.7	ASP 73, ILE 78, GLU 50, PRO 79
13a	-6.7	GLU50, ASN 46, ILE 78, VAL 167, ALA 47, THR 165
13b	-7.3	THR165, VAL 71, VAL 167, ALA 47, GLU 50, ILE 78, VAL 120
13c	-7.5	THR 165, VAL 71, VAL 167, ALA 47, GLU 50, ASN 46, VAL 120, ILE 78
14a	-8.7	VAL 118, SER 121, GLY 117, ILE 90, ASN 46, THR 165, ILE 78, PRO 79, ARG 76, GLU 50
14b	-8.9	THR 165, ILE 78, GLU 50, ARG 76, PRO 79, ASN 46, ILE 90, VAL 118, HIS 95, GLY 117
14c	**-9**	GLU 50, THR 165, ILE 78, ARG 76, PRO 79, ASN 46, ILE 90, VAL 118, GLY 117
15a	-8.4	ASP 73, ASN 46, PRO 79, GLU 50, ILE 78, ILE 90, ALA 96, VAL 93, GLY 119
15b	-8.4	ASP 73, ALA 47, ILE 78, GLU 50, ASN 46, ASP 49, ASP 45
15c	-8.5	ASP 73, ILE 78, ALA 47, ASN 46, ASP 49, GLU 50
Clorobiocin	-8.9	ALA 96, ILE 90, ASN 46, THR 165, ASP 73, ALA 47, VAL 43, VAL 71

The best docking scores for DNA gyrase were recorded for hybrids **14 a-c** with values ranging between -8.7 and -9 kcal/mol. Compared to the monomer intermediates (**10-11**, **13a-c**) the hybrids **14 a-c** and **15 a-c** showed better docking scores for both OmpA and DNA gyrase.

(a)

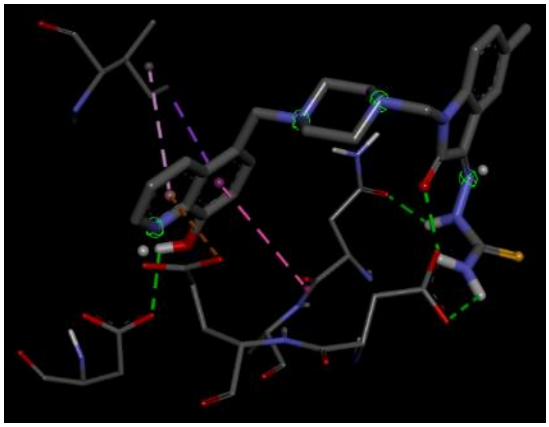

(b)

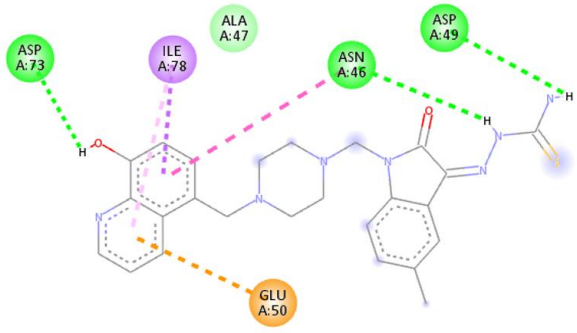

Figure 8. Representations of the molecular model of complex formed between compound **15 c** and DNA gyrase. **(a)** 3D representation of the ligand-enzyme binding interactions. **(b)** 2D schematic representation of the hydrogen bonding and hydrophobic interactions.

As shown in **Figure 8**, **15 c** interacted with amino acids ASP 73, ASN 46 through hydrogen bonding via the alcohol group on hydroxyquinoline, the hydrazinic hydrogen of the TSC moiety and the hydrogen of the primary thioamide of the same moiety, respectively. The binding scores for all three hybrids are very close with binding scores of -8.4 kcal/mol for **15 a** and **b** and -8.5 kcal/mol for hybrid **15 c.**

Figure 9 shows that compound **14c** formed a hydrogen bond with amino acid THR 165, as well as electrostatic interactions with amino acids ARG 76 and GLU 50. It also shows unfavorable interactions with amino acid VAL 118. Compounds **14 a** and **14 b** shows very similar binding scores to that of **14 c** which could be because all amino acids binding with **14 c** also binds with **14 a** and **14 b**.

(a)

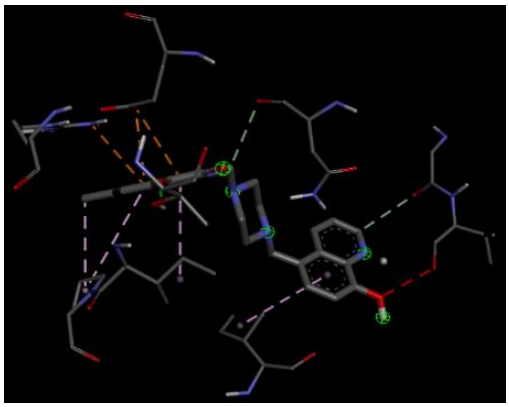

(b)

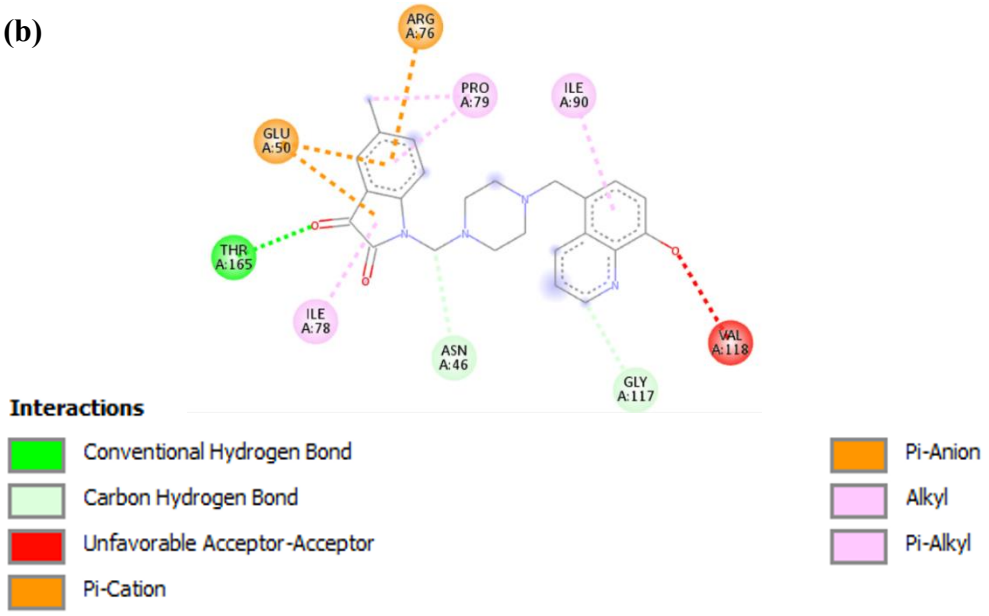

Figure 9. Representations of the molecular model of complex formed between compound **14 c** and DNA gyrase **(a)** 3D representation of the ligand-enzyme binding interactions; **(b)** 2D schematic representation of the hydrogen bonding and hydrophobic interactions.

4.2 Synthesis of piperazine-linked 8-hydroxyquinoline-isatin 14a-c

This section outlines the results from the synthesis and structural confirmation of the intermediates **10, 11, 13** and hybrids **14**.

4.2.1 Synthesis of 5-chloromethyl-8-hydroxyquinoline hydrochloride, 10

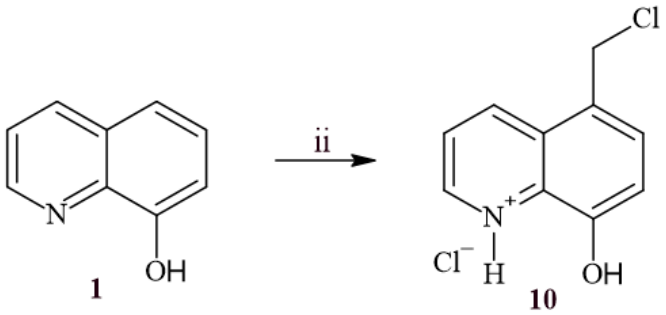

Scheme 4. Synthesis of intermediate, **10**. *Reagents and conditions:* (i) 35% formaldehyde, Conc. HCHO, Conc. HCl, 25°C

The chloromethylation of 8HQ **(scheme 4)** afforded **10** in 84% yield as a yellow amorphous powder with a melting point of 280°C which differs slightly from the literature melting point of 282 °C [39]. IR data confirmed the presence of the OH group with a broad band between 3200 and 3300 cm^{-1} **(Appendix B: Figure A1).** The ^{1}H-NMR spectrum of **10 (Figure 10)** shows five signals in the aromatic region which is one less than what was expected for the starting material 8HQ. This observation and the signal resonating at δ 4.88 ppm that integrates for two hydrogens was assigned to the methylene hydrogens and confirmed the formation of **10**. The ^{1}H-NMR also showed the presence of minor impurities.

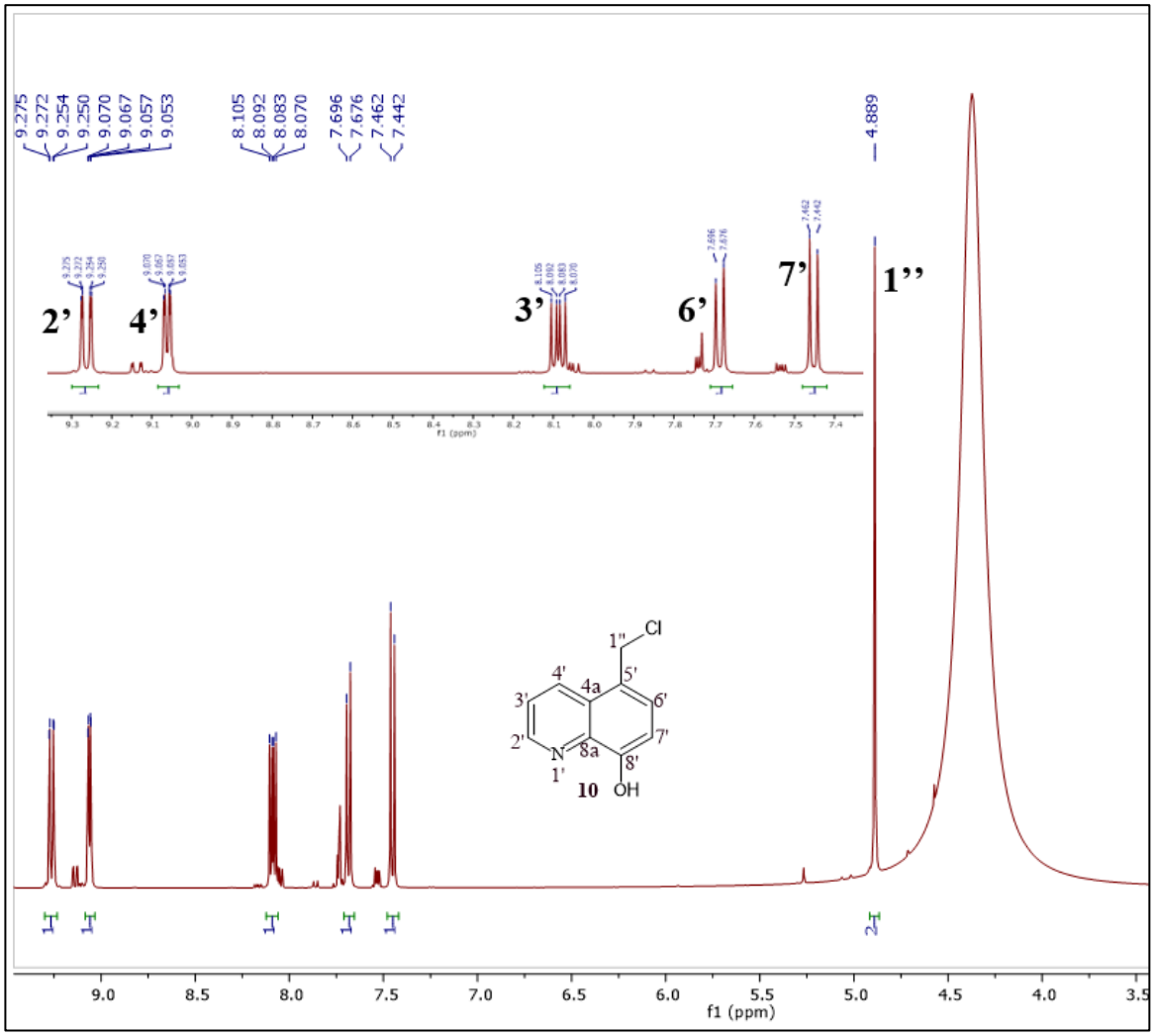

Figure 10. ^{1}H-NMR spectrum of intermediate **10** in DMSO-d_6 at 400 MHz

4.2.2 Synthesis of 5-(piperazin-1-yl) quinoline-8-ol, 11

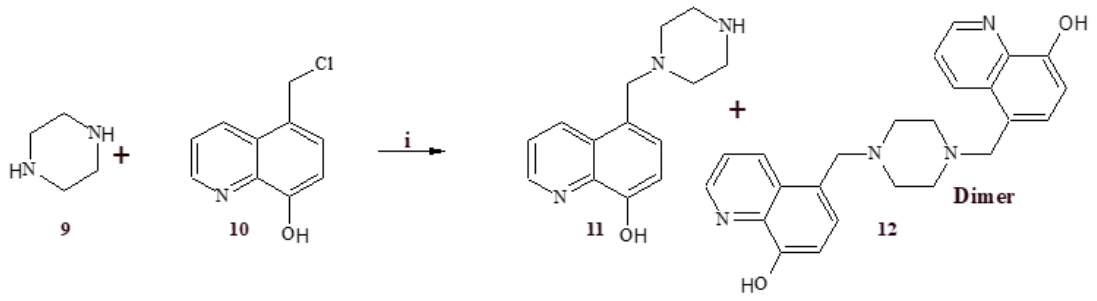

Scheme 5 Synthesis of intermediate, **11.** *Reagents and conditions*: (i) $CHCl_3$, 0 °

Synthesis of intermediate **11**, as outlined in scheme 5, followed a direct N-alkylation or nucleophilic substitution reaction. One of the reported shortcomings of this reaction was over-alkylation, which was evidenced by the formation of a byproduct, dimer **(scheme 5).** Compound **11** was obtained in low yield (48%) due to the formation of the byproduct dimer. A similar result was reported by Singh, T. et, al (1970). They attempted to optimize the reaction yield by employing four-equivalence of anhydrous piperazine which made the work-up difficult [110]. It is plausible that the yield could have been increased by using a N-Boc-protected piperazine which was unfortunately not available [111]. Nonetheless, the desired product was obtained as an off-white amorphous powder with a melting point of 229.4 °C which differed slightly from the literature melting point of 232–234 °C. The melting point for the dimer was lower at 227-228 °C [88]. IR spectrum of compound **11** showed a band at 3190 cm^{-1}, assignable to NH of the isatin and an OH band at 3400 cm^{-1} of the 8HQ ring system **(Appendix B: Figure A2).** The ^{1}H-NMR spectrum (**Figure 11**) confirmed the structure for compound **11** and not the dimer as inferred by the signals assigned to the protons of the piperazine moiety, which appeared as two multiplets at δ 2.75 ppm and δ 2.41 ppm each integrating for 4 protons. Also noted was the slight upfield shift of the methylene hydrogens (H-1'') which resonated at δ 4.88 ppm in compound **10** compared to the

chemical shift of δ 3.76 ppm for compound **11**. The observed up-field shift is due to the replacement of the more electronegative chlorine (in **10**) with a less electronegative nitrogen atom (in **11**). The ^{13}C-NMR **(Appendix B: Figure A12)** showed the twelve carbon signals associated with the expected product and not eleven - due to the symmetry in the structure - as would have been expected for the dimer.

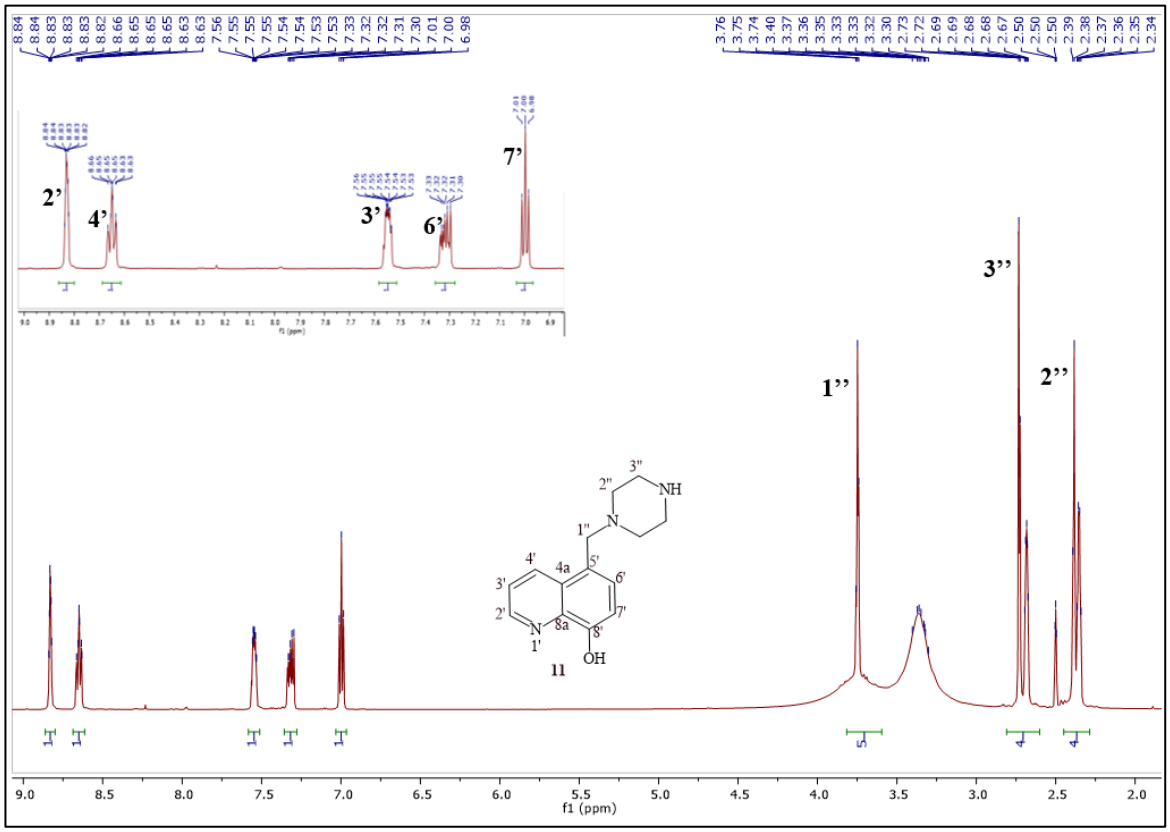

Figure 11. ^{1}H-NMR spectrum of intermediate **11** in DMSO-d_6 at 400 MHz

4.2.3 Synthesis of piperazine-linked 8-hydroxyquinoline-isatin hybrids, 14a-c

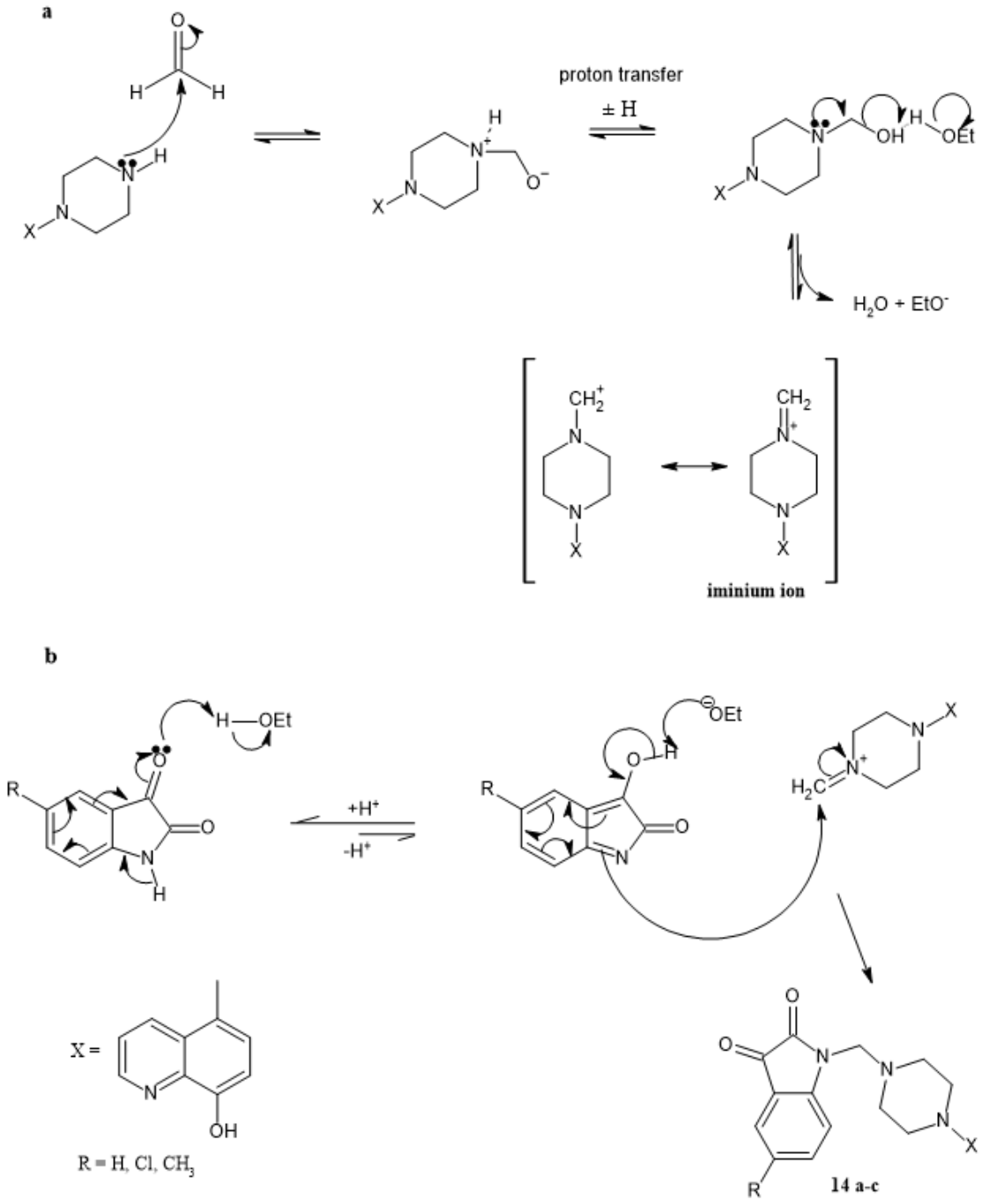

Figure 12. Mechanism of the *N*-Mannich reaction to yield hybrids **14.**

Mannich bases can combine various types of heterocyclic systems in their structure, making them interesting candidates for further chemical modifications. These

modifications can result in the creation of new derivatives with potential biological activity [112].

According to the literature, Mannich bases are highly reactive and have been demonstrated to display powerful medicinal properties [113]. The Mannich reaction, or amine methylation, is an organic reaction where an amine is added to a carbonyl group of formaldehyde to form an intermediate followed by acid-catalyzed dehydration to give the iminium ion. In the absence of an acid catalyst, ethanol was the most likely proton donor during the dehydration as shown in **(a) (Figure 12)**. The carbonyl group undergoes tautomerization to give the enol form **(b) (Figure 12)** which attacks the iminium ion yielding the Mannich base. The resulting product is an α, β-amino carbonyl compound, known as a Mannich base. This reaction is crucial and is used in the synthesis of many drugs and natural products [114]. In medicinal chemistry, Mannich bases have several practical applications and can improve the physicochemical properties of potential drug attempts.

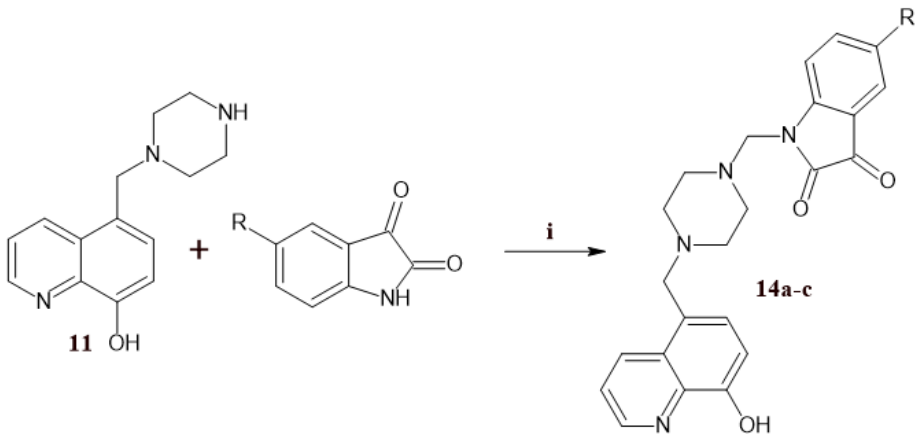

Scheme 6. Synthesis of piperazine-linked 8-hydroxyquinoline-isatin hybrids, **14a-c**
Reagents and conditions: 35% aqueous formaldehyde, anhydrous EtOH, 25ºC, 2 hrs

The N-Mannich base reaction, **scheme 6** yielded the novel hybrid **14** in moderate yield as shown in **Table 5.**

Table 5. Melting point and yield for hybrids **14 a-c**

Compound	R	Yield (%)	Mp (°C)	colour
14a	H	60	183	**Yellow orange**
14b	Cl	56	220	**orange**
14c	CH_3	58	212	**Light orange**

Hybrids **14a-c** are novel compounds. The IR spectrum for **14c (appendix B: Figure A8)** showed peaks for the carbonyl groups at 1726 cm^{-1} for the ketonic and at 1622 cm^{-1} for the amidic carbonyl groups of the isatin. Also noted was the absence of the NH band present in intermediate **11,** this confirmed the formation of hybrids **14**. Further evidence to support the formation of **14** was obtained from ^{1}H-NMR data **(Figure 13)**. The presence of the methyl group was evidenced by the singlet resonating at δ 2.3 ppm that integrated for three protons. Two sets of methylene hydrogens **(Figure 13)** resonating at δ 3.8 ppm and δ 4.4 ppm were assigned to H-1'' and H-4'', respectively.

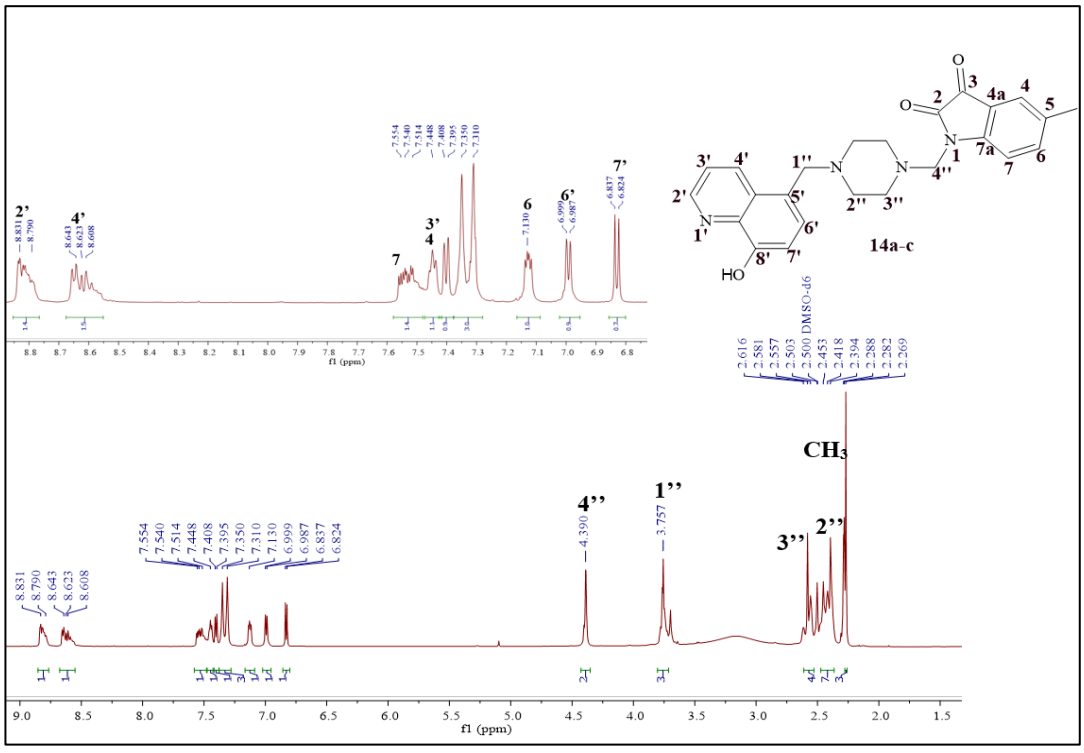

Figure 13. [1]H-NMR spectrum of hybrid **14c** in DMSO-d_6 at 400 MHz

It was evident from both the [1]H-NMR (**Figure 13**) and [13]C-NMR (**Figure 14**) spectra that compound **14c** was not pure. For example, the intense signal in the aromatic region of the [1]H-NMR spectra example δ 7.33 ppm indicated the presence of unreacted isatin starting material, while excess signals in the [13]C NMR spectra was indicative of the presence of impurities.

The [13]C-NMR spectra, **Figure 14** showed the two carbonyl carbons resonating at 184.7 ppm for ketonic carbonyl carbon **3** and 159.6 ppm for amidic carbonyl carbon **2**.

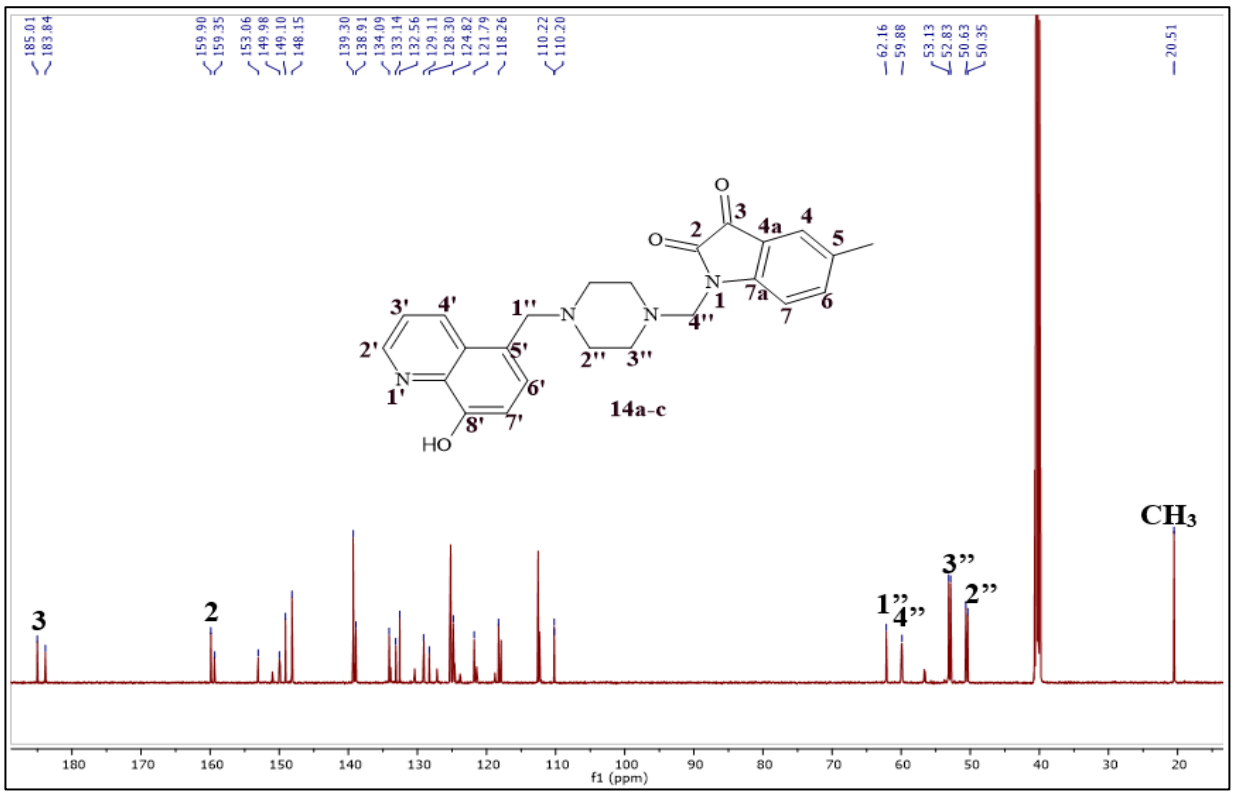

Figure 14. [13]C NMR spectrum of **14c** in DMSO-d_6 at 100MHz.

4.3 Synthesis of 8-hydroxyquinoline-isatin-thiosemicarbazone hybrids, 15a-c

An attempt was made to synthesize 8-hydroxyquinoline-isatin-thiosemicarbazones **15** by means of a Schiff base condensation reaction of TSC and piperazine-linked 8-

hydroxyquinoline-isatin hybrid, **14 (Scheme 7)**. This reaction, however, failed as only starting material was recovered after 48 hours, as evidenced by the TLC profile of the product mixture. An alternative method was followed, which commenced with the synthesis of the isatin thiosemicarbazone intermediates **13 a-c** which was in turn reacted with 5-(piperazin-1-yl)quinoline-8-ol **11**, as outlined in section 3.4.

4.3.1 Synthesis of isatin thiosemicarbazone derivatives, 13a-c

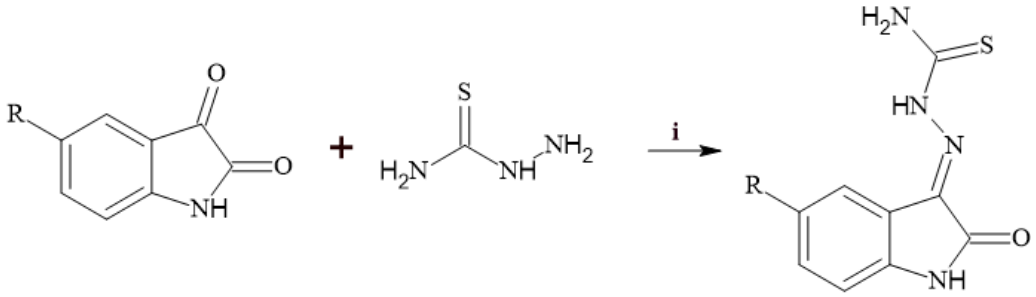

Scheme 7 Synthesis of intermediate **13a-c** *Reagents and conditions***:** (i) EtOH, Reflux at 100 °C.

The synthesis of **13a-c (Scheme 7)** formed part of an alternative synthesis protocol for hybrids **15a-c**. Isatin thiosemicarbazone derivatives **13** are known compounds and were obtained as brightly coloured solids in yields ranging from 61-74% (**Table 6)**. Correlation of the literature melting point with the experimentally determined values shown in **Table 6**, served in part as confirmation of the proposed structures.

Table 6. Melting point and yields of intermediates **13a-c**

Code	R	Yield (%)	M.p. (ºC)	Literature M.p. (ºC)
13a	H	74	225	235[115]
13b	Cl	65	196	190 [116]
13c	CH_3	61	224	232–234 [117]

IR data for **13c (appendices: Figure A5)** showed the presence of the amidic C=O and imine C=N groups appearing at absorption bands 1682 and 1610 cm^{-1}, respectively, and the ^{1}H-NMR spectra (**Figure 15**) of **13 c** agreed with literature data [119].

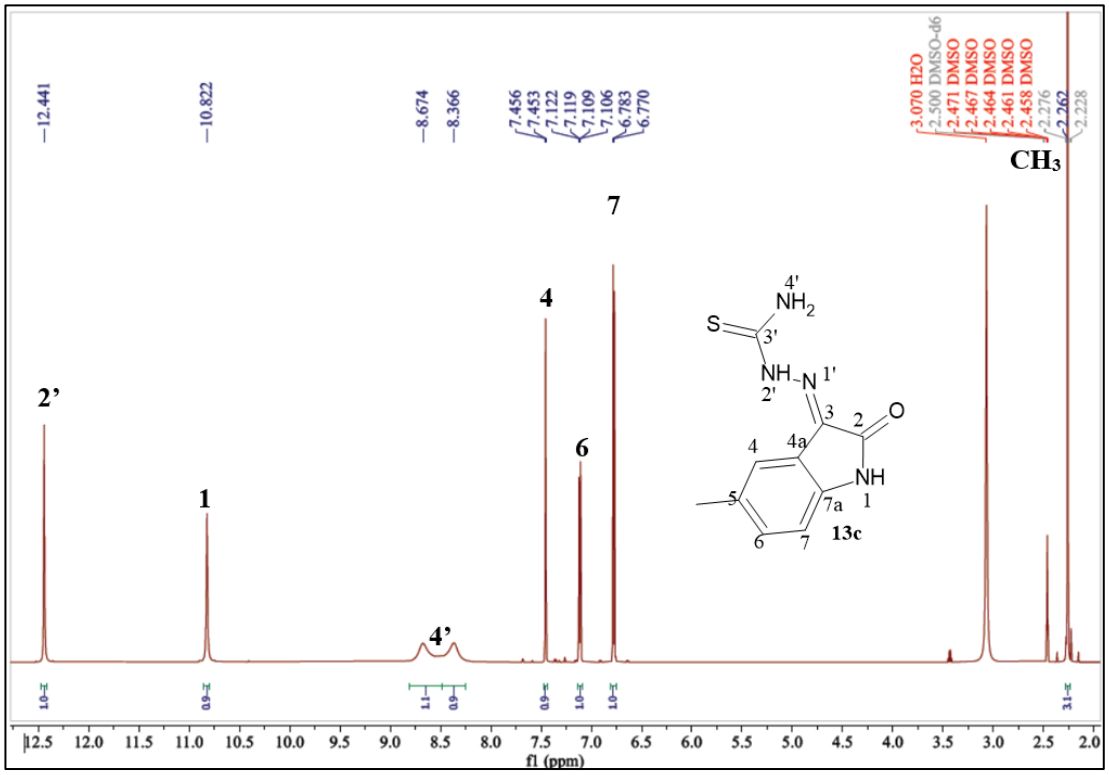

Figure 15 ^{1}H-NMR spectrum of hybrid **13c** in DMSO-d_6 at 400 MHz

4.3.2 Synthesis of piperazine linked 8-hydroxyquinoline-isatin-thiosemicarbazone hybrids, 15 a-c

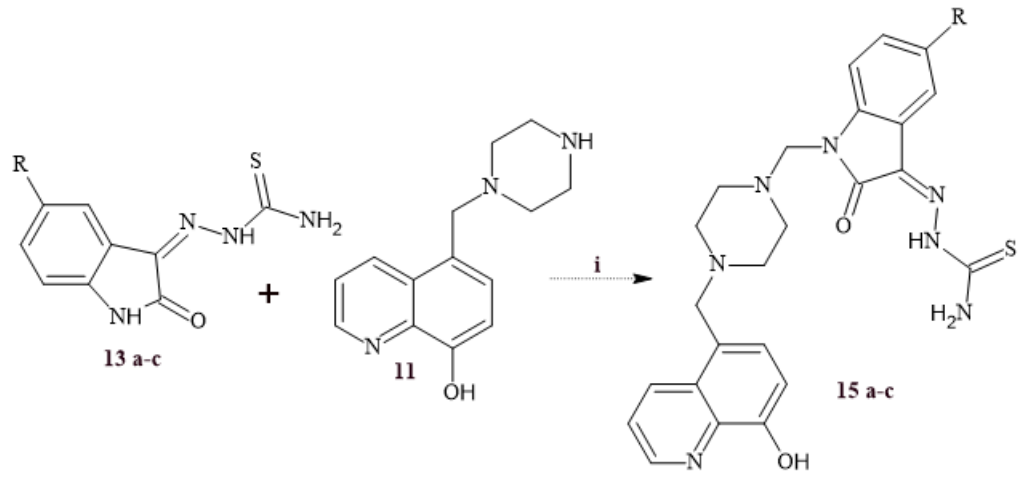

Scheme 8 Synthesis of hybrids **15a-c.** *Reagents and conditions*: (i) glacial acetic acid, EtOH, Reflux at 100 °C

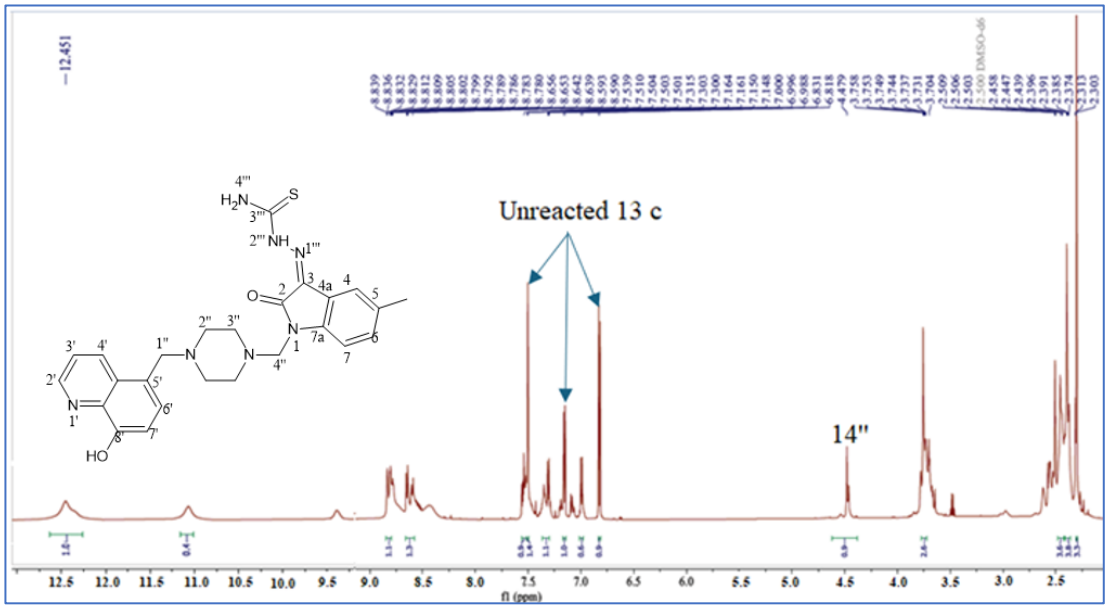

Figure 16: H^1NMR spectrum of hybrid **15c** in DMSO-d_6 at 400 MHz

Scheme 8 shows the synthesis protocol used for hybrids **15**. The TLC profiles showed that even after running for two days the reaction did not go to completion. Also,

purification of the hybrids **15a-c** was challenging due to their poor solubility in water and other organic solvents (methanol, ethanol, water acetone, diethyl ether ethyl acetate and DCM) as mentioned in section 3.3.2. The proton NMR data **(Figure 16)** clearly shows the hybrids formed, but were not pure, the intense signals in the aromatic region δ 6.5-7.5 ppm were assigned to the unreacted TSC intermediate **13c** (**Figure 16**). The signal at δ 4.48 assigned to the methylene protons, H-4'', confirms the formation of the product but in small quantities. Attempts to further purify the product resulted in significant losses. Purification of compounds 15 a-c involved sonicating the crude product in ethanol at 40 °C for 45 minutes. This was followed by filtering the mixture and washing the solid with warm ethanol. A further attempt to purify the product entailed preparative layer chromatography on silica gel plates using ethyl acetate: MeOH: H_2O (10:1:0.5) as solvent system.

Hybrids **15 a-c** are compounds that have not been synthesized before. However, because the spectral data could not be unambiguously assigned, i.e., to confirm the proposed structures, and as a result of many impurities, the hybrids **15** were not subjected to antimicrobial testing.

4.4 Antimicrobial activity

All compounds with the exception of **15 a-c**, were subjected to antimicrobial activity testing against a Gram +ve (*S. aureus*) and two *Gram -ve* (*E. coli, K. pneumonia*) bacterial strains, as well as a fungal strain *C. albicans.* It is noteworthy that three of the microbial strains, S. *aureus, E. coli* and *C. albicans* are on the WHO's list of high priority pathogens [118]. Preliminary screening was done using the agar disc diffusion method with ampicillin as positive control.

Table 7. Growth inhibition activity of intermediates **10, 11** and hybrids **13a-c** and **14 a-c**

Compound	**Zone of inhibition (mm) at 10 mg/mL**			
	E. coli	***C. albicans***	***K. pneumonia***	***S. aureus***
10	22	20	22	19.5
11	13.5	ND	11.5	11
13a	ND	ND	ND	ND
13b	ND	ND	ND	ND
13c	ND	ND	ND	ND
14a	14.5	15	13	12.5
14b	19.5	15	**15**	12.5
14c	ND	ND	ND	ND
Ampicillin	18	17	14	11
DMSO	ND	ND	ND	ND

ZOI: ≥ 25 mm (very strong); 24 – 15 mm (strong); 14 – 11 moderate; 10-8 (weak) ≤ 8 no activity [119]

Table 7 shows the antimicrobial effect of the intermediates and hybrids at a concentration of 10 mg/ml on bacterial strains, *E. coli*, *K. pneumonia, S. aureus* and fungal strain *C. albicans*. The isatin-thiosemicarbazone intermediates **13a-c** showed no activity against any of the strains and intermediate **11** showed moderate activity toward all three bacterial strains. Intermediate **10** showed strong activity against all bacterial and fungal strains. Of the hybrids only **14a, b** showed activity of which **14a** showed moderate activity towards all bacterial strains while **14b** showed strong activity against *E. coli*, *K. pneumonia,* and *C. albicans*, and moderate activity against *S. aureus*.

Table 8. Minimum inhibitory concentration (MIC) of intermediates and hybrids against four microbial strains.

	MIC (mg/mL)			
Compound	***E. coli***	***C. albicans***	***K. pneumonia***	***S. aureus***
10	1.25	2.5	1.25	2.5
11	5	ND	5	10
14a	2.5	5	2.5	2.5
14b	1.25	5	1.25	1.25
Ampicillin	1.25	1.25	1.25	1.25

ND = Not Detected

For the Minimum Inhibitory Concentration (MIC) the following concentrations were used, 10 mg/mL, 5 mg/mL. 2.5 mg/mL and 1.25 mg/mL. A MIC value of ≤ 1.25 mg/mL was observed for intermediate **10 (Table 8)** against *E. coli* and *K. pneumonia*, and by hybrid **14b** against all selected bacterial strains. Hybrid **14a** showed a MIC value of ≤ 2.5 mg/mL against all selected bacterial strains. Compared to the positive control ampicillin, **14b** showed equipotent MIC value of 1.25 mg/mL against *E. coli*, *K. pneumonia* and *S.aureus*, while ampicillin showed two fold higher activity than **14a**. Ampicillin also showed 4 fold higher activity than both **14a** and **14b** against *C. albicans*.

It is plausible that the lack of activity observed for intermediates **13** was due to poor solubility which hindered their ability to diffuse through the agar. The delineation of the SAR cannot be done because the library is too small to draw conclusions regarding the effective substituent groups on the C-5 of the isatin moiety biological activity, but it would seem that the chlorinated substituent showed superior activity compared to the unsubstituted and methylated isatin derivative for hybrids **14**.

4.5 Experimental

Synthesis of 5-chloromethyl-8-hydroxyquinoline hydrochloride 10

The 8-hydroxyquinoline (10.0 g, 68 mmol), concentrated hydrochloric acid (11 ml 36%, 11.85 N) and formaldehyde (11 ml, 397 mmol 37% (w/v)) were mixed and treated with hydrogen chloride gas that was bubbled through the solution. The mixture was stirred for 24 hours at room temperature. Upon completion, the solution was allowed to stand at room temperature for 2 hours without stirring. The yellow precipitate that formed was collected by filtration, washed three times with acetone and allowed to dry [39].

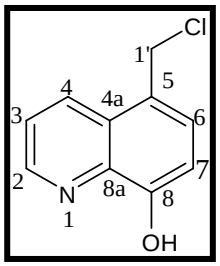

Yellow amorphous solid 84% yield; m. p. 280°C; IR (cm^{-1}) 3300-3200 (OH), 1493 (C-Cl), 1305(C=N); δ_H (400 MHz, DMSO-d_6), 9.26 (1H, dd, *J* 1.6 and 8.8, H-2'), 9.06 (1H, dd, *J* 1.6 and *J* 5.6, H-4), 8.09 (1H, dd, *J* 5.2 and *J* 8.8, H-3), 7.70 (1H, d, *J* 8 H-6), 7.45 (1H, d, *J* 8 H-7), 4.89 (2H, s, H-1). δ_C (100 MHz, DMSO-d_6); δ_{ppm} 42.79, 115.46, 121.62, 122.36, 129.04, 129.23, 143.27, 144.17, 147.50, 149.56;

Synthesis of 5-(piperazin-1-yl)quinoline-8-ol, 11

Anhydrous piperazine (9 g, 0.21 mol) dissolved in 30 ml chloroform was added dropwise to 5-chloromethyl-8-hydroxyquinoline hydrochloride **10** (2.1 g) dissolved in chloroform at 0 ºC. The resulting mixture was stirred for 24 hours at 25 ºC. Upon completion, the product was neutralized using 150 ml of saturated $NaHCO_3$ followed by 150 ml of H_2O; stirring was continued for 45 minutes. Approximately 300 mL of chloroform was added, and the mixture was stirred for an additional hour. After liquid-

liquid extraction, the organic layer was collected and dried over Na_2SO_4, filtered, and concentrated. The product was obtained as an off-white powder (Zhou, et al., 2015).

5-(piperazin-1-ylmethyl) quinolin-8-ol -8-ol, 11

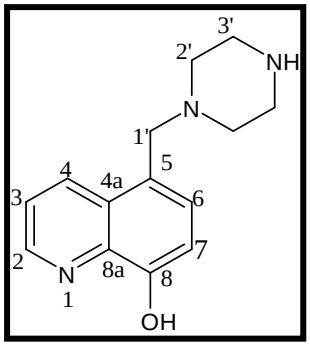

Off white amorphous solid; 48% yield; m. p 229.4°C, lit. mp. 232–234 °C ; R_f ($CHCl_3$:MeOH:NH_3 9:1:0.25) 0.26; IR cm^{-1}: 3190 (N-H) 2931 (OH), 1356 (C=N); δ_H (400 MHz, DMSO-d_6), 3.78 (2H, s, H1''), 2.76 (4H, m, H2''), 2.42 (4H, m, H3''); δ_C (100 MHz, DMSO-d_6) 45.37, 52.47, 59.29, 109.57, 121.14,124.06, 127.68, 128.51, 133.48, 138.66; 147.52; 152.44.

General procedure for preparation of compounds 14 a-c

A mixture of 5-(piperazin-1-ylmethyl) quinolin-8-ol **11** (10 mmol), 5-substituted /unsubstituted isatin (0.4 g, 1.64 mmol), and aqueous formaldehyde (0.075 ml of a 37% w/v) solution, 2.73 mmol) in anhydrous EtOH (10 mL) was refluxed for 1 hour. The mixture was stirred at 25ºC for 24 hours. The resulting precipitate was filtered, washed with cold EtOH, and then dried (Elsayed M. Afsah, et al., 2015).

piperazine-linked 8-hydroxyquinoline-isatin, 14a

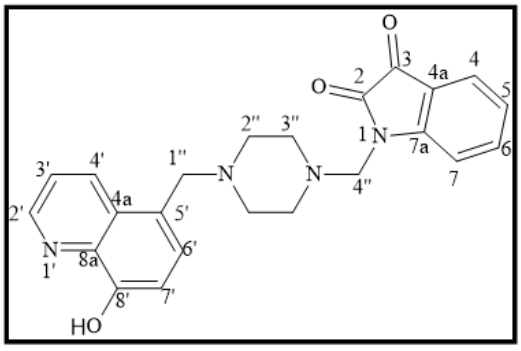

Yellow orange amorphous solid; 60% yield; m. p. 183 °C; R_f ($CHCl_3$:MeOH:NH_3 9:1:0.25) 0.79; IR cm^{-1}: 3305 (OH), 1724 (C=O keto), 1613 (C=O amide), 1577 (C=N). Anal. Calcd. For $C_{23}H_{24}N_4O_3$ is C 68.298%, H 5.981%, N 13.853%, O 11.868%.

piperazine-linked 8-hydroxyquinoline-chloroisatin, 14b

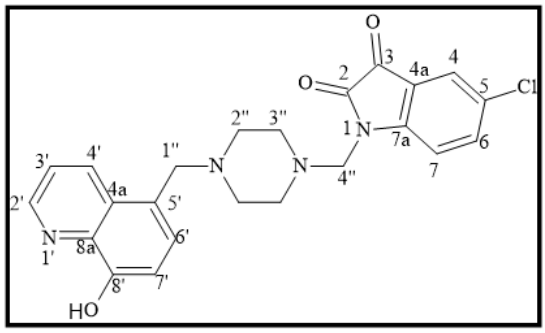

Orange amorphous solid; % yield 56 %; m. p. 220 °C; R_f ($CHCl_3$:MeOH:NH_3 9:1:0.25) 0.77; IR cm^{-1}: 3331 (OH), 1738 (C=O keto), 1609 (C=O amide); δ_H (400 MHz, DMSO-d_6), 4.40 (2H, s, H-4''), 3.77 (2H, s, H-1''), 2.57 (4H, m H-3''), 2.43 (4H, m H-2''); δ_C (100MHz, DMSO-d_6), 181.83, 158.26, 152.36, 152.33, 149.79, 149.07, 147.42, 138.56, 133.36, 128.39, 128.35, 127.57, 127.34, 126.70, 123.35, 121.06, 118.80, 118.62, 109.48, 61.58, 59.14, 52.09, 49.50; Anal. Calcd. For $C_{23}H_{23}ClN_4O_3$ is C 62.939%, H 5.282%, Cl 8.077%, N 12.766%, O 10.937%.

piperazine-linked 8-hydroxyquinoline-methylisatin, 14c

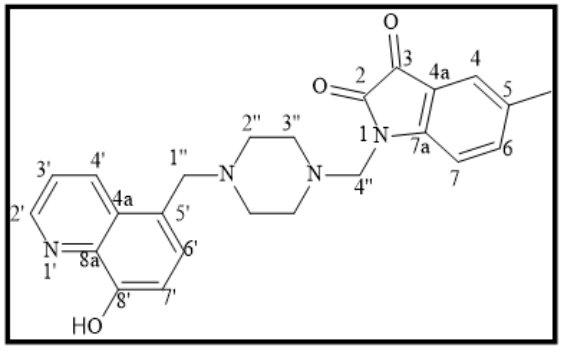

Orange amorphous solid; yield 58%; m. p. 212 °C; R_f ($CHCl_3$:MeOH:NH_3 9:1:0.25) 0.89; IR cm^{-1}: 3335 (O-H), 1726 (C=O keto), 1622 (C=O amide); δ_H (400 MHz, DMSO-d_6), 4.39 (2H, s, H-4''), 3.76 (2H, s, H-1'') 2.58 (4H, m, H-3''), 2.39 (4H, m, H-2''), 2.27 (3H, s, CH_3); δ_C (100MHz, DMSO-d_6), 183.84, 159.35, 153.06, 149.98, 149.10, 148.15, 139.30, 138.91, 134.09, 133.14, 132.56, 129.11, 128.30, 124.82, 121.79, 118.26, 110.22,110.20, 62.16, 59.88, 52.83, 50.35; Anal. Calcd. For $C_{24}H_{26}N_4O_3$ is C 68.879%, H 6.262%, N 13.389%, O 11.470%.

General procedure for compounds, 13 a-c

Equimolar (10 mmol) quantities of TSC and the 5-substituted/unsubstituted isatin were refluxed in ethanol for 2 hrs. The resulting precipitate was filtered and washed with cold ethanol.

Isatin-thiosemicarbazone, 13 a

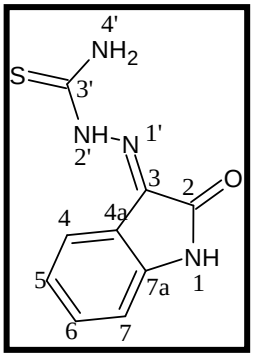

Yellow Powder; % yield 74%; m. p. 225 ºC; R_f ($CHCl_3$:MeOH:NH_3 9:1:0.25) 0.59; IR cm^{-1}: 3420 (N-H), 1680 (C=O), 1131(C=S); δ_H (400 MHz, DMSO-d_6) 12.48 (1H, s, H-2'), 10.98 (1H, s, H-1), 8.75-8.43 (1H, d, H4'); δ_C (100MHz, DMSO-d_6), 179.16, 162.52, 142.34, 132.01, 131.10, 122.24, 120.81, 119.96, 110.34. Anal. Calcd. For $C_9H_8N_4OS$ is C 49.078%, H 3.661%, N 25.439%, O 7.265% S 14.557%.

5-chloroisatin-thiosemicarbazone, 13 b

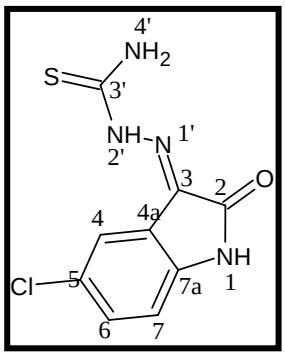

Yellow crystals; % yield 65%; m.p. 196 ºC; R_f ($CHCl_3$:MeOH:NH_3 9:1:0.25) 0.71; IR cm^{-1}: 3424 (N-H), 1683 (C=O), 1140 (C=S); δ_H (400 MHz, DMSO-d_6) 12.35 (1H, s, H-2'''), 11.08 (1H, s, H-1), 8.84 – 8.59 (2H, d, H4'''); δ_C (100MHz, DMSO-d_6), 178.94, 162.0, 149.0, 140.65, 130.44, 130.05, 121.29, 120.26, 112.31; Anal. Calcd. For $C_9H_7ClN_4OS$ is C 42.442%, H 2.770%, Cl 13.918, N 21.999%, O 6.282% S 12.588%.

5-Methylisatin-thiosemicarbazone, 13 c

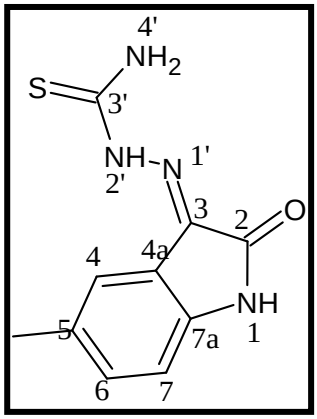

Orange crystals; yield: 61%; m.p. 24 ºC; R_f ($CHCl_3$:MeOH:NH_3 9:1:0.25) 0.69; IR cm^{-1}: 3420 (N-H), 1682 (C=O), 1596 (C=N), 1125 (C=S); δ_H (400 MHz, DMSO-d_6), 12.44 (1H, s, H-2’’’), 10.82 (1H, s, H-1), 8.67 – 8.37 (2H, d, H4’’’). 7.45 (1H, d, *J* 1.2 H4), 7.114 (1H, dd, J 1.2 and J 5.2 H6), (1H d, J 5.2 H7), 2.296 (3H, s, CH_3); δ_C (100MHz, DMSO-d_6), 179.15, 162.64, 140.11, 132.16, 131.41, 131,35, 121.37, 120.14, 110.71, 20.54; Anal. Calcd. For $C_{10}H_{10}N_4OS$ is C 51.267%, H 4.302%, N 23.916%, O 6.830% S 13.685%.

General procedure for compounds, 15 a-c

The conditions employed for the preparation of this compound were the same as that for the synthesis of compounds **14 a-c**.

5. CONCLUSION AND RECOMMENDATIONS

5.1 Conclusion

The objectives of the study were met. Novel piperazine linked 8-hydroxyquinoline-isatin hybrids **14a-c** of which **14a** and **b** displayed promising antimicrobial activity were prepared. Of note, both hybrids **14a** and **b** displayed broad-spectrum antimicrobial activity. The delineating of SAR for hybrids **14a-c** is limited because of the small number of compounds synthesized. Based on the antimicrobial activity, it is plausible that the presence of the chloro group at C-5 of the isatin scaffold enhanced antimicrobial activity.

Attempts to synthesize hybrids **15a-c** using two different synthesis routes failed. It is worth pointing out that *in silico* predictions revealed poor permeability, moderate solubility, poor absorption as well as non-compliance with Lipinski's rule of 5 for hybrids **15**. The poor activity reported for intermediates **13a-c** offered further support for the deprioritization of hybrids **15a-c.** Also revealed by the docking results was that the hybrids showed stronger binding interactions compared to the monomers with the two enzyme systems selected for the study. *In silico* data however showed that the hybrids cannot be subjected to further structural modifications because of their high molecular weights.

Overall, the study contributed new knowledge on and demonstrated the value of hybrid formation as a drug design approach for antimicrobial agents; more specifically, it supports the privileged status of the 8-hydroxyquinoline and isatin scaffolds and their potential to yield novel antimicrobial compounds.

5.2 Recommendations

Only a few hybrids could be synthesized. Expanding the hybrid library by varying substituents on the aromatic rings of the isatin and quinoline ring systems. Exploring alternative linker strategies other than piperazine that might enhance the efficacy of the compounds, for example, the triazole ring system, for the hybrid constructs, will contribute towards the generation of SAR data for future lead identification and optimization. Not knowing what the pharmacophore of the hybrid structures are, we cannot affect significant changes but what can be improved upon is the water solubility that was flagged by the in silico data and experimentally. Converting the compounds into salts such as hydrochloride salts or different salt derivatives is an effective technique to enhance solubility. Explore and use other synthesis methodologies, including greener methods, to synthesize thiosemicarbazide derivatives, and use the so obtained derivatives to prepare metal complexes as a means to enhance the antimicrobial properties. Subjecting the hybrids to antibiofilm activity testing is strongly recommended. Scaling up the synthesis of the hybrids 14 followed by extensive purification and subsequent testing in other disease models such as anticancer, anti-HIV, antimalaria, etc. will demonstrate the potential value of the hybrid constructs.

REFERENCE LIST

1. O'Neill, J. Tackling drug-resistant infections globally: final report and recommendations. Government of the United Kingdom, 2016.

2. Murray CJ, Ikuta KS, Sharara F, Swetschinski L, Aguilar GR, Gray A, Han C, Bisignano C, Rao P, Wool E, Johnson SC. Global burden of bacterial antimicrobial resistance in 2019: a systematic analysis. The Lancet. 2022 Feb 12; 399(10325): p. 629-55.

3. Walsh TR, Gales AC, Laxminarayan R, Dodd PC. Antimicrobial resistance: addressing a global threat to humanity. PLoS medicine. 2023 Jul 3;20(7):e1004264.

4. Elton L, Thomason MJ, Tembo J, Velavan TP, Pallerla SR, Arruda LB, Vairo F, Montaldo C, Ntoumi F, Abdel Hamid MM, Haider N. Antimicrobial resistance preparedness in sub-Saharan African countries. Antimicrobial Resistance & Infection Control. 2020 Dec;9:1-1.

5. Newman DJ, Cragg GM. Natural products as sources of new drugs over the nearly four decades from 01/1981 to 09/2019. Journal of Natural Products 2020 Mar 12;83(3):770-803.

6. Prachayasittikul V, Prachayasittikul S, Ruchirawat S, Prachayasittikul V. 8-Hydroxyquinolines: a review of their metal chelating properties and medicinal applications. Drug design, Development and Therapy. 2013 Oct 4:1157-78.

7. Bugalia S, Dhayal Y, Sachdeva H, Kumari S, Atal K, Phageria U, Saini P, Gurjar OP. Review on isatin-a remarkable scaffold for designing potential therapeutic complexes and its macrocyclic complexes with transition metals. Journal of Inorganic and Organometallic Polymers and Materials. 2023 Jul;33(7):1782-801.

8. Nain S, Mathur G, Anthwal T, Sharma S, Paliwal S. Synthesis, characterization, and antibacterial activity of new isatin derivatives. Pharmaceutical Chemistry Journal. 2023 May;57(2):196-203.

9. Xu H, Chen W, Zhan P, Liu X. 8-Hydroxyquinoline: A privileged structure with a broad-ranging pharmacological potential. MedChemComm. 2015;6(1):61-74.

10. Shukla M, Dubey M, Kulshrashtha H, Seth DS. Synthesis of bioactive thiosemicarbazides: Antimicrobial agents against drug resistant microbial pathogens. Chemistry of Phytopotentials: Health, Energy and Environmental Perspectives. 2012:9-12.

11 Choudhary S, Singh PK, Verma H, Singh H, Silakari O. Success stories of natural product-based hybrid molecules for multi-factorial diseases. European journal of Medicinal Chemistry.. 2018 May 10;151:62-97.

12 Alkhzem AH, Woodman TJ, Blagbrough IS. Design and synthesis of hybrid compounds as novel drugs and medicines. RSC Advances. 2022;12(30):19470-84.

13. Pires DE, Blundell TL, Ascher DB. pkCSM: predicting small-molecule pharmacokinetic and toxicity properties using graph-based signatures. Journal of Medicinal Chemistry. 2015 May 14;58(9):4066-72.

14. Dulsat J, López-Nieto B, Estrada-Tejedor R, Borrell JI. Evaluation of free online ADMET tools for academic or small biotech environments. Molecules. 2023 Jan 12;28(2):776.

15. Smith RD, Coast J. Antimicrobial resistance: a global response. Bulletin of the World Health Organization. 2002;80:126-33.

16. Chokshi A, Sifri Z, Cennimo D, Horng H. Global contributors to antibiotic resistance. Journal of Global Infectious Diseases. 2019 Jan 1;11(1):36-42.

17. Miethke M, Pieroni M, Weber T, Brönstrup M, Hammann P, Halby L, Arimondo PB, Glaser P, Aigle B, Bode HB, Moreira R. Towards the sustainable discovery and development of new antibiotics. Nature Reviews Chemistry. 2021 Oct;5(10):726-49.

18. Atanasov AG, Zotchev SB, Dirsch VM, Supuran CT. Natural products in drug discovery: advances and opportunities. Nature reviews Drug discovery. 2021 Mar;20(3):200-16.

19. Naseri G. A roadmap to establish a comprehensive platform for sustainable manufacturing of natural products in yeast. Nature Communications. 2023 Apr 6;14(1):1916.

20.. Evans BE, Rittle KE, Bock MG, DiPardo RM, Freidinger RM, Whitter WL, Lundell GF, Veber DF, Anderson PS, Chang RS, Lotti VJ. Methods for drug discovery: development of potent, selective, orally effective cholecystokinin antagonists. Journal of Medicinal Chemistry. 1988 Dec 1;31(12):2235-46.

21. DeSimone RW, Currie KS, Mitchell SA, Darrow JW, Pippin DA. Privileged structures: applications in drug discovery. Combinatorial Chemistry & High Throughput Screening. 2004 Aug 1;7(5):473-93.

22. Grewal AS. Isatin derivatives with several biological activities. International Journal of Pharmaceutical Research. 2014 Jan;6(1):1-7.

23. Premanathan M, Radhakrishnan S, Kulangiappar K, et al. Antioxidant & anticancer activities of isatin (1H-indole-2,3-dione), isolated from the flowers of *Couroupita guianensis* Aubl, Indian Journal of Medical Research, 2012; 136(5): 822-826.

24. Singh UK, Pandeya SN, Singh A, Srivastava BK, Pandey M. Synthesis and antimicrobial activity of Schiff's and *N*-Mannich bases of isatin and its derivatives with 4-amino-N-carbamimidoyl benzene sulfonamide. International Journal of Pharmaceutical Sciences and Drug Research. 2010;2(2):151-4.

25. Panneerselvam P, Reddy RS, Murali K, Kumar RR, Synthesis, analgesic, anti-inflammatory and antimicrobial activities of some novel Schiff's bases of 5-subsituted Isatin, Der Pharma Chemica, 2010; 2(1): 28-37.

26. Mondal P, Jana S, Balaji A, Ramakrishna R, Kanthal LK. Synthesis of some new isoxazoline derivatives of chalconised indoline 2-one as a potential analgesic, antibacterial and anthelmimtic agents. Journal of Young Pharmacists. 2012 Jan 1;4(1):38-41.

27. Malawska B. New anticonvulsant agents. Current topics in Medicinal Chemistry. 2005 Jan 1;5(1):69-85.

28. Varma RS, Nobles WL, Antiviral, antibacterial and antifungal activities of isatin N-mannich bases, Journal of Pharmaceutical Sciences, 1975; 64(5): 881-882.

29. Teitz YA, Ronen D, Vansover A, Stematsky T, Riggs JL. Inhibition of human immunodeficiency virus by N-methylisatin-β4′: 4′-diethylthiosemicarbazone and N-allylisatin-β-4′: 4′-diallythiosemicarbazone. Antiviral Research. 1994 Aug 1;24(4):305-14.

30. Pal M, Sharma NK, Priyanka, Jha KK, Synthetic and biological multiplicity of isatin: A Review, Journal of Advanced Scientific Research, 2011; 2(2): 35-44.

31. Liu B, Jiang D and Hu G. The antibacterial activity of isatin hybrids. Current Topics in Medicinal Chemistry. 2022; 22: p. 25-40.

32. Hassan M, Ghaffari R, Sardari S, Farahani YF, Mohebbi S. Discovery of novel isatin-based thiosemicarbazones: synthesis, antibacterial, antifungal, and antimycobacterial screening. Research in Pharmaceutical Sciences. 2020 Jun 1;15(3):281-90.

33. Koçyiğit ÜM, Doğan M, Muğlu H, Taslimi P, Tüzün B, Yakan H, Bal H, Güzel E, Gülçin İ. Determination of biological studies and molecular docking calculations of isatin-thiosemicarbazone hybrid compounds. Journal of Molecular Structure. 2022 Sep 15;1264:133249.

34. Tehrani KH, Hashemi M, Hassan M, Kobarfard F, Mohebbi S. Synthesis and antibacterial activity of Schiff bases of 5-substituted isatins. Chinese Chemical Letters. 2016 Feb 1;27(2):221-5.

35. Gupta R, Luxami V, Paul K. Insights of 8-hydroxyquinolines: A novel target in medicinal chemistry. Bioorganic chemistry. 2021 Mar 1;108:104633.

36. Zhang RH, Guo HY, Deng H, Li J, Quan ZS. Piperazine skeleton in the structural modification of natural products: a review. Journal of enzyme inhibition and Medicinal Chemistry. 2021 Jan 1;36(1):1165-97.

37. Oliveri V, Vecchio G. 8-Hydroxyquinolines in medicinal chemistry: A structural perspective. European Journal of Medicinal Chemistry. 2016 Sep 14;120:252-74.

38. Peng X, Chen Q, Han B, Zhang H, Li J, Zhang Q. Applications of piperazine scaffold in drug design. In Privileged Scaffolds in Drug Discovery 2023 Jan 1 (pp. 273-299). Academic Press.

39. El Faydy M, Dahaief N, Rbaa M, Ounine K, Lakhrissi B. Synthesis, Characterization and Biological Activity of Some Novel 5-((4-Alkyl piperazin-1-yl) methyl) quinolin-8-ol Derivatives. chemistry. 2016;17:18.

40. TG S, Subramanian S, Eswaran S. Design, synthesis and study of antibacterial and antitubercular activity of quinoline hydrazone hybrids. Heterocyclic Communications. 2020 Oct 15;26(1):137-47.

41. Kumar HM, Herrmann L, Tsogoeva SB. Structural hybridization as a facile approach to new drug candidates. Bioorganic & Medicinal Chemistry Letters. 2020 Dec 1;30(23):127514.

42. Gediya LK, Njar VC. Promise and challenges in drug discovery and development of hybrid anticancer drugs. Expert Opinion on Drug Discovery. 2009 Nov 1;4(11):1099-111.

43. Domalaon R, Idowu T, Zhanel GG, Schweizer F. Antibiotic hybrids: the next generation of agents and adjuvants against Gram-negative pathogens? Clinical Microbiology Reviews. 2018 Apr;31(2):10-128.

44. Prakash CR, Raja S. Synthesis, characterization and in vitro antimicrobial activity of some novel 5-substituted Schiff and Mannich base of isatin derivatives. Journal of Saudi Chemical Society. 2013 Jul 1;17(3):337-44.

45. Koh AJ, Thombare V, Hussein M, Rao GG, Li J, Velkov T. Bifunctional antibiotic hybrids: A review of clinical candidates. Frontiers in Pharmacology. 2023 Jun 12;14:1158152.

46. Fisher CR, Schmidt-Malan SM, Ma Z, Yuan Y, He S, Patel R. In vitro activity of TNP-2092 against periprosthetic joint infection–associated staphylococci. Diagnostic Microbiology and Infectious Disease. 2020 Jul 1;97(3):115040.

47. Yuan Y, Wang X, Xu X, Liu Y, Li C, Yang M, Yang Y, Ma Z. Evaluation of a dual-acting antibacterial agent, TNP-2092, on gut microbiota and potential application in the treatment of gastrointestinal and liver disorders. ACS Infectious Diseases. 2019 Dec 18;6(5):820-31.

48. Niazi SK, Mariam Z. Computer-aided drug design and drug discovery: a prospective analysis. Pharmaceuticals. 2023 Dec 22;17(1):22.

49. Prieto-Martínez FD, López-López E, Juárez-Mercado KE, Medina-Franco JL. Computational drug design methods—current and future perspectives. In: Kunal Roy. In silico drug design. Academic Press; 2019 Jan 1:19-44.

50. Ganesan A. The impact of natural products upon modern drug discovery. Current Opinion in Chemical Biology. 2008 Jun 1;12(3):306-17.

51. Schmitz U, Swaminathan S. Discovery and development of oseltamivir at Gilead Sciences. Antiviral Therapy. 2022 Apr 20;27(2):13596535211067598.

52. Kubitza D, Perzborn E, Berkowitz SD. The discovery of rivaroxaban: translating preclinical assessments into clinical practice. Frontiers in Pharmacology. 2013 Nov 25; 4:145.

53. Peluso P, Chankvetadze B. Recent developments in molecular modeling tools and applications related to pharmaceutical and biomedical research. Journal of Pharmaceutical and Biomedical Analysis. 2023 Nov 3:115836.

54. Hanwell MD, Curtis DE, Lonie DC, Vandermeersch T, Zurek E, Hutchison GR. Avogadro: an advanced semantic chemical editor, visualization, and analysis platform. Journal of Cheminformatics. 2012 Dec; 4:1-7.

55. Smith TJ. MolView: a program for analyzing and displaying atomic structures on the Macintosh personal computer. Journal of Molecular Graphics. 1995 Apr 1;13(2):122-5.

56. Biovia DS. Discovery Studio Visualizer. San Diego, CA, USA. 2018. https://discover.3ds.com/discovery-studio-visualizer-download.

57. Hofmann S, Merz L. Contribution of the Swiss Chemistry Community to SDGs–Perspective of the SCNAT Platform Chemistry. Chimia. 2024 Jun 26;78(6):379-83.

58. Eberhardt J, Santos-Martins D, Tillack AF, Forli S. AutoDock Vina 1.2. 0: New docking methods,New docking methods expanded force field, and python bindings. Journal of Chemical Information and Modeling. 2021 Jul 19;61(8):3891-8.

59. Santos-Martins D, Solis-Vasquez L, Tillack AF, Sanner MF, Koch A, Forli S. Accelerating AutoDock4 with GPUs and gradient-based local search. Journal of Chemical Theory and Computation. 2021 Jan 6;17(2):1060-73.

60. Jones G, Willett P, Glen RC, Leach AR, Taylor R. Development and validation of a genetic algorithm for flexible docking. Journal of Molecular Biology. 1997 Apr 4;267(3):727-48.

61. Friesner RA, Banks JL, Murphy RB, Halgren TA, Klicic JJ, Mainz DT, Repasky MP, Knoll EH, Shelley M, Perry JK, Shaw DE. Glide: a new approach for rapid, accurate docking and scoring. 1. Method and assessment of docking accuracy. Journal of Medicinal Chemistry. 2004 Mar 25;47(7):1739-49.

62. Daina A, Michielin O, Zoete V. SwissADME: a free web tool to evaluate pharmacokinetics, drug-likeness and medicinal chemistry friendliness of small molecules. Scientific Reports. 2017 Mar 3;7(1):42717.

63. Silverman RB, Holladay MW. The organic chemistry of drug design and drug action. Academic press; 2014 Mar 29.

64. Bhunia SS, Saxena M, Saxena AK. Ligand-and structure-based virtual screening in drug discovery. In Biophysical and Computational Tools in Drug Discovery 2021 Aug 7 (pp. 281-339). Cham: Springer International Publishing.

65. Fu L, Shi S, Yi J, Wang N, He Y, Wu Z, Peng J, Deng Y, Wang W, Wu C, Lyu A. ADMETlab 3.0: an updated comprehensive online ADMET prediction platform enhanced with broader coverage, improved performance, API functionality and decision support. Nucleic Acids Research. 2024 Apr 4:gkae236.

66. Swanson K, Walther P, Leitz J, Mukherjee S, Wu JC, Shivnaraine RV, Zou J. ADMET-AI: a machine learning ADMET platform for evaluation of large-scale chemical libraries. Bioinformatics. 2024 Jun 24:btae416.

67. Lee SK, Lee IH, Kim HJ, Chang GS, Chung JE, No KT. The PreADME Approach: Web-based program for rapid prediction of physico-chemical, drug absorption and drug-

like properties. EuroQSAR 2002 Designing Drugs d Crop Protectants: processes, problems and solutions. 2003;2003:418-20.

68. Patlewicz G, Jeliazkova N, Safford RJ, Worth AP, Aleksiev B. An evaluation of the implementation of the Cramer classification scheme in the Toxtree software. SAR and QSAR in Environmental Research. 2008 Jul 1;19(5-6):495-524.

69. Azzam KA. SwissADME and pkCSM webservers predictors: An integrated online platform for accurate and comprehensive predictions for *in silico* ADME/T properties of artemisinin and its derivatives. Kompleksnoe Ispolzovanie Mineralnogo Syra= Complex use of mineral resources. 2023;325(2):14-21.

70. Kaniga P. *Insilico, Synthesis, Characterization and Biological Evaluation of Novel Isatin Analogues* (Doctoral dissertation, Arulmigu Kalasalingam College of Pharmacy, Krishnankoil).

71. Ashraf SA, Elkhalifa AE, Mehmood K, Adnan M, Khan MA, Eltoum NE, Krishnan A, Baig MS. Multi-targeted molecular docking, pharmacokinetics, and drug-likeness evaluation of okra-derived ligand abscisic acid targeting signaling proteins involved in the development of diabetes. Molecules. 2021 Oct 1;26(19):5957.

72. Audu OY. *In-Silico* Guided Design, Synthesis and Bio-Evaluation of Potential Chemotherapeutic Agents Against Malaria, Cancer and Disease-Causing Pathogens (Doctoral dissertation, University of Pretoria (South Africa)).

73. Jofily P, Pascutti PG, Torres PH. Improving blind docking in DOCK6 through an automated preliminary fragment probing strategy. Molecules. 2021 Feb 25;26(5):1224.

74. Torres PH, Sodero AC, Jofily P, Silva-Jr FP. Key topics in molecular docking for drug design. International Journal of Molecular Sciences. 2019 Sep 15;20(18):4574.

75. BioSignature Lab. pkCSM: Prediction of Kinase-Specific Phosphorylation Site Motifs. [Internet]. The University of Queensland; [cited 2023 November 2023]. Available from: https://biosig.lab.uq.edu.au/pkcsm/prediction.

76. Elseginy SA, Anwar MM. Pharmacophore-based virtual screening and molecular dynamics simulation for identification of a novel DNA gyrase B inhibitor with benzoxazine acetamide scaffold. ACS omega. 2021 Dec 22;7(1):1150-64.

77. Berman HM, Bhat TN, Bourne PE, Feng Z, Gilliland G, Weissig H, Westbrook J. The Protein Data Bank and the challenge of structural genomics. Nature Structural Biology. 2000 Nov;7(11):957-9.

78. Pautsch A, Schulz GE. Structure of the outer membrane protein A transmembrane domain. Nature Structural Biology. 1998 Nov;5(11):1013-7.

79. Zhao Q, Wu Y, Li B, He L, Sun J, Pang X, Gu S, Li X. OmpA is Involved in the early response of *Escherichia coli* to antibiotics as a hub outer membrane protein. Applied Biochemistry and Microbiology. 2023 Oct;59(5):608-21.

80. Saadeh HA, Sweidan KA, Mubarak MS. Recent advances in the synthesis and biological activity of 8-hydroxyquinolines. Molecules. 2020 Sep 21;25(18):4321.

81. Rose PW, Prlić A, Altunkaya A, Bi C, Bradley AR, Christie CH, Costanzo LD, Duarte JM, Dutta S, Feng Z, Green RK. The RCSB protein data bank: integrative view of protein, gene and 3D structural information. Nucleic Acids Research. 2016 Oct 27:gkw1000.

82. Pautsch A, Schulz GE. Structure of the outer membrane protein A transmembrane domain. Nature structural biology. 1998 Nov;5(11):1013-7.

83. Lafitte D, Lamour V, Tsvetkov PO, Makarov AA, Klich M, Deprez P, Moras D, Briand C, Gilli R. DNA gyrase interaction with coumarin-based inhibitors: the role of the hydroxybenzoate isopentenyl moiety and the 5 '-methyl group of the noviose. Biochemistry. 2002 Jun 11;41(23):7217-23.

84. Shaquiquzzaman M, Verma G, Marella A, Akhter M, Akhtar W, Khan MF, Tasneem S, Alam MM. Piperazine scaffold: A remarkable tool in generation of diverse pharmacological agents. European Journal of Medicinal Chemistry. 2015 Sep 18; 102: p. 487-529.

85. Hall MD, Salam NK, Hellawell JL, Fales HM, Kensler CB, Ludwig JA, Szakács G, Hibbs DE, Gottesman MM. Synthesis, activity, and pharmacophore development for isatin-β-thiosemicarbazones with selective activity toward multidrug-resistant cells. Journal of Medicinal Chemistry. 2009 May 28;52(10):3191-204.

86. Aly AA, Abdallah EM, Ahmed SA, Rabee MM, Bräse S. Transition metal complexes of thiosemicarbazides, and their corresponding carbazones with Cu (I), Cu (II), Co (II), Ni (II), Pd (II), and Ag (I)—A review. Molecules. 2023 Feb 14;28(4):1808.

87. Chiyanzu I, Clarkson C, Smith PJ, Lehman J, Gut J, Rosenthal PJ, Chibale K. Design, synthesis and anti-plasmodial evaluation in vitro of new 4-aminoquinoline isatin derivatives. Bioorganic & Medicinal Chemistry. 2005 May 2;13(9):3249-61.

88. Pitucha M, Karczmarzyk Z, Swatko-Ossor M, Wysocki W, Wos M, Chudzik K, Ginalska G, Fruzinski A. Synthesis, in vitro screening and docking studies of new

thiosemicarbazide derivatives as antitubercular agents. Molecules. 2019 Jan 11;24(2):251.

89. Zhou A, Wu H, Pan J, Wang X, Li J, Wu Z, Hui A. Synthesis and evaluation of paeonol derivatives as potential multifunctional agents for the treatment of Alzheimer's disease. Molecules. 2015 Jan 14;20(1):1304-18.

90. Warshawsky et al., 2005. United States Patent Documents. US6,855,711B1, February 15 2005.

91. Ali AQ, Teoh SG, Salhin A, Eltayeb NE, Ahamed MB, Majid AA. Synthesis of isatin thiosemicarbazones derivatives: In vitro anti-cancer, DNA binding and cleavage activities. Spectrochimica Acta Part A: Molecular and Biomolecular Spectroscopy. 2014 May 5;125:440-8.

92. Afsah EM, Elmorsy SS, Abdelmageed SM, Zaki ZE. Synthesis of some new mixed azines, Schiff and Mannich bases of pharmaceutical interest related to isatin. Zeitschrift für Naturforschung B. 2015 Jun 1;70(6):393-402.

93. Zeidan R, Oran S. Antioxidant activity of leaf and fruit extracts of Jordanian *Rubus sanguineus* Friv.(Rosaceae). Journal of Medicinal Plants Research. 2014 Nov 26;8(39):1179-90.

94. Tsaioun K, Jacewicz M. De-Risking Drug Discovery with ADDME—Avoiding Drug Development Mistakes Early. Alternatives to Laboratory Animals. 2009 Sep;37(1_suppl):47-55.

95. Lipinski CA, Lombardo F, Dominy BW, Feeney PJ. Experimental and computational approaches to estimate solubility and permeability in drug discovery and development settings. Advanced Drug Delivery Reviews. 1997 Jan 15;23(1-3):3-25.

96. Gao Y, Gesenberg C, Zheng W. Oral formulations for preclinical studies: principle, design, and development considerations. In Developing solid oral dosage forms 2017 Jan 1 (pp. 455-495). Academic Press.

97. Ibrahim ZY, Uzairu A, Shallangwa G, Abechi S. Molecular docking studies, drug-likeness and in-silico ADMET prediction of some novel β-Amino alcohol grafted 1, 4, 5-trisubstituted 1, 2, 3-triazoles derivatives as elevators of p53 protein levels. Scientific African. 2020 Nov 1;10:e0057094.

98. Maximo da Silva M, Comin M, Santos Duarte T, Foglio MA, De Carvalho JE, do Carmo Vieira M, Nazari Formagio AS. Synthesis, antiproliferative activity and molecular properties predictions of galloyl derivatives. Molecules. 2015 Mar 25;20(4):5360-73.

99. Janicka M, Sztanke M, Sztanke K. Modeling the Blood-Brain Barrier Permeability of Potential Heterocyclic Drugs via Biomimetic IAM Chromatography Technique Combined with QSAR Methodology. Molecules. 2024 Jan 5;29(2).

100. Dahlin JL, Nissink JW, Strasser JM, Francis S, Higgins L, Zhou H, Zhang Z, Walters MA. PAINS in the assay: chemical mechanisms of assay interference and promiscuous enzymatic inhibition observed during a sulfhydryl-scavenging HTS. Journal of Medicinal Chemistry. 2015 Mar 12;58(5):2091-113.

101. Kus M, Ibragimow I, Piotrowska-Kempisty H. Caco-2 cell line standardization with pharmaceutical requirements and in vitro model suitability for permeability assays. Pharmaceutics. 2023 Oct 24;15(11):2523.

102. Stielow M, Witczyńska A, Kubryń N, Fijałkowski Ł, Nowaczyk J, Nowaczyk A. The bioavailability of drugs—the current state of knowledge. Molecules. 2023 Dec 11;28(24):8038.

103. Durán-Iturbide NA, Díaz-Eufracio BI, Medina-Franco JL. *In silico* ADME/Tox profiling of natural products: A focus on BIOFACQUIM. ACS Omega. 2020 Jun 25;5(26):16076-84.

104. Zhao M, Ma J, Li M, Zhang Y, Jiang B, Zhao X, Huai C, Shen L, Zhang N, He L, Qin S. Cytochrome P450 enzymes and drug metabolism in humans. International Journal of Molecular Sciences. 2021 Nov 26;22(23):12808.

105. Pires DE, Kaminskas LM, Ascher DB. Prediction and optimization of pharmacokinetic and toxicity properties of the ligand. Computational Drug Discovery and Design. 2018:271-84.

106. Venkateshan N, Rajapandi R, Kaniga P. Synthesis, antibacterial evaluation and docking studies of some novel isatin derivatives. Indian Drugs. 2018 Mar 1;55(3).

107. Elfaky MA, Abdel-Hamid MI, Khalifa E, Alshareef WA, Mosbah RA, Elazab ST, Ghoneim MM, Al-Sanea MM, Bendary MM. Innovative next-generation therapies in combating multi-drug-resistant and multi-virulent Escherichia coli isolates: Insights

from in vitro, in vivo, and molecular docking studies. Applied Microbiology and Biotechnology. 2022 Feb;106(4):1691-703.

108. Ugurlu SY, McDonald D, Lei H, Jones AM, Li S, Tong HY, Butler MS, He S. Cobdock: an accurate and practical machine learning-based consensus blind docking method. Journal of Cheminformatics. 2024 Jan 11;16(1):5.

109. Abdullah T. Blind Docking Vs Site-specific Docking. [internet]. [Cited 2024 April]. Available from: https://bioinformaticsreview.com/20210226/blind-docking-vs-site-specific-docking/.

110. Singh T, Stein RG, Hoops JF, Biel JH, Hoya WK, Cruz DR. Antimalarials. 7-Chloro-4-(substituted amino) quinolines. Journal of Medicinal Chemistry. 1971 Apr;14(4):283-6.

111. Durand C, Szostak M. Recent advances in the synthesis of piperazines: focus on C–H functionalization. Organics. 2021 Oct 8;2(4):337-47.

112. Janowska S, Andrzejczuk S, Gawryś P, Wujec M. Synthesis and Antimicrobial Activity of New Mannich Bases with Piperazine Moiety. Molecules. 2023 Jul 21;28(14):5562

113. Raju SK, Vengadhajalaphathy P, Sundaram R, Periyasamy S, Chinnaraj T, Sekar P. Recent advances in biological applications of Mannich bases—An overview. International Journal of Pharmaceutical Chemistry and Analysis. 2023;10(1):15-27.

114. Pu MX, Guo HY, Quan ZS, Li X, Shen QK. Application of the Mannich reaction in the structural modification of natural products. Journal of Enzyme Inhibition and Medicinal Chemistry. 2023 Dec 31;38(1):2235095.

115. Justim JD, Bohs LM, Martins BB, Bandeira KC, Melo AP, Gervini VC, Bresolin L, Godoi M, Peixoto CR. Electrochemical characterization of isatin-thiosemicarbazone derivatives. Journal of Chemical Sciences. 2021 Dec;133(4):124.

116. Saranya S, Haribabu J, Palakkeezhillam VN, Jerome P, Gomathi K, Rao KK, Babu VH, Karvembu R, Gayathri D. Molecular structures, Hirshfeld analysis and biological investigations of isatin based thiosemicarbazones. Journal of Molecular Structure. 2019 Dec 15;1198:126904.

117. Akinchan NT. Spectroscopic studies on Isatin-3-Semicarbazone and Isatin-3-Thiosemicarbazone. Global Journal of Pure and Applied Sciences. 2004 Nov 10;10(4):545-53.

118. World Health Organization. World Health Organization publishes list of bacteria for which new antibiotics are urgently needed. Geneva: World Health Organization. 2017.

119. Nematollahi A, Aminimoghadamfarouj N, Wiart C. Anti-bacterial, Antioxidant activity and phytochemical study of *Diospyros wallichii*—an Interesting Malaysia's endemic species of Ebenaceae. International Journal of PharmTech Research. 2011;3(3):1732-6.

APPENDICES

Appendix A: University of Namibia Ethical Clearance Certificate

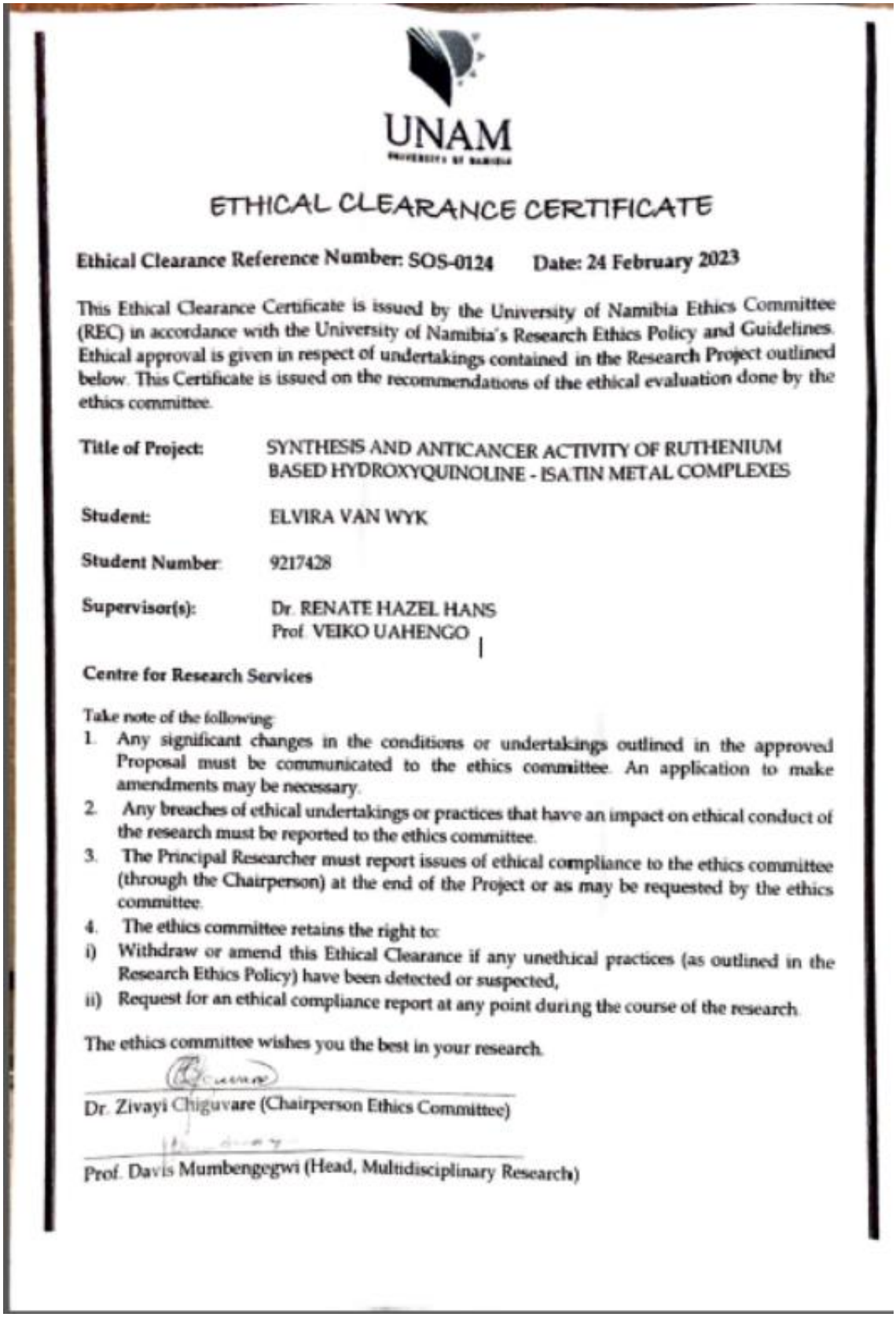

UNAM

ETHICAL CLEARANCE CERTIFICATE

Ethical Clearance Reference Number: SOS-0124 **Date: 24 February 2023**

This Ethical Clearance Certificate is issued by the University of Namibia Ethics Committee (REC) in accordance with the University of Namibia's Research Ethics Policy and Guidelines. Ethical approval is given in respect of undertakings contained in the Research Project outlined below. This Certificate is issued on the recommendations of the ethical evaluation done by the ethics committee.

Title of Project:	SYNTHESIS AND ANTICANCER ACTIVITY OF RUTHENIUM BASED HYDROXYQUINOLINE - ISATIN METAL COMPLEXES
Student:	ELVIRA VAN WYK
Student Number:	9217428
Supervisor(s):	Dr. RENATE HAZEL HANS Prof. VEIKO UAHENGO

Centre for Research Services

Take note of the following:

1. Any significant changes in the conditions or undertakings outlined in the approved Proposal must be communicated to the ethics committee. An application to make amendments may be necessary.
2. Any breaches of ethical undertakings or practices that have an impact on ethical conduct of the research must be reported to the ethics committee.
3. The Principal Researcher must report issues of ethical compliance to the ethics committee (through the Chairperson) at the end of the Project or as may be requested by the ethics committee.
4. The ethics committee retains the right to:

i) Withdraw or amend this Ethical Clearance if any unethical practices (as outlined in the Research Ethics Policy) have been detected or suspected,

ii) Request for an ethical compliance report at any point during the course of the research.

The ethics committee wishes you the best in your research.

Dr. Zivayi Chiguvare (Chairperson Ethics Committee)

Prof. Davis Mumbengegwi (Head, Multidisciplinary Research)

Appendix B: Supplementary information

Table A1. Code names, formula and SMILES codes of all intermediates and hybrids

Compound	Formula	Canonical Smiles
10	$C_{10}H_8ClNO$	OC1=C2N=CC=CC2=C(CCl)C=C1
11	$C_{14}H_{17}N_3O$	OC1=C(N=CC=C2)C2=C(CN3CCNCC3)C=C1
13a	$C_9H_8N_4OS$	O=C(NC1=C/2C=CC=C1)C2=N/NC(N)=S
13b	$C_9H_7ClN_4OS$	O=C(NC1=C/2C=C(Cl)C=C1)C2=N/NC(N)=S
13c	$C_{10}H_{10}N_4OS$	O=C(NC1=C/2C=C(C)C=C1)C2=N/NC(N)=S
14a	$C_{23}H_{24}N_4O_3$	O=C1N(CN2CCN(CC3=CC=C(O)C4=NC=CC=C43)CC2)C5=C(C=CC=C5)C1=O
14b	$C_{23}H_{23}ClN_4O_3$	O=C1N(CN2CCN(CC3=CC=C(O)C4=NC=CC=C43)CC2)C5=C(C=C(Cl)C=C5)C1=O
14c	$C_{24}H_{26}N_4O_3$	O=C1N(CN2CCN(CC3=CC=C(O)C4=NC=CC=C43)CC2)C5=C(C=C(C)C=C5)C1=O
15a	$C_{24}H_{27}N_7O_2S$	OC1=C(N=CC=C2)C2=C(CN3CCN(CN4C(C=CC=C5)=C5/C(C4=O)=N/NC(N)=S)CC3)C=C1
15b	$C_{24}H_{26}ClN_7O_2S$	O=C1N(CN2CCN(CC3=C4C(N=CC=C4)=C(C=C3)O)CC2)C5=C(/C1=N/NC(N)=S)C=C(Cl)C=C5
15c	$C_{25}H_{29}N_7O_2S$	OC1=C(N=CC=C2)C2=C(CN3CCN(CN4C(C=CC(C)=C5)=C5/C(C4=O)=N/NC(N)=S)CC3)C=C1

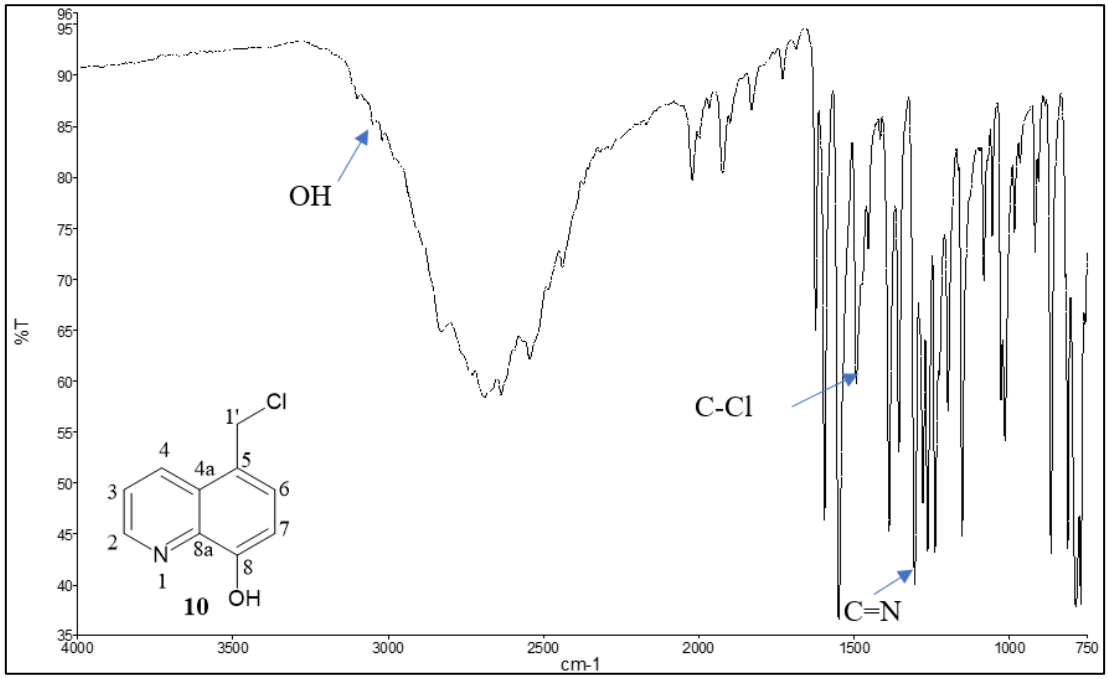

Figure A1: IR spectrum intermediate **10**

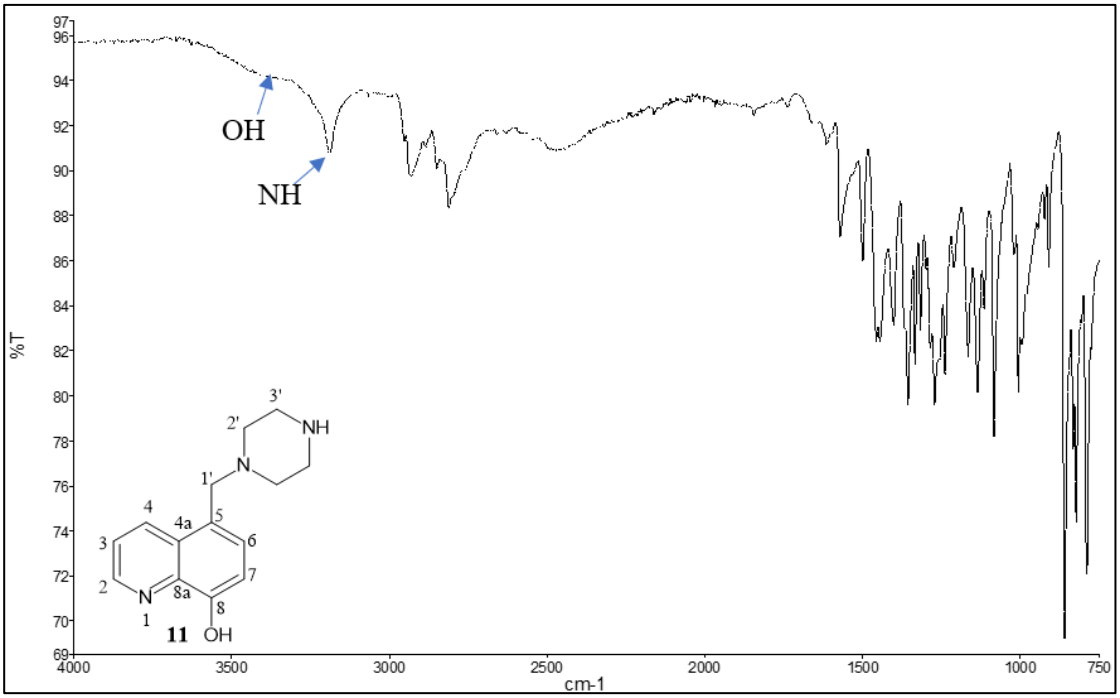

Figure A2: IR spectrum of intermediate **11**

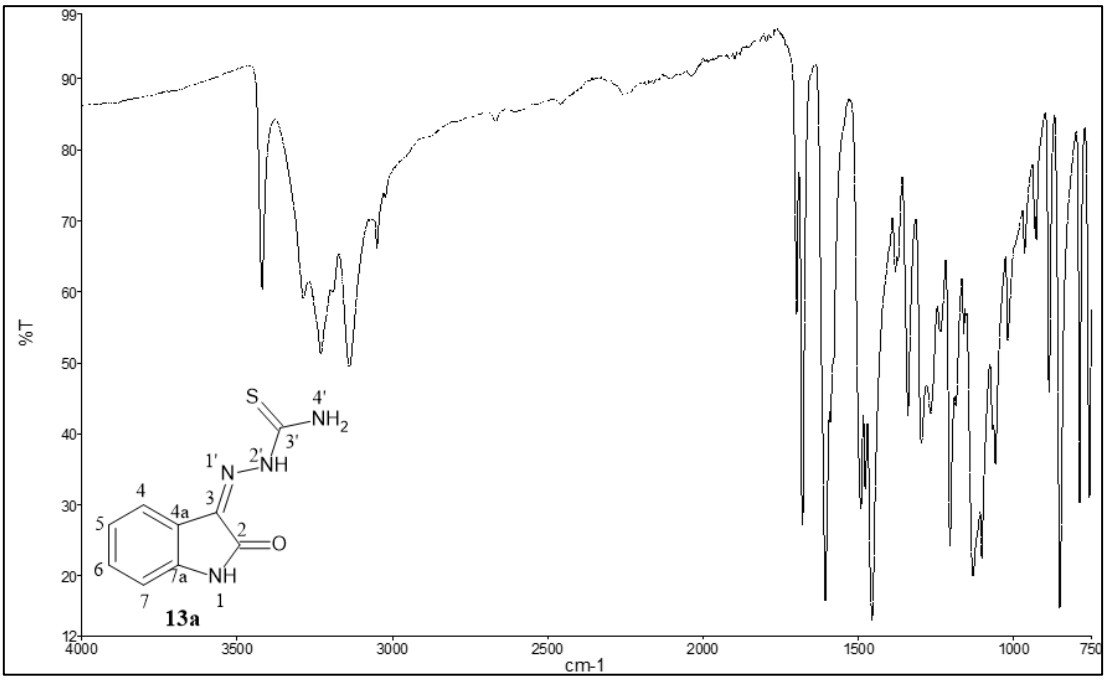

Figure A3: IR spectrum of intermediate **13a**

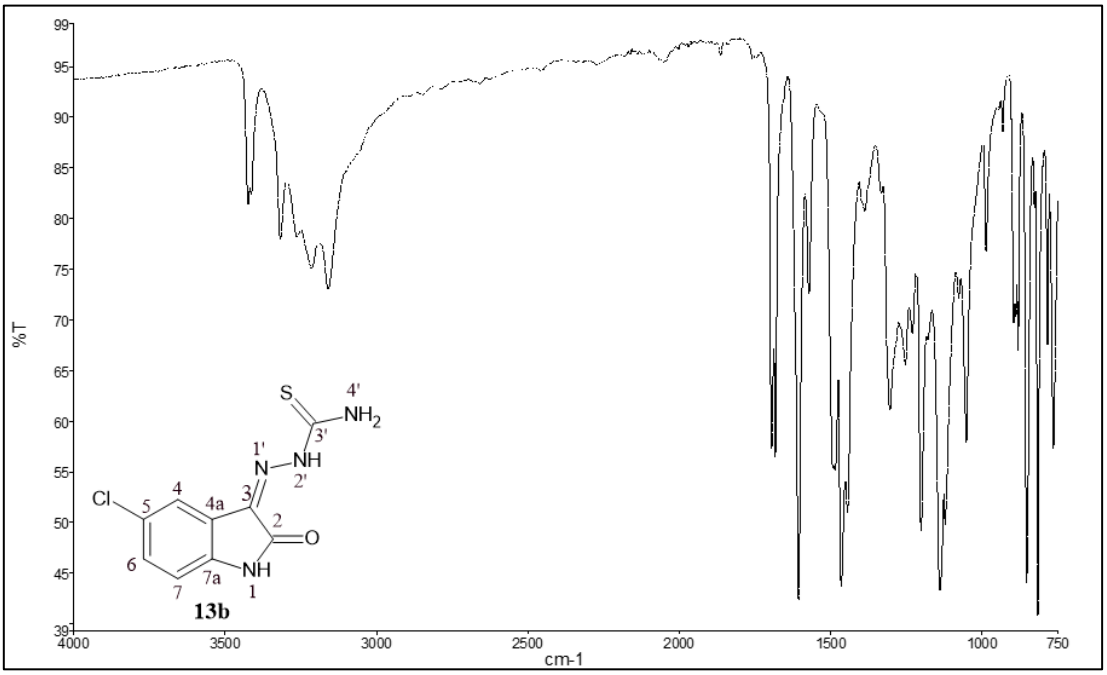

Figure A4: IR spectrum of intermediate **13b**

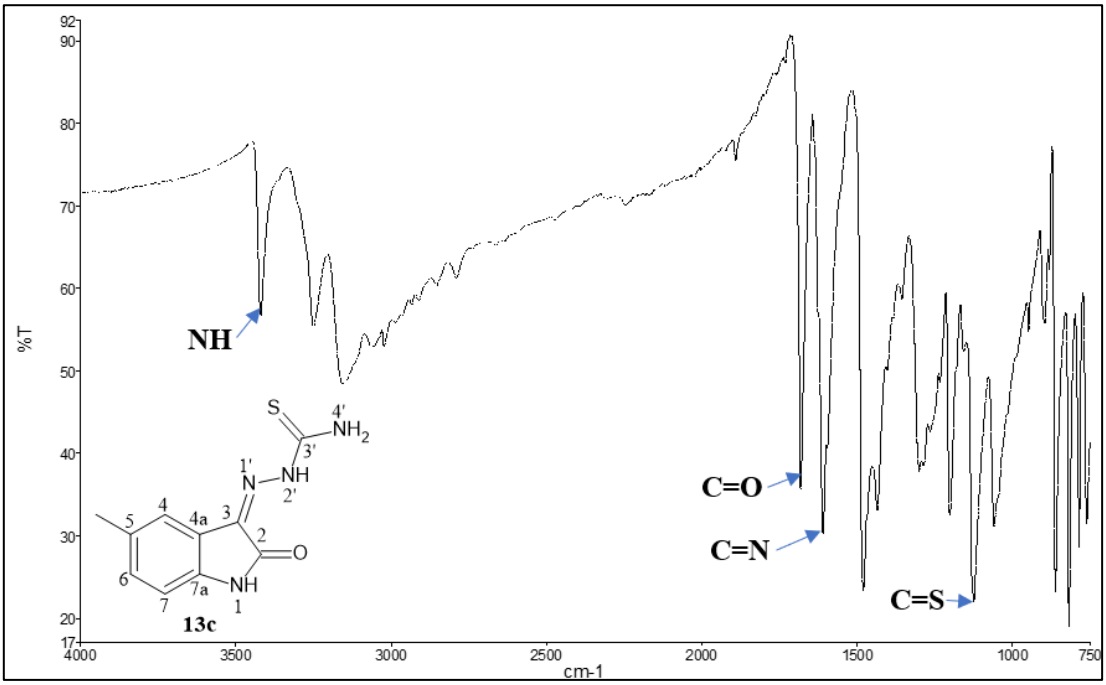

Figure A5: IR spectrum of intermediate **13c**

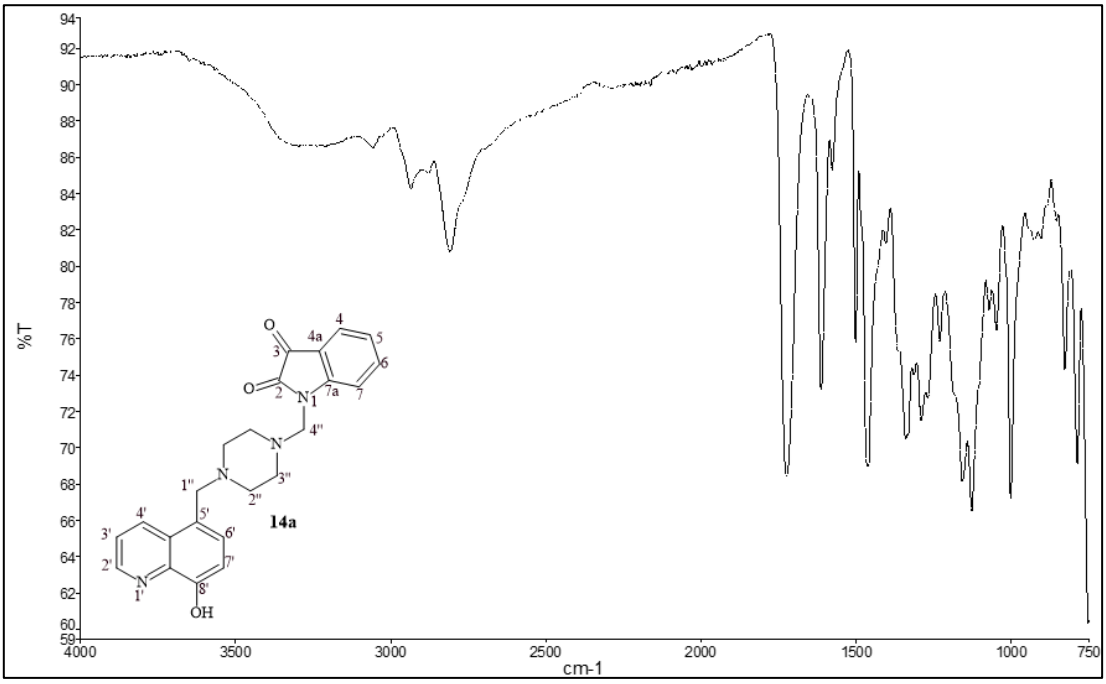

Figure A6: IR spectrum of intermediate **14a**

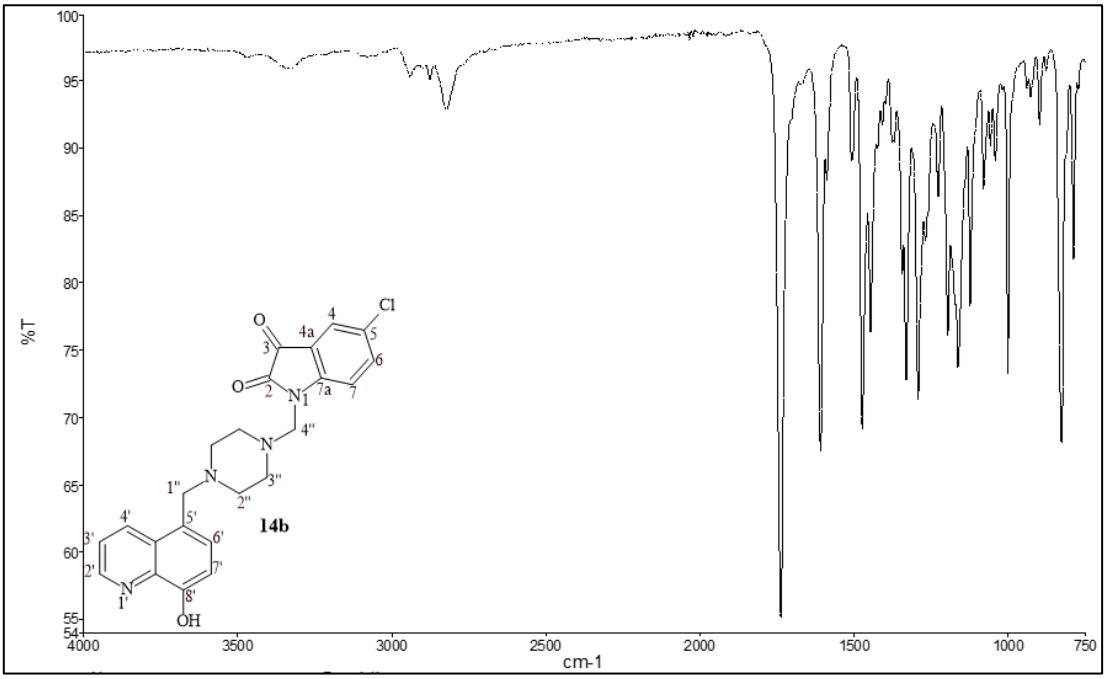

Figure A7: IR spectrum of intermediate **14b**

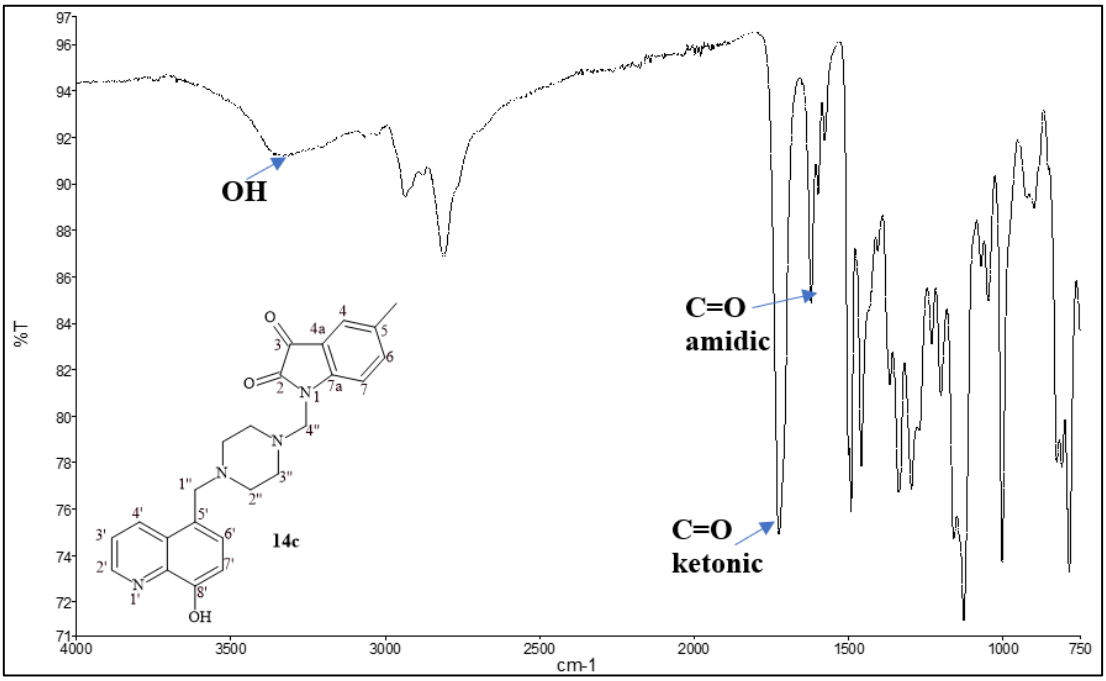

Figure A8: IR spectrum of intermediate **14c**

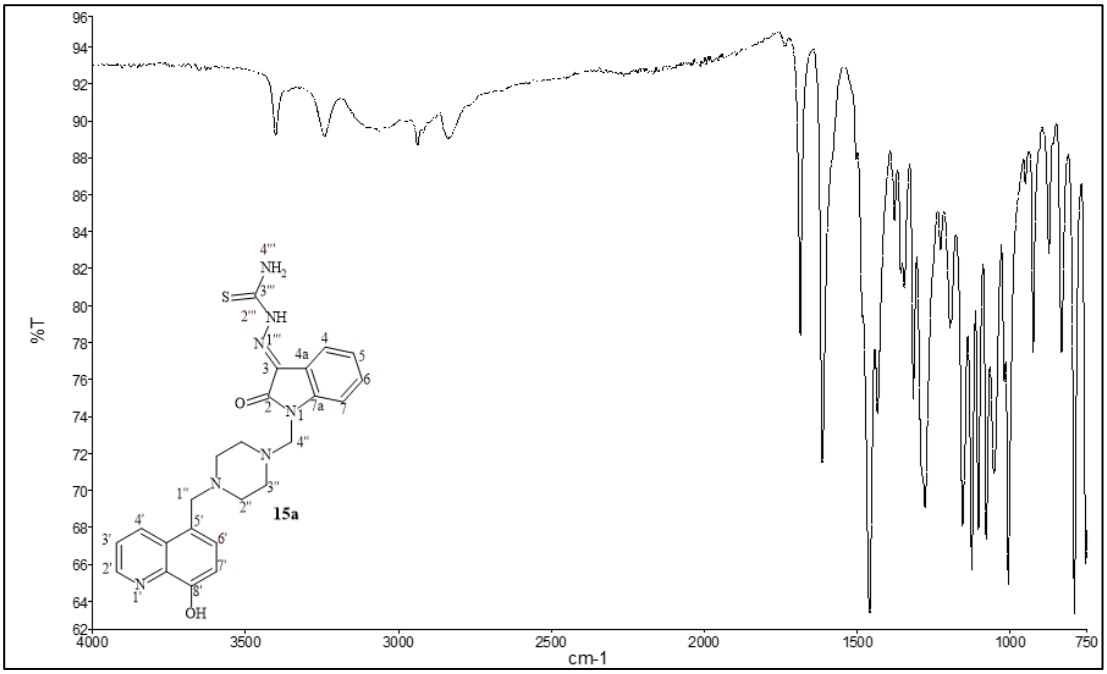

Figure A9: IR spectrum of intermediate **15a**

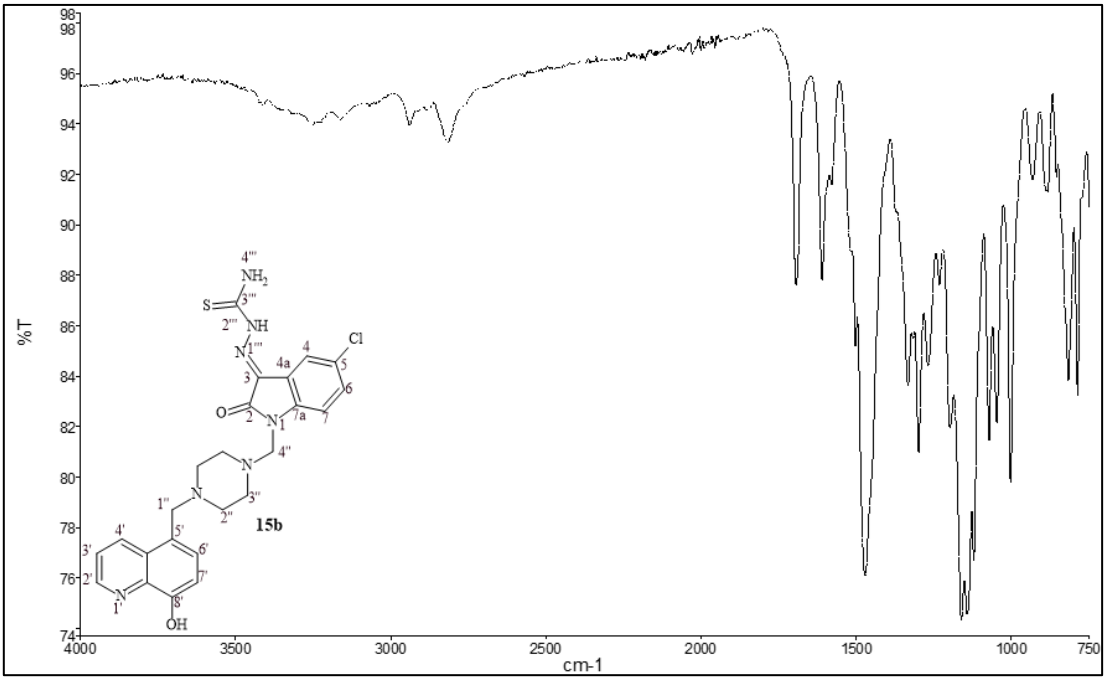

Figure A10: IR spectrum of intermediate **15b**

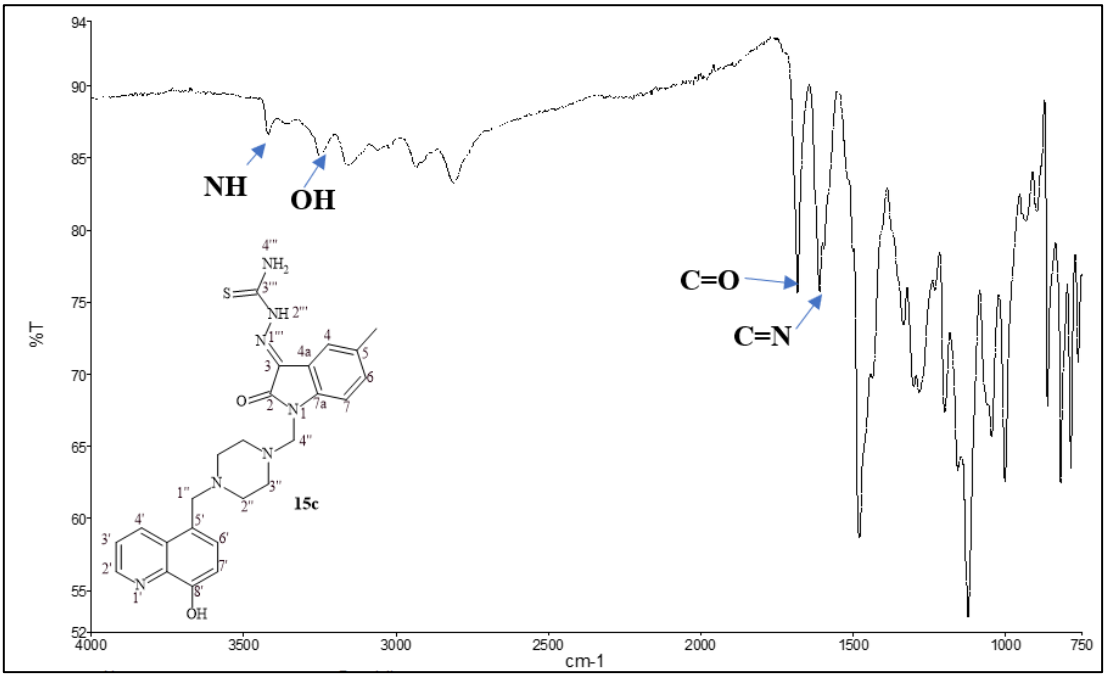

Figure A11: IR spectrum of intermediate **15c**

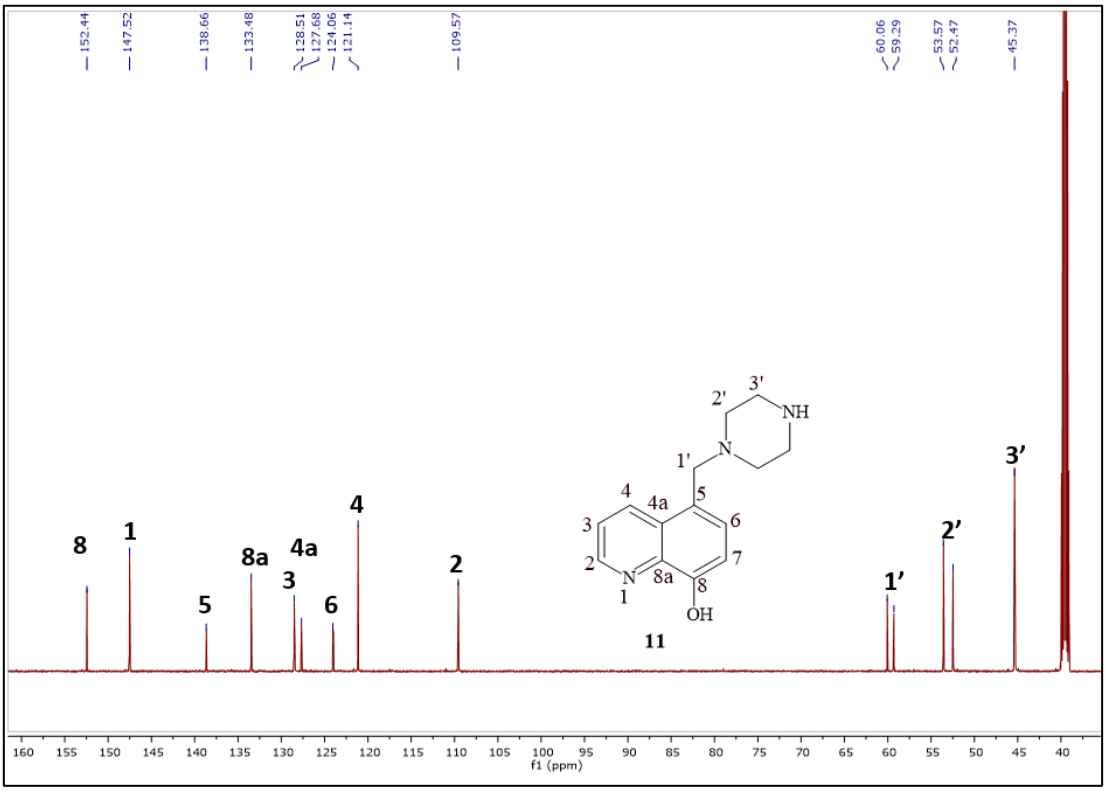

Figure A12: ^{13}C NMR spectrum of intermediate **11** in DMSO-d_6 at 100MHz.

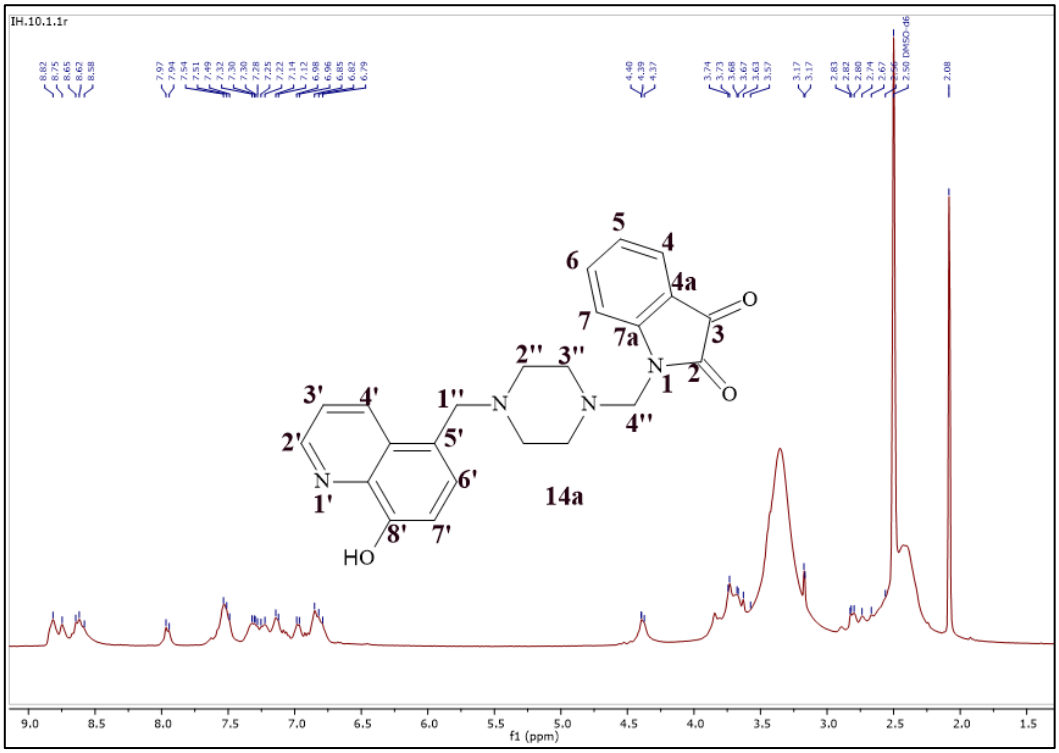

Figure A13: ^{1}H-NMR spectrum of hybrid **14 a** in DMSO-d_6 at 400 MHz

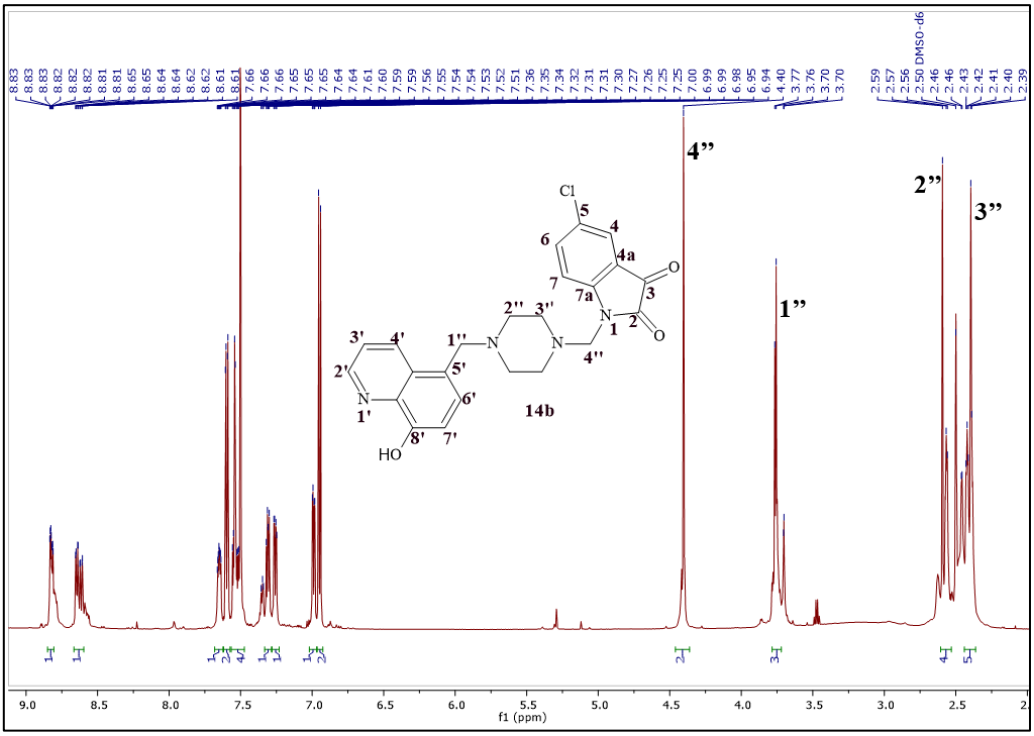

Figure A14: ^{1}H-NMR spectrum of hybrid **14 b** in DMSO-d_6 at 400 MHz

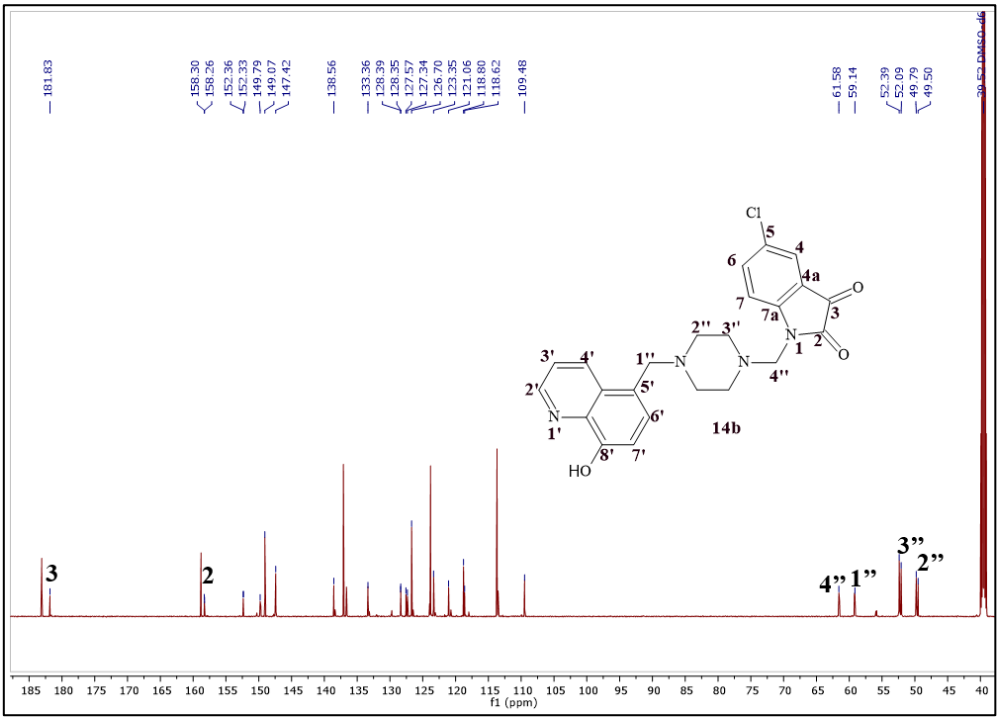

Figure A15: ^{13}C NMR spectrum of hybrid **14b** in DMSO-d_6 at 100MHz.

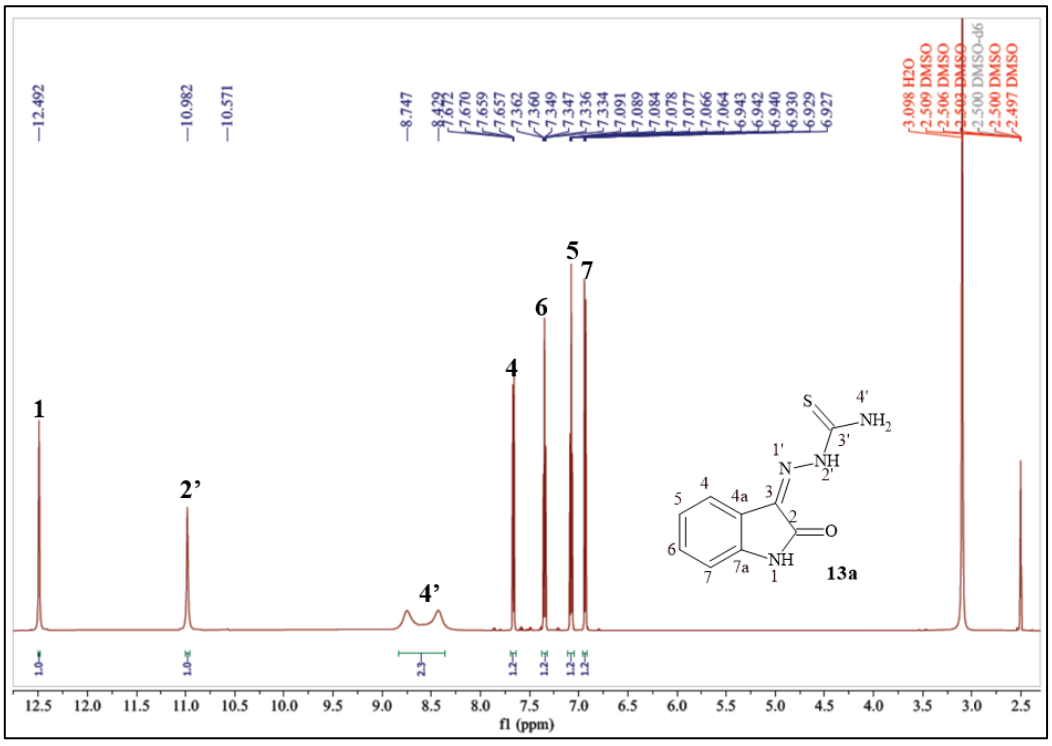

Figure A16: ^{1}H-NMR spectrum of intermediate **13 a** in DMSO-d_6 at 400 MHz

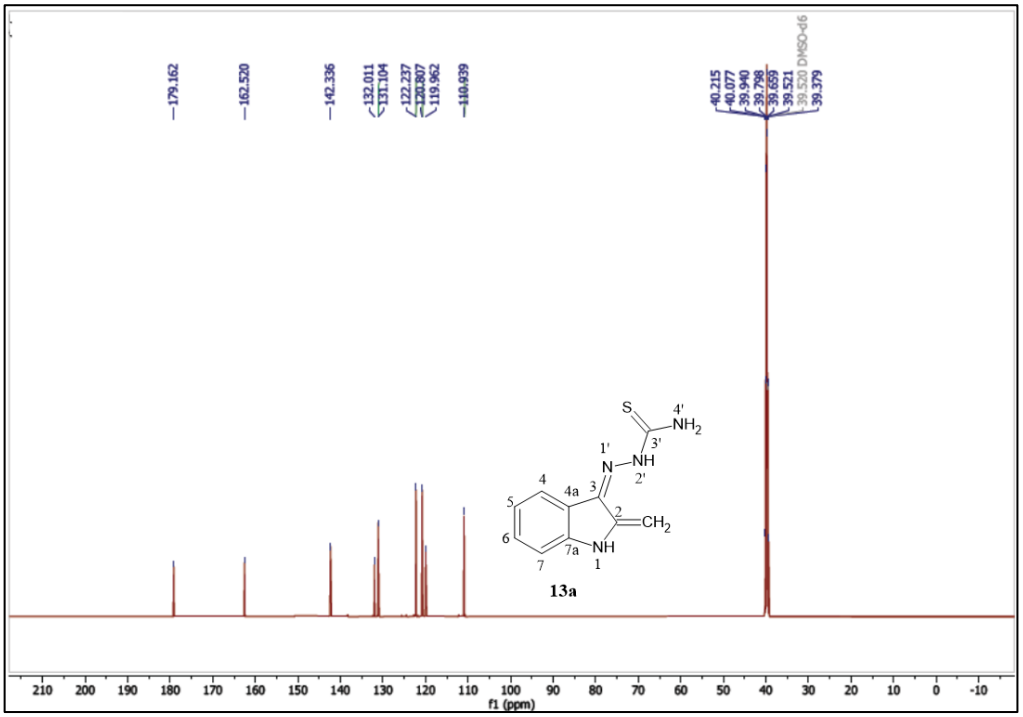

Figure A17: ^{13}C NMR spectrum of intermediate **13a** in DMSO-d_6 at 100MHz.

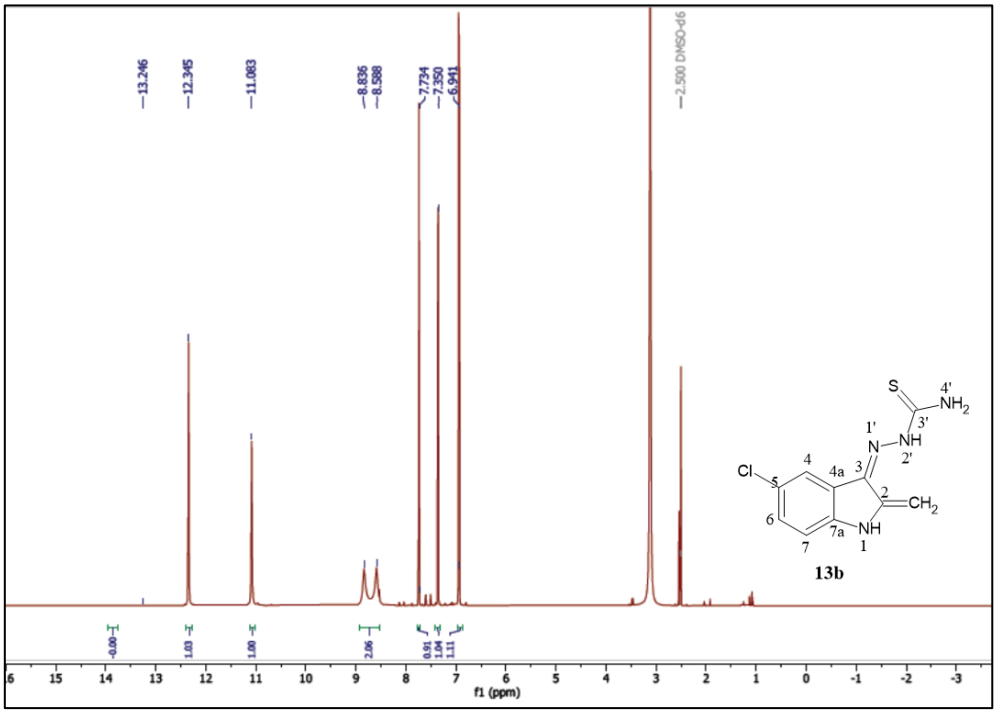

Figure A18: ^{1}H-NMR spectrum of intermediate **13 b** in DMSO-d_6 at 400 MHz

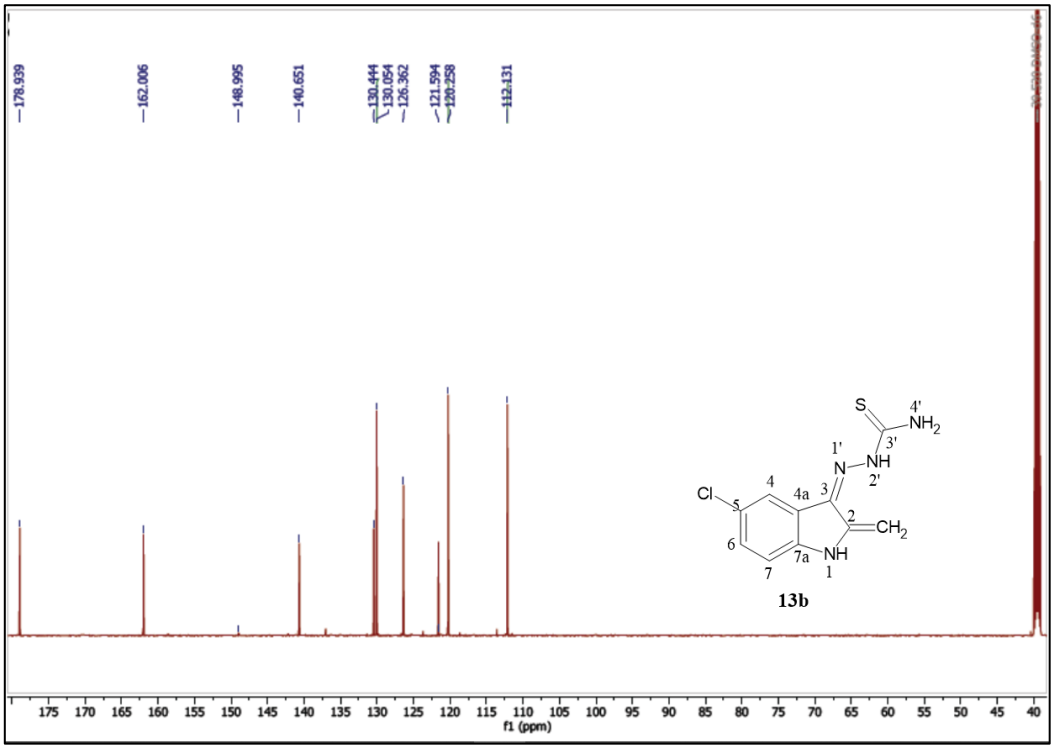

Figure A19: ^{13}C NMR spectrum of intermediate **13b** in DMSO-d_6 at 100MHz.

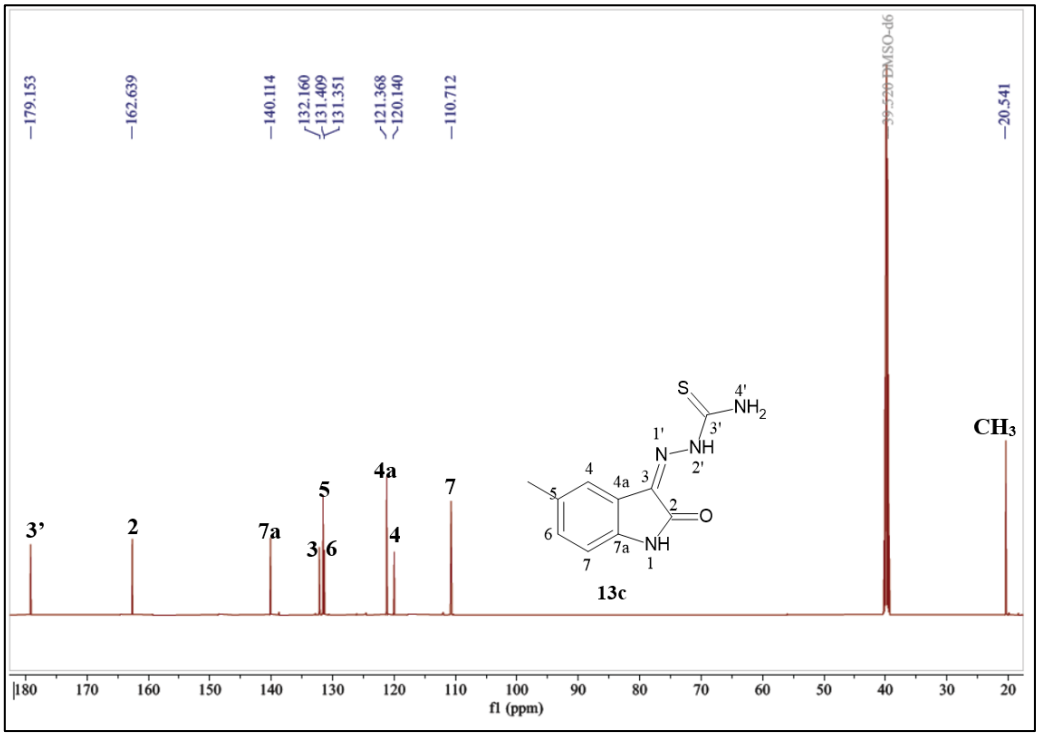

Figure A20: ^{13}C NMR spectrum of intermediate **13c** in DMSO-d_6 at 100MHz.

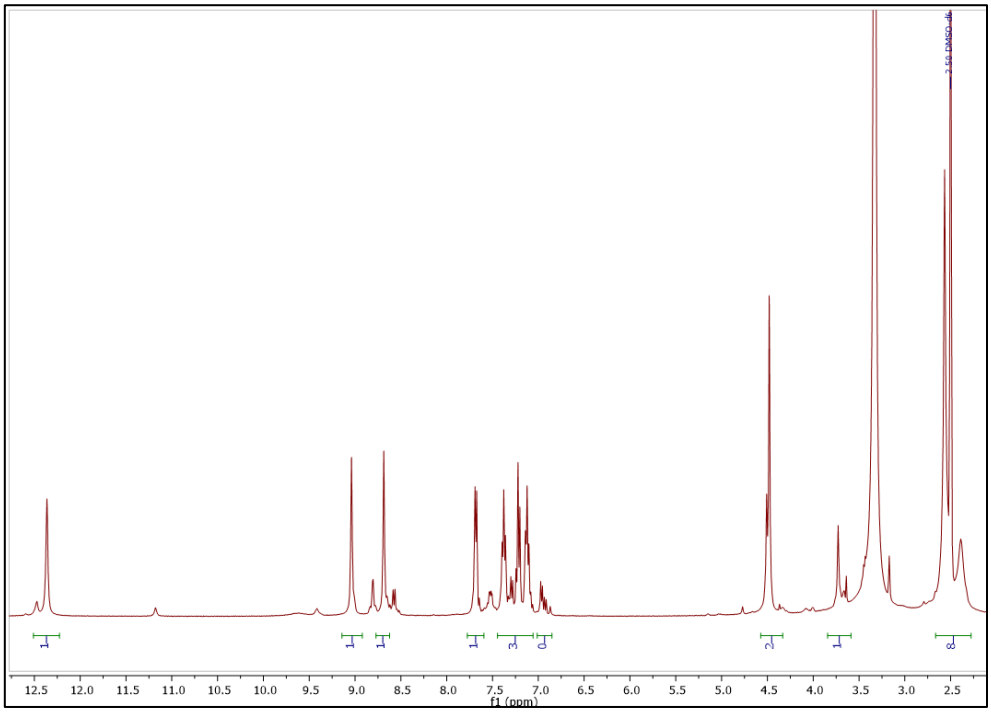

Figure A21: : ^{1}H-NMR spectrum of hybrid **15a** in DMSO-d_6 at 400 MHz

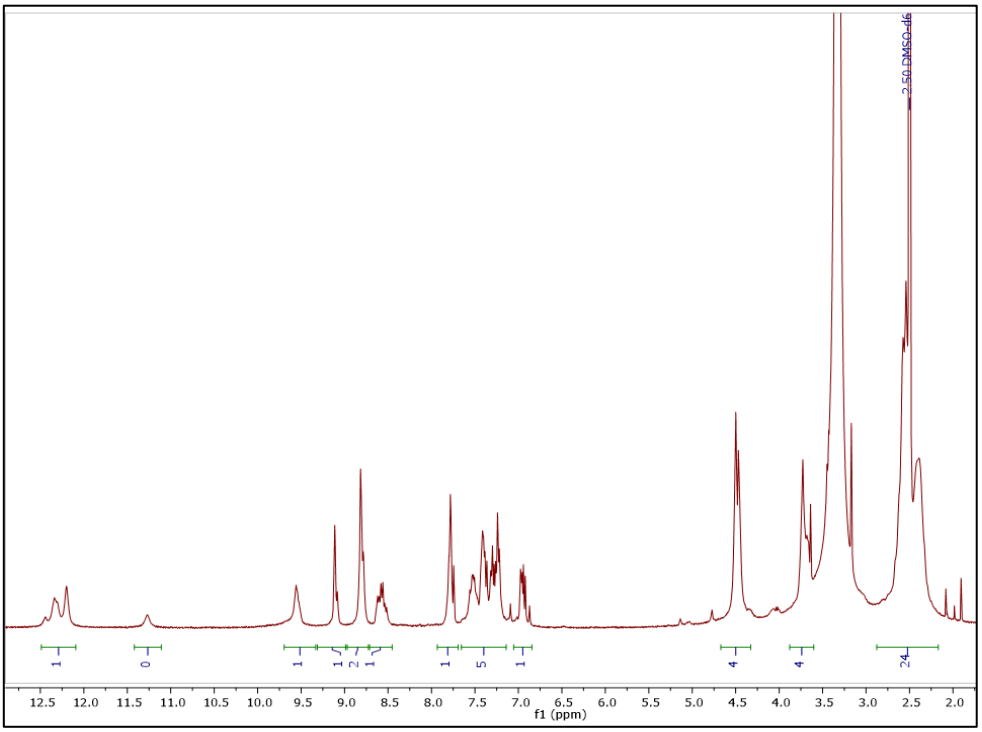

Figure A22: : ^{1}H-NMR spectrum of hybrid **15b** in DMSO-d_6 at 400 MHz

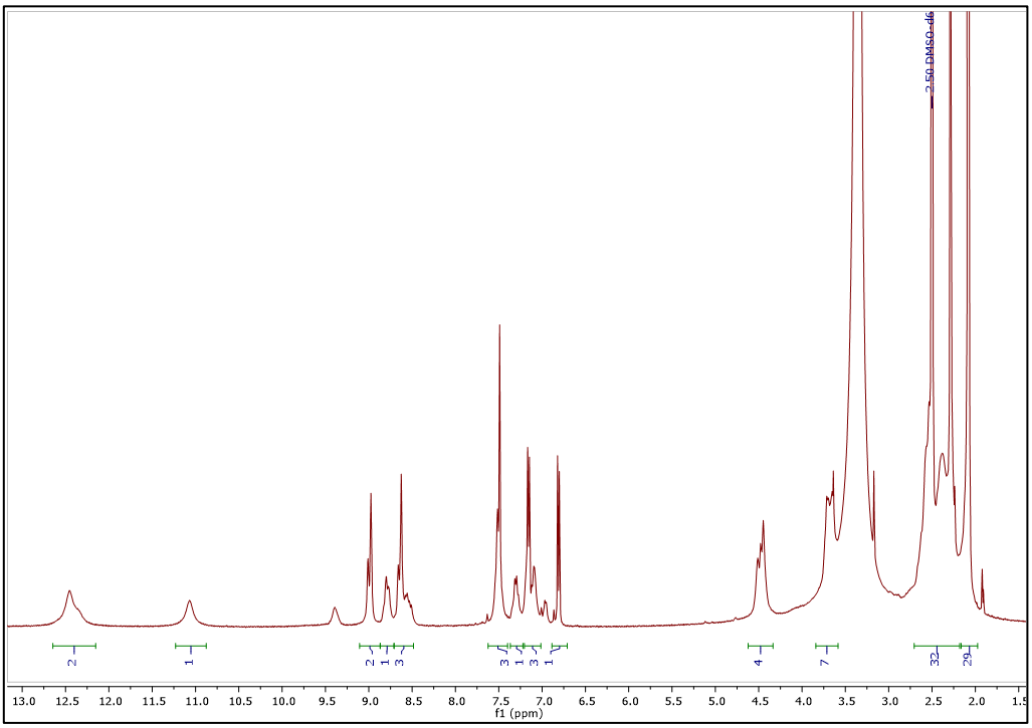

Figure A23: : ^{1}H-NMR spectrum of Hybrid **15c** in DMSO-d_6 at 400 MHz